THE
PHYSICAL REVIEW
A journal of experimental and theoretical physics established by E. L. Nichols in 1893

SECOND SERIES, VOL. 65, NOS. 7 AND 8 APRIL 1 AND 15, 1944

High Energy Particles in Auger Showers

ANATOLE ROGOZINSKI
Ryerson Physical Laboratory, University of Chicago, Chicago, Illinois
(Received January 17, 1944)

The results are given of counter experiments carried out at an altitude of 10,618 feet (Echo Lake, Colorado) on extensive atmospheric showers, or Auger showers, of a minimum spread of 22 meters. An efficient method (the master group method) of investigation of such showers is described. It was found that high energy electrons or photons, initiating a shower below a lead screen of 10-cm thickness, are accompanied, above the absorber, by a shower of high particle density, located either in the central part of the core of the Auger shower or in its close neighborhood.

DURING the summer of 1943, different kinds of counter experiments on extensive atmospheric showers, or Auger showers (here referred to as A showers) were carried out at Echo Lake, Colorado, at the altitude of 10,618 feet above sea level. A detailed account of all the results obtained, of the experimental arrangements, and of the method used in these investigations will be given at a later date. In this paper we will describe only experiments on particles which are able to penetrate up to 10 cm of lead and belong to A showers having a spread of at least 22 meters.

PRINCIPLE OF THE METHOD

The general principle of the method, which we shall call the master group method, is the following:

n counters M_1, $M_2 \cdots M_n$ are in coincidence, and p counters T_1, $T_2 \cdots T_p$, in coincidence between themselves, can be connected in anticoincidence to the first set of n counters. These two sets of counters together form the master group. k other counters (analyzing counters) A_1, $A_2 \cdots A_k$[1] are connected to the master group in such a way that a discharge, which occurs in any one of these k analyzing counters, can be recorded only if it is coincident with an output pulse of the master group. A photographic record of neon lamp flashes—each of the neon lamps being flashed only by its corresponding analyzing counter—thus shows directly how many and which ones of these analyzing counters were discharged simultaneously with the master group.

Now, this record gives not only the coincidences between the master group and any of the analyzing counters, but also, at the same time, all the possible 2^k-1 combinations of coincidences between the k analyzing counters, provided a simultaneous discharge of the master group occurs. In addition, the same record gives a number of anticoincidences, that is, coincidences which are *not* accompanied by other types of coincidences.

For instance, if $k=10$, the total number of

[1] More generally, an analyzing counter can be replaced by a set of coincident and anticoincident counters.

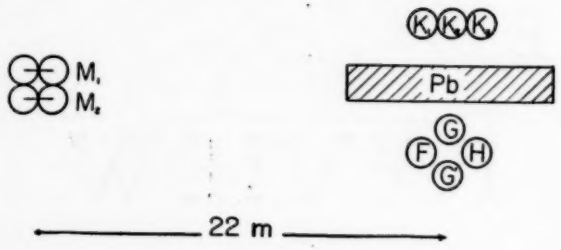

FIG. 1. Arrangement of counters.

possible types of coincidences provided by the record exceeds 1000. However, there is a practical limit on the number of analyzing counters to be used which is set by the prohibitive time required for evaluating the coincidence data. It should, on the other hand, be pointed out that frequently it is not really important to evaluate all the coincidence data thus available since many are of minor interest because various factors, like the geometry of the counter arrangement, prevent a direct interpretation of the corresponding data.

This shows directly that the method described above has a much higher efficiency than all other methods previously[2] used in experiments on A showers.

EXPERIMENTAL ARRANGEMENT AND RESULTS

In the particular case of the present experiment, the master group consists of only two counters, M_1 and M_2,[3] put in a vertical twofold coincidence (Fig. 1). Seven counters, F, G, G', H, K_1, K_2, K_3, are placed at a horizontal distance of 22 meters from the master group. The lower set of counters, F, G, G', H, can be separated from the upper set of counters, K_1, K_2, K_3, by lead absorbers up to a thickness of 10 cm. The whole outfit thus records only particles in an A shower having a minimum spread of 22 meters.

With k equal to 7, in the present case, the number of available coincidences was 127; but only 31 were actually evaluated.

These 31 types of coincidences are divided into 3 categories: In the first category are listed 7 types of coincidences, according to whether *only* one, or *only* two, or all three upper counters K_1, K_2, K_3 are discharged. The second category comprises three types of coincidences in the lower set, namely: (a) when a discharge occurs in both counters G and G' *alone;* (b) when the (a)-type discharge is accompanied by a discharge in counter F or H, but not in both; and (c) when it is accompanied by a discharge in both. The third category consists of the 21 combinations of all individual cases of the first two categories. It must be borne in mind that in each of the 31 cases the master group was simultaneously discharged.

The first type of coincidences of the second category and the corresponding 7 cases of the third category are of special interest since they might be attributed to penetrating non-shower producing particles, like mesotrons or protons. However, these particular cases will be discussed in another paper, and here we shall give only the results concerning high energy shower-producing particles in A showers, such as electrons or photons.

These results are given in Table I. The first column gives the time of recording for measurements with thicknesses of lead which are indicated in the second column. All the data in the other columns represent frequencies expressed in number of coincidences per 10 hours. The third column gives the frequencies of the sixfold coincidences $M_1M_2FGG'H$ in different thicknesses of the lead absorber. Columns IV to X give the frequencies of the coincidences between $M_1M_2FGG'H$ and the 7 cases of the first category, which have already been mentioned. The last column Δ represents, for a given thickness of lead, the difference between the frequency of $M_1M_2FGG'H$ and the sum of the frequencies listed in columns IV to X. The Δ values give the frequencies of the $M_1M_2FGG'H$ events which are *not* accompanied by a discharge in any of the upper counters. The mean coincidence-frequencies in this upper set alone (first category) were, respectively, 320, 80, and 170, when *just* one of the K counters was discharged, *just* two of the K counters were discharged simultaneously, and all three counters K_1, K_2, K_3 were discharged simultaneously. All the counters used in these experiments have a diameter of 5 cm, and an

[2] P. Auger, R. Maze, T. Grivet-Meyer, Comptes rendus **206**, 1721 (1938). P. Auger, P. Ehrenfest, R. Maze, J. Daudin, Robley, and A. Freon, Rev. Mod. Phys. **11**, 288 (1939). W. Kolhörster, J. Matthes, and E. Weber, Naturwiss. **26**, 576 (1938). N. Hilberry, Phys. Rev. **60**, 1 (1941).

[3] Actually, M_1 and M_2 consist, each, of two counters connected in parallel.

TABLE I. Coincidences, per 10 hours, occurring between the master group M_1M_2 and the different analyzing counters F, G, G', H, K_1, K_2, K_3. In column Δ are listed such coincidences $M_1M_2FGG'H$ which are *not* accompanied simultaneously by discharges in any of the upper counters K_1, K_2, K_3.

I Hours of recording	II cm Pb	III $M_1M_2FGG'H$	IV K_1	V K_2	VI K_3	VII $M_1M_2FGG'H$ K_1K_2	VIII K_1K_3	IX K_2K_3	X $K_1K_2K_3$	XI Δ
7	2.5	66	3	3	4.5	9	3	12	22.5	9
29.8	5.0	64.8	1.7	3.7	3.4	6.4	3.7	6	33	6.8
20.5	10.0	26	1	0.5	0.5	1	1	0.5	20	1.5

effective area of 250 cm²; they are filled with a mixture of argon and alcohol and operate at 1200 volts. The resolving time of the coincidence circuits is about 4×10^{-6} sec., so chance coincidences were negligible in the case of the higher order coincidences here reported. The question of the solid angles, subtended by any counter or set of counters, is of minor importance in the present experiment since the particle-densities in the showers which are involved here are high, as will be seen hereafter.

DISCUSSION

Consider first values obtained for a lead absorber of 10-cm thickness. An event $M_1M_2FGG'H$ represents then a shower of at least 3 particles, emerging below a lead screen of a thickness equivalent to about 20 radiation units; moreover, this shower is associated with one or more particles which reach the counters placed at a horizontal distance of 22 meters from the counters located below the lead. The same shower must have originated from at least one particle of an energy sufficiently high to penetrate such a thickness of lead. However, if the particle responsible for the creation of the shower emerging below the lead is a mesotron, its energy could have been relatively low—of the order of a few times 10^8 ev. But since the probability of a mesotron being in an A shower and, moreover, creating in the lead absorber even a small shower is quite low, this possibility might be disregarded. Therefore, the creation of the shower emerging below the lead should be attributed mainly to high energy electrons or photons. In this case, the energy of such particles (electrons or photons) must be of the order of magnitude of at least 10^{10} ev.

Now, particles of such high energy can be created only in the central part of their parent A shower because the average angle of their emission, with respect to the direction of the particle from which they directly originate, is given approximately by the ratio between the rest energy of an electron and the energy of the created particle. For an energy of 10^{10} ev, this angle is extremely small—of the order of a few seconds—and has a negligible influence on the scattering of the particle. A mechanism which could play here a more appreciable role would be the multiple scattering of the particle out of the core of the A shower, since the average angle of this scattering, per radiation unit, is about 40 times as high as the mean angle of emission mentioned above.[4] Even in this case, the distance of the particle from the core of the A shower would not become appreciable, unless the particle was created very far above the observation point—for example, in the first few radiation units from the top of the atmosphere. But then, in order to reach the absorber with a residual energy of at least 10^{10} ev, the initial energy of the particle created close to the top of the atmosphere should have had a much higher value. Such a particle would have to cross a thickness of air equivalent to some 15 radiation units, and, consequently, would arrive at the lead absorber accompanied by its own cascade shower. Hence one sees that the particle initiating a shower under the lead would always be accompanied, either by a shower of particles belonging to the core of the same parent A shower, or by its own cascade shower, or by both.

The values given in Table I are in agreement with the foregoing interpretation. Indeed, in 20 out of 26 cases an event $M_1M_2FGG'H$ is accom-

[4] B. Rossi and K. Greisen, Rev. Mod. Phys. 13, 240 (1941).

panied above the lead by a shower discharging all three upper counters K_1, K_2, K_3. The table shows, furthermore, that cases where none, or only one, of the K counters is discharged, or only two of the K counters are discharged simultaneously with the event $M_1M_2FGG'H$, are very infrequent. This indicates that the mean particle density in the portion of the showers which strikes the lead absorber, under the described conditions, must be very high and, as calculations show, of at least several hundred particles per m^2.

Now, counters of the size used in the present experiments become practically saturated for such particle-densities. This means that the probability of discharging such a counter is then very close to unity. Therefore, the actual densities might have had much higher values than those just quoted. More accurate values could be provided by using counters of a much smaller size. But then, the time required to carry out such experiments would be considerably longer.

Let us notice now that the ratio between the coincidence frequencies of an $M_1M_2FGG'HK_1K_2K_3$ event and an $M_1M_2FGG'H$ event decreases with decreasing thickness of the lead absorber. This is in agreement with the fact that a particle able to produce a shower below the lead absorber might have a lower energy in case the lead absorber has a smaller thickness, and thus could be present in a lower density region of the A shower. Inversely, one can expect that the same ratio will reach a value of 100 percent for a sufficient thickness of the absorber. This point should be carefully verified because if confirmed, it could give a different interpretation of counter experiments on multiple mesotrons,[5] even though the absorber thicknesses used in such experiments might have been very large. Indeed, since a knock-on shower accompanying a mesotron should be considered as a very infrequent event, the most reliable criterion for the identification of a mesotron in counter experiments is its practical inability to produce showers in absorbers of a thickness equivalent to a sufficiently high number of radiation units. Therefore, so long as it is not proved, by means of several counters as there are in the present experiment, that a particle is not accompanied by a shower below a thick absorber, there will always be a high probability that the shower below the absorber is initiated by a high energy electron or photon, and is accompanied, *above* the absorber, by a dense shower belonging to the core of an A shower.

The same remarks apply to experiments on the presence of mesotrons in the A showers.

I wish to express my deep appreciation to Dean A. H. Compton for making available to me many facilities, and to the Rockefeller Foundation for its generous support. I am also very grateful to Professor Pierre Auger for his friendly and inspiring interest in this work, and to Professor Marcel Schein for many valuable discussions of the problems regarding the present experiments. I should like to express my thanks to General L. A. Lawson and to Captain A. Innis-Taylor for their generous hospitality at the Echo Lake Camp.

[5] M. Damy de Souza Santos, P. A. Pompeia, and G. Wataghin, Phys. Rev. **59**, 902 (1941). V. Josephson, D. K. Froman, and J. C. Stearns, Phys. Rev. **57**, 335 (1940).

PHYSICAL REVIEW VOLUME 65, NUMBERS 7 AND 8 APRIL 1 AND 15, 1944

Disintegration Schemes of Radioactive Substances. VII. Mn^{54} and Co^{58}*

MARTIN DEUTSCH AND LLOYD G. ELLIOTT**
Massachusetts Institute of Technology, Cambridge, Massachusetts

(Received January 20, 1944)

The radiations emitted by Mn^{54} and by Co^{58} have been studied by means of the magnetic lens spectrometer and coincidence techniques. Mn^{54} decays by orbital electron capture to an excited state of Cr^{54}, followed by the emission of a 0.835-Mev gamma-ray. A study of the x-rays emitted following the capture process indicates that a large—or even an overwhelming—fraction of the captured electrons are K electrons. Few if any capture transitions lead directly to the ground state. Co^{58} decays to a state of Fe^{58} 0.805 Mev above the ground state which in turn decays by the emission of a single gamma-ray. About 90 percent of the disintegrations of Co^{58} occur by K-electron capture. In the remaining 10 percent positrons of maximum energy 0.47 Mev are emitted. This ratio of the two modes of decay is consistent with the idea that the transition takes place with a change of angular momentum of one unit or zero, whether the parity changes in the transition or not, if the tensor theory of beta-decay is the correct one. The lowest known excited states of Cr^{54}, Fe^{56}, and Fe^{58} have excitation energies differing by less than five percent. The difference between the masses of the neutral atoms of Co^{58} and Fe^{58} should be $2.46\pm0.03\times10^{-3}$ a.m.u.

INTRODUCTION

IN contrast to the very complex radiations described in paper VI,[1] this paper is concerned with two nuclear species whose disintegration schemes are quite simple. Inspection of the isotope chart (Fig. 1) discloses that both Mn^{54} and Co^{58} have two stable isobaric neighbors and could thus decay either by increasing or by decreasing the nuclear charge. However, both decay only by the change of a proton into a neutron, i.e., by positron emission or orbital electron capture, with relatively long half-lives. The product nuclei Cr^{54} and Fe^{58}, respectively, both belong to the stable sequence of nuclear type $(4n+2)$ with isotopic number 6 which extends from Ca^{46} to Kr^{78}. Both disintegration schemes were studied by the magnetic spectrometer and coincidence techniques described in the preceding papers of this series.[1]

Mn^{54}

The radioactivity of manganese with about 500-day half-life was definitely assigned to the species of mass number 54 by Livingood and Seaborg.[2] These same authors also reported that this activity emits no charged particles of nuclear origin but does emit gamma-rays of about 0.85-Mev energy as shown by absorption measurements. Alvarez[3] also demonstrated the emission of chromium K x-rays.

Sources of Mn^{54} used in our experiments were prepared from iron bombarded with deuterons. The iron was removed by precipitation with pyridine (paper IV), cobalt by precipitation with KNO_2 (paper VI), and finally the manganese was precipitated as the oxide in nitric acid solution. The sources were allowed to age for about two months because of the presence of the 6.5-day activity of Mn^{52}.

Under the bombarding conditions of the M.I.T. cyclotron at the time when these experiments were performed, i.e., with a deuteron energy of about 11 Mev and thick targets, the great majority of all the gamma-rays emitted by the long-lived activities induced in the iron target are contributed by the soft gamma-rays of Co^{57}. Since the cross section for production of photoelectrons by gamma-rays of these energies (0.119 and 0.131 Mev) is very large, even a slight residual contamination of radiocobalt will be detected when photoelectron spectra are studied in the spectrometer. It will be recalled that such a contamination was found in sources of Fe^{59} prepared from the same targets as the Mn^{54} (paper IV). Deutsch and Roberts[4] reported a 0.850-Mev and a 0.120-Mev gamma-ray from

* Some of these results have been presented at the New York Meeting of the American Physical Society, January 22–23, 1943.

** Now with the Canadian National Research Council, Radiological Committee, Montreal.

[1] L. G. Elliott and M. Deutsch, Phys. Rev. **64**, 321 (1943). The previous papers of this series are listed under reference 1 of paper VI, and are referred to here as papers I to VI.

[2] J. J. Livingood and G. T. Seaborg, Phys. Rev. **54**, 391 (1938).

[3] L. Alvarez, Phys. Rev. **54**, 486 (1938).

[4] M. Deutsch and A. Roberts, Phys. Rev. **60**, 362 (1941).

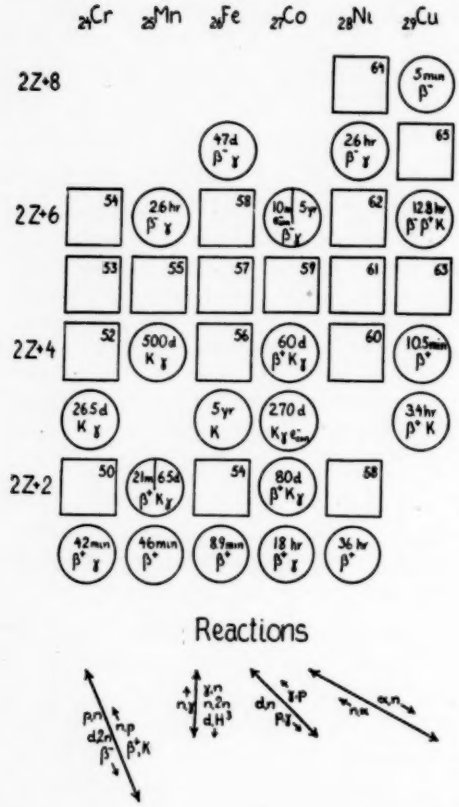

FIG. 1. The known nuclear species of the elements between $Z=24$ and $Z=29$. Squares indicate stable isotopes, circles radioactive isotopes.

Mn^{54}. Because of our experience with Fe^{59}, we re-examined the low energy region, using a source of Mn^{54} which had been freed of cobalt several times, adding inactive carrier material in each purification. No gamma-rays other than the 0.85-Mev radiation were found. Therefore it seems certain that the low energy gamma-ray reported previously[4] was due to a slight contamination by Co^{57}.

The energy of the 0.85-Mev gamma-ray was also redetermined with greater accuracy and is now found to be 0.835 ± 0.015 Mev. (Compare Fig. 9 of paper VI.[1]) In agreement with other observers, we failed to find any charged particles emitted by thin sources of Mn^{54}.

Since Mn^{54} decays only by orbital electron capture, it remained to be shown whether the decay always leaves the Cr^{54} nucleus in an excited state or whether it leads sometimes directly to the ground state. Therefore coincidences between K x-rays and gamma-rays were studied. Our standard "bell" type beta-ray counters, equipped with mica windows and filled with helium at atmospheric pressure (paper II), are quite unsuited for the detection of x-rays of this wave-length. Several of these counters were therefore equipped with thin Cellophane or beryllium windows and filled with pure tank argon at a pressure of about 60 cm Hg. About half of the rays entering these counters should be absorbed in the filling gas and therefore be counted.

Such an x-ray counter was placed in the standard coincidence arrangement (paper V). The observed number of x-gamma-coincidences per recorded x-ray was 1.25 ± 0.04, in good agreement with the known efficiency of the gamma-ray counter for a single gamma-ray of energy 0.835 Mev. (The efficiency of the gamma-ray counter used in this experiment was slightly larger than that of the counter described in paper V). No gamma-gamma coincidences were found. It follows, then, that each K x-ray of chromium emitted following the K-electron capture process is accompanied by a single gamma-ray of energy 0.835 Mev. This scheme is shown in Fig. 2. The disintegration energy is not known, but because of the complete absence of positron emission, it seems reasonable to assume that the energy difference between initial and final states of the disintegration is less than or, at most, very close to mc^2. The particular value chosen in Fig. 2, namely, 0.1 Mev, was arrived at by assuming both Mn^{54} and Co^{58} to perform allowed transitions with the same matrix element.

Marshak[5] has raised the question whether L-electron capture might not occur with a fre-

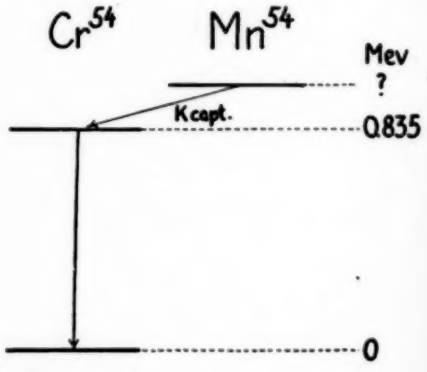

FIG. 2. Disintegration scheme of Mn^{54}.

[5] R. E. Marshak, Phys. Rev. **61**, 431 (1942).

quency comparable to that of K-electron capture in the case of Mn^{54}. It seems quite certain, for theoretical reasons, that abundant L-electron capture, if it occurs at all, must also lead to the excited state of Cr^{54}. If the net detection efficiency of the x-ray counter were known as well as the efficiency of the gamma-ray counter, it should be possible to compare directly the number of gamma-rays and the number of K x-rays emitted by noting the corresponding counting rates. A comparison of the observed number of x-rays with the number from a source of Co^{58}, taking into account the variation of the absorption of the two different radiations in the counter gas and in the beryllium window and the different fluorescent yield of iron and chromium, all of which enter into the net detection efficiency, leads to the conclusion that our observations are consistent with the assumption that Mn^{54} decays overwhelmingly by K-electron capture. The experiment is crude, at best, because of the large and uncertain absorption of the x-rays in the source material itself.

Co^{58}

Livingood and Seaborg[6] showed that Co^{58} decays by positron emission to Fe^{58}. They reported the maximum energies of the beta- and gamma-rays, found by absorption methods to be 0.5 Mev and 0.8 Mev, respectively. The assignment of this activity to Co^{58} is definite because it is produced by alpha-particle bombardment of manganese. This distinguishes it from Co^{56} which has a very similar half-life (compare paper VI).[1]

The results of Jensen,[7] which contradict these findings as well as ours, were probably due either to a contamination or to the well-known unreliability of cloud-chamber data.

We have produced Co^{58} by an (n, p) reaction on nickel. About 5 g of nickel metal were fixed to the back of a beryllium target which was bombarded by about 10-milliampere-hours of 14-Mev deuterons. The chemical separations followed the same lines as those described in paper VI[1] for the preparation of sources of Co^{56}. Inspection of Fig. 1 shows that the only known

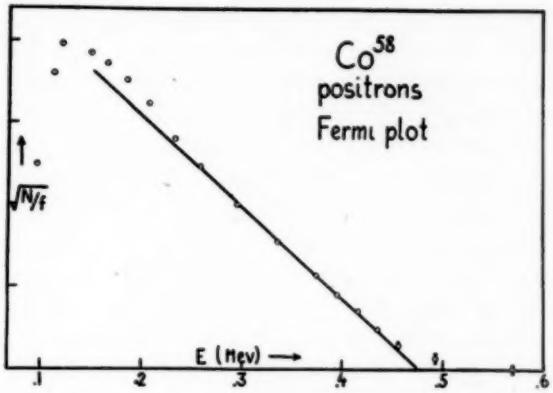

FIG. 3. Fermi plot of the positron spectrum of Co^{58}. The Fermi function was evaluated for $Z=26$.

radioactive species of cobalt expected from fast neutron bombardment of nickel are Co^{58} and Co^{60}. The radiations accompanying the decay of the latter species are well known[8] and consist of soft negatrons and hard gamma-rays. If equal cross sections for the two (n, p) reactions are assumed, a consideration of the relative isotope abundance and half-lives indicates that one should observe about one hundred times as many disintegrations of Co^{58} as of Co^{60}. In fact the number of negatrons was found to be too small to be reliably detected, in the presence of the secondary electron due to the Co^{58} gamma-rays.[9] A small amount of Co^{57} might be found as the decay product of Ni^{57}, produced by an $(n, 2n)$ reaction. However, the intensity of the soft gamma-rays and conversion electrons emitted by this activity, if present at all, was too small to be detected.

Figure 3 shows a Fermi plot of the positron spectrum emitted by Co^{58}. The specific activity of the active material was not sufficient to permit the preparation of a source which could be considered thin for electrons of so low an energy. The shape of the Fermi plot is therefore probably distorted by scattering in the source. Extrapolation of the straight line portion of the plot yields the value 0.470 ± 0.015 Mev for the maximum energy. The apparent tailing off beyond the end point is due to the poor resolution

[6] J. J. Livingood and G. T. Seaborg, Phys. Rev. **60**, 913 (1941).
[7] A. S. Jensen, Phys. Rev. **60**, 430 (1941).
[8] M. Deutsch and L. G. Elliott, Phys. Rev. **62**, 558 (1942).
[9] The magnetic lens spectrometer ordinarily does not distinguish between positrons and negatrons. A special baffle system is provided for this purpose.

necessary because of the low intensity available. The value of the maximum energy is in good agreement with that found with thinner sources containing a mixture of Co^{56} and Co^{58} (paper VI).

Figure 4 shows the secondary electron spectrum produced in a lead radiator (35 mg/cm²) by the gamma-rays of Co^{58}. Two very pronounced photoelectron lines are found, corresponding to gamma-ray energies of 0.507 ± 0.008 Mev and 0.805 ± 0.012 Mev, respectively. The *L*-photoelectron group, due to the same gamma-rays, also appears as much smaller peaks. The lower energy line is certainly due to annihilation radiation. The small number of counts at energies above 0.8 Mev is probably due to the Co^{60} gamma-rays of 1.10- and 1.30-Mev energy.[8]

It is apparent from Fig. 4 that the 0.805-Mev radiation is considerably more intense than the 0.51-Mev gamma-ray. When account is taken of the variation of the photoelectric cross section with gamma-ray energy and of the effect of finite radiator thickness on the height of the photoelectron lines, it is found that the 0.805-Mev gamma-ray is 5 ± 2 times as intense as the annihilation radiation. The relatively large uncertainty in this ratio is due to the fact that the effective source of annihilation radiation is slightly larger than the dimensions of the source material because of the finite range of the positrons. Since *two* annihilation quanta are emitted for each positron that is annihilated, we conclude that there are 10 ± 4 times as many 0.805-Mev quanta emitted as positrons.

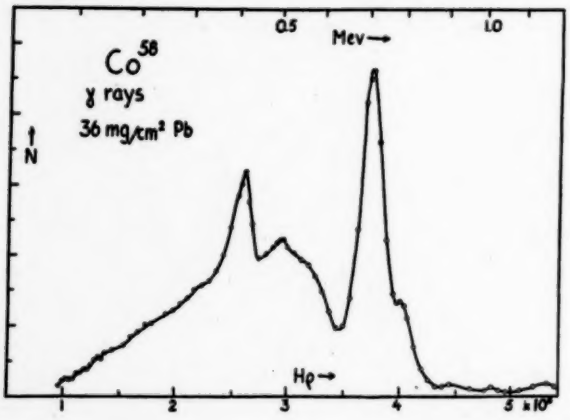

FIG. 4. Secondary electrons due to gamma-rays of Co^{58}. The peaks are photoelectrons ejected from the lead foil. The continuous distribution is due to Compton recoil electrons.

Coincidences between positrons and gamma-rays were observed in the spectrometer since the great abundance of gamma-rays and the presence of negatrons due to Co^{60} interfered with accurate measurements in the standard counter arrangement (paper V). It was found that the coincidence rate per recorded positron was independent of positron energy. One may conclude from this that all disintegrations proceed to the same excited state.

The observed coincidence rate for the positrons of Co^{58} was in good agreement with the efficiency of the gamma-ray for a 0.8-Mev gamma-ray in the geometry used as determined by observing coincidences with the high energy beta-ray spectrum of Mn^{56} (paper VI).

We may conclude that each positron emitted by Co^{58} is accompanied by one 0.805-Mev gamma-ray.

In order to study coincidences between iron *K* x-rays which are emitted following the *K*-electron capture process and gamma-rays, the beta-ray counter of the standard arrangement was replaced by an argon-filled x-ray counter as described above in the discussion of Mn^{54}. When all of the positrons were absorbed in beryllium, a true coincidence rate of $1.23\pm0.04\times10^{-3}$ per recorded x-ray was observed in the standard arrangement. This is in good agreement with the expected efficiency for detecting a 0.8-Mev gamma-ray which is $1.19\pm0.05\times10^{-3}$. One may conclude that the orbital electron capture process, too, always leaves the Fe^{58} nucleus in the excited state. This is, of course, to be expected since no high energy positrons are observed.

The observations of Co^{58} are summarized in the disintegration scheme shown in Fig. 5.

From this disintegration scheme the mass difference between the neutral atoms of Co^{58} and Fe^{58} is found to be $2.46\pm0.03\times10^{-3}$ a.m.u. The threshold for the reaction Fe^{58} (p, n) Co^{58} should be 3.10 ± 0.03 Mev.

DISCUSSION

It appears that the determination of the relative probabilities of positron emission and orbital electron capture by Co^{58} represents the first case in which the ratio of the two processes has been found with sufficient accuracy to permit a close quantitative comparison with theory.

The various formulations of the Fermi theory[5] all lead to the same ratio of the probabilities in the case of allowed transitions, $\lambda_+/\lambda_K \simeq 0.1$ for Co^{58} in good agreement with the observed value. With the tensor interaction which is most likely to be the correct one, the calculation of the ratio for forbidden transitions is complicated by the occurrence of several matrix elements of unknown ratio. The observed ratio of about 1 : 10 is consistent with a special case of first forbidden transition with a change in nuclear angular momentum of one unit or without change in angular momentum. In particular, the tensor theory predicts the observed value of the ratio if the angular momenta of the initial and final states are 1 and 0 (or vice versa), whether the parity changes or not. For other values of the angular momenta (involving a change of one or zero) the ratio of the transition probabilities may still agree with the observed value if the dominant matrix element is $\int \alpha$ [Eq. (17a), reference 5], which is not unreasonable in this particular case. For larger changes in angular momentum, the tensor theory predicts a smaller relative probability of positron emission at least in some cases. For example, the calculations of Marshak[5] lead to a ratio $\lambda_+/\lambda_K \simeq 0.01$ for an angular momentum change of 2 units and parity change. It may then be said that on the tensor theory the decay of Co^{58} involves an angular momentum change of zero or one, with or without parity change.

If this interpretation of the relative probabilities of the modes of decay is correct, the shape of the positron spectrum of Co^{58} should be that predicted for an allowed transition. It seems difficult, although not impossible, to obtain sources of sufficient specific activity to verify this point.

The similarity between the modes of decay of Mn^{54} and Co^{58} is rather striking: In both cases the transformation of a proton leaves the product nucleus in a state with about 0.8-Mev excitation energy which is then given up in a single gamma-ray. It may be noted that the lowest known excited state of Fe^{56} also has an excitation energy of about 0.8 Mev (paper VI). The excitation energies of the three nuclei are Cr^{54} : 0.835 Mev, Fe^{56} : 0.845 Mev, Fe^{58} : 0.805 Mev (compare Fig. 9 of paper VI). The differences between these energies are known to about ± 0.005 Mev even though the absolute values may be in error by three times this amount.[10]

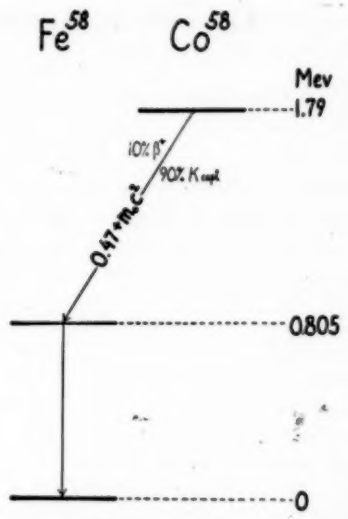

FIG. 5. Disintegration scheme of Co^{58}.

It may be recalled that Rosenblum and collaborators[11] found such similarities of energy level spacings in the case of several natural radioactivities. Another striking similarity exists in the case of Co^{59} (paper IV) and Ni^{60}.[8] The very similar isomeric states of the two stable species of silver,[12] the isomeric states of Br^{78}, of Br^{80}, and of Kr^{83},[12,13] the gamma-ray energies of about 0.05 Mev found in the 19-minute gallium,[13] and the 100-day arsenic[14] activities may be cited as further examples. Sufficient data are not yet available to decide whether these similarities between excitation energies are significant or fortuitous. A study of excited states of isobaric nuclei may shed further light on this question.

The authors wish to express their gratitude to Professor R. D. Evans for his continued interest, to Professor M. S. Livingston and the M.I.T. cyclotron crew for the bombardments, and to Professor J. W. Irvine, Jr., for help with the chemical procedures.

[10] B. R. Curtis, Phys. Rev. **55**, 1136 (1939), reported a gamma-ray of about 0.8 Mev from Co^{58}. A preliminary study of this activity in the spectrometer showed that the gamma-ray energy nearest to this value is 0.915 Mev.

[11] S. Rosenblum and M. Guillot, Comptes rendus **204**, 975 (1937).

[12] A. C. Helmholtz, Phys. Rev. **60**, 415 (1941).

[13] G. E. Valley and R. L. McCreary, Phys. Rev. **56**, 863 (1929).

[14] L. G. Elliott and M. Deutsch, Phys. Rev. **63**, 457 (1943).

PHYSICAL REVIEW VOLUME 65, NUMBERS 7 AND 8 APRIL 1 AND 15, 1944

Alpha-Helium Method for Determining Geological Ages

ROBLEY D. EVANS AND CLARK GOODMAN
Department of Physics, Massachusetts Institute of Technology, Cambridge, Massachusetts

(Received May 13, 1943)

New techniques for determining the rate of helium production in igneous rocks by direct counting of the alpha-rays, combined with the removal and measurement of the helium accumulated in a rock specimen during geologic time, provide a direct physical method of helium age analysis which is free from complicated chemical manipulation, makes possible more rapid measurement of the helium and radioactivity of terrestrial materials, and has only a second-order dependence upon radioactive standards. Equations are derived which relate the true rate of production of helium to the observed rate of alpha-particle emission from a thin source. Age relationships are derived which allow a simple, but accurate, correction to be applied to the approximate age in obtaining the true age of geologically old materials, in which the decay of the parent radioactive elements has been appreciable. Intercheck radioactivity measurements have established the mutual reliability of the alpha-count method and the radon-thoron method of determining the total radioactive content of rocks and ores and have shown that there are no unknown, strong, alpha-emitting, radioactive elements in ordinary terrestrial materials. The agreement between the "alpha-helium" and "radon-thoron-helium" ages on the same samples indicates that the accepted decay constants of the parent elements, thorium and uranium, are correct to within the experimental uncertainty of the measurements (±5 to 10 percent). The application of the alpha-helium method to igneous rocks has revealed that certain mineral constituents allow a significant amount of their radiogenic helium to escape during geologic time. For this reason the revised helium time scale is based on measurements of selected retentive minerals, magnetite being one of the most promising. As a by-product of these researches, the alpha-activity of 81 rock specimens has been found to range from 0.0 to 5.8 with an average of 1.23 alpha-rays per hour per milligram.

I. INTRODUCTION

THE rate of helium production in terrestrial materials can be calculated from the measured uranium and thorium contents,[1] if we assume radioactive equilibrium to obtain. The present paper describes a direct, physical method of determining this rate.[2] This method possesses the distinct advantage of being free from chemical manipulation and having only a second-order dependence upon standard radium or thorium solutions and on the decay constants of uranium, thorium, and actino-uranium.

The only known natural source of helium in rocks is from the alpha-particles emitted by radioactive sources.[3] The true rate of production of helium is given directly by the total rate of alpha-ray emission within a rock. It has already been shown[4] that such measurements are complicated by the small range of α-rays in these materials, and the variation of range for α-rays from different radioactive elements. For sources thick to α-rays, the conversion of the observed count to the true emission depends *directly* upon an accurate knowledge of the stopping power of the rock for alpha-rays, the proportion and ranges of the various α-rays emitted, and an experimental factor involving the minimum detectable range of an α-ray in the counting apparatus.[4] While each of these quantities is either known or can be measured within a probable error of about 10 percent, the combined corrections result in considerable uncertainty of measurement for thick sources. Although sources sufficiently thin to cause only a fractional absorption of even the shortest range α-rays give a somewhat lower counting rate than can be obtained from thick sources, the conversion of the observed count to the true emission involves only the above factors in terms of second-order importance. Consequently, considerable improvement in accuracy is obtained by the use of thin sources, and the present discussion is limited almost exclusively to such deposits, the preparation of which is described in Section IIC. Although these techniques have been applied specifically to terrestrial ma-

[1] W. D. Urry, J. Chem. Phys. **4**, 34–48 (1936); A. Holmes and F. A. Paneth, Proc. Roy. Soc. London **A154**, 385–412 (1936); N. B. Keevil, Trans. Roy. Soc. Can. **32**, 123–150 (1938).

[2] R. D. Evans and C. Goodman, Phys. Rev. **52**, 255A (1937); *ibid.* **53**, 916A (1938).

[3] The recently discovered stable isotope, He^3, in ordinary helium has a relative abundance of $<10^{-7}$, and its origin is not yet known. L. W. Alvarez and R. Cornog, Phys. Rev. **56**, 613 (1939).

[4] G. D. Finney and R. D. Evans, Phys. Rev. **48**, 503–511 (1935).

terials, the same methods and equations are applicable, with only minor modifications, to many other nuclear problems involving heavy particle counting.

II. INTERPRETATION OF OBSERVED COUNTING RATES IN TERMS OF THE RATE OF HELIUM PRODUCTION

A. Nomenclature

m = mass of source, in grams.
A = area of source, in cm².
R = mean range of an α-ray group, in air-cm, i.e., cm of dry air at 15°C and 760 mm Hg.
μ = ratio of the α-ray range μR in source to its range R in air.
d = density of the source in g/cm³.
τ = thickness of the source, in equivalent air-cm.
ρ = minimum residual α-ray range in air-cm which can be detected with certainty by the counting apparatus.
N = specific rate of production of α-rays having the mean range R air-cm; in α-rays per hour per gram of source.
N_U, N_A, N_T = rate of production of α-rays within the source, by the parent elements uranium I, actino-uranium, and thorium, respectively, each in α-rays per hour per gram of source.
n = observed α-ray emission from the source, due to α-rays having the mean range R, in α-rays per hour per gram of source.
n_U, n_A, n_T = total *observed* α-ray emission from the source, due to α-rays from the uranium, actino-uranium, and thorium series, respectively, each in observed alpha-counts per hour per gram of source.
a = thickness of a non-radioactive absorbing film covering the source, in equivalent air-cm.
F = fraction of total α-ray production due to uranium and actino-uranium series.

B. Thickness of Source

The α-ray activity of terrestrial materials is usually small, hence the source should contain as much material as possible. But the short range of α-rays results in excessive internal absorption in thick sources, leading to uncertainty in the estimation of the absolute emission in terms of the observed emission. Accordingly, the source must be sufficiently thick to give an easily measured α-ray activity, yet thin enough to allow the corrections for internal absorption to be made accurately. Finney and Evans[4] have derived these corrections in detail, and Fig. 2 of their paper shows that the observed counting rate is proportional to source thickness for extremely thin sources only. When the source is thicker than about one-sixth of the range of the α-ray in the source, the emission falls below linear proportionality with the source thickness, and approaches the constant value for thick sources. Thus the emission is governed by the α-ray range μR in the solid. This quantity varies with the type of mineral grain being traversed by the α-ray. For most rock constituents an uncertainty of about 5 percent exists in the knowledge of μ. Accordingly rather thin rock sources are used, in which μ enters as a small correction term only.

Expressed in air-cm, that is, in the number of cm of dry air at 15°C and 760 mm Hg which offers the same deceleration to the α-ray, the source thickness is

$$\tau = m/A\mu d. \qquad (1)$$

Direct measurements of μ are not practicable, but can be estimated from the atomic stopping power of the mineral constituents with the aid of the Bragg-Kleeman rule. Numerical values of μd for a number of the common mineral constituents of igneous rocks, and average values for various rock types are given in Table I.

In general, the sources contain 30 to 70 milligrams of rock, and cover an area of 44 cm². From Eq. (1) such sources are 0.4 to 1.0 air-cm thick. Thicker sources are used for feebly radioactive rocks, but 2.0 air-cm is never exceeded because at 2.15 air-cm the source is "thick" for uranium I α-rays, as seen in Table II.

C. Preparation of Source

Cut and polished thin sections, used for petrographic analysis, are unsuitable α-ray sources. Not only is the area small, but the section may easily fail to represent the average composition. Moreover, radon and thoron escape more easily from polished surfaces than from the dense and uniform films prepared by deposition of finely powdered samples. In the alpha-helium method alpha-ray counts and the helium determination

TABLE I. Values of μd calculated from chemical and mineral compositions, using the Bragg-Kleeman rule, $\mu d = d_a W_g^4 / W_a^4$, where d_a is the density of dry air, 0.001226 g/cm³ at 15°C and 760 mm Hg; W_g^4 is the sum of the atomic fraction times the square root of the atomic weight of each of the chemical constituents of the mineral grain; and $W_a^4 (= 3.84)$ is the similarly computed mean square root of the atomic weight for dry air.

Rock mineral	Average composition*	Calculated μd in 10^{-3} g/cm³
Quartz	SiO_2	1.48
Orthoclase	$KAlSi_3O_8$	1.54
Plagioclase	$NaAlSi_3O_8 + CaAl_2Si_2O_8$	1.51
Biotite	$(H_2, K)_2Fe_2Mg_2Al_2Si_3O_{24}$	1.67
Amphibole	$H_2NaCa_2(Mg, Fe)_4Al_2Si_6O_{24}$	1.72
Pyroxene	$Ca(Mg, Fe, Al)Si_2O_6$	1.73
Magnetite	$FeFe_2O_4$	2.08
Olivine	$(Mg, Fe)_2SiO_4$	1.88

Rock type	Assumed average mineral composition in percent	Average μd in 10^{-3} g/cm³
Granite	qtz. 30, ortho. 30, plag. 30, bio. 10	1.53
Syenite	qtz. 5, ortho. 35, plag. 40, amph. 20	1.56
Granodiorite	qtz. 15, ortho. 20, plag. 50, pyr. 5, amph. 5, bio. 5	1.54
Diorite	qtz. 4, ortho. 10, plag. 50, pyr. 20, amph. 15, mag. 1	1.59
Gabbro	plag. 55, pyr. 30, oliv. 10, mag. 5	1.64
Peridotite	amph. 50, oliv. 50	1.90
	Mean** (excluding peridotite) =	1.57

* A. N. Winchell, *Optical Mineralogy* (John Wiley & Sons, Inc., New York, 1933), Part II.
** The mean value is sufficiently accurate for most rocks. For other specimens, such as peridotites, meteorites, and magnetites, appropriate values of μd are used.

are made on separate portions of the rock. Care in sampling and quartering the specimen appears to overcome this possible source of error in substantially all cases. For most rocks two or more deposits of the same sample agree in activity within the range of probable error dictated by the statistical fluctuations in the α-ray emission. In the few cases where inhomogeneity is indicated, a number of measurements are made and the mean value is taken as representative within the probable error calculated from the squares of the residuals of the separate measurements.

The standard procedure adopted consists in (1) screening the coarsely broken sample into three portions, coarse (−10+30 mesh), medium (−30+60 mesh), and fine (−60 mesh), sufficient specimen being used to give about 25 grams of coarse portion; (2) determining the helium content of 5 to 10 grams of coarse; (3) powdering *ca.* 5 grams of a separate portion of the coarse; (4) grinding *ca.* 1 gram of this powdered material in an agate mortar under reagent ethyl alcohol to a grain size thin to α-rays (i.e., $\lesssim 15$ microns); and (5) depositing 30 to 70 mg of this rock powder in suspension on a previously weighted aluminum disk.

Deposition of the finely ground sample is performed by means of a very simple device. A thin rubber gasket containing a 7.5-cm diameter opening is placed over the aluminum disk which is supported by a flat, brass plate. A cylindrical brass cage, also 7.5-cm I.D., is placed on the

TABLE II. Mean range R in air at 15°C and 760 mm Hg for the α-ray emitters of the uranium, actino-uranium, and thorium series. Evaluation of the summations over $(R-\rho)^{-1}$ for each series [see Eqs. (3), (4), and (5)], using $\rho = 0.5$ air-cm. Here RaC, AcC′, and Ac are omitted because their small branching ratios (0.0004, 0.003, and 0.01, respectively) make their contribution to $\Sigma 1/(R-\rho)$ negligible. The individual contributions of ThC and ThC′ to $(R-\rho)^{-1}$ are weighted according to the branching ratio (0.34 for ThC, and 0.66 for ThC′).[a]

Uranium series	R	$R-\rho$	$(R-\rho)^{-1}$	Reference for R
U I	2.65	2.15	0.465	*b, c*
U II	3.21	2.71	0.369	*b, c*
Io	3.09	2.59	0.386	*d*
Ra	3.26	2.76	0.362	*d*
Rn	4.05	3.55	0.282	*b*
RaA	4.66	4.16	0.240	*b*
RaC′	6.91	6.41	0.156	*b*
RaF	3.84	3.34	0.300	*b*
$\Sigma^U 1/(R-\rho)$			2.560	

Actino-uranium series	R	$R-\rho$	$(R-\rho)^{-1}$	Reference for R
AcU	2.9	2.4	0.42	*c*
Pa	3.57	3.07	0.326	*d*
RdAc (Av.)	4.60	4.10	0.244	*e*
AcX (Av.)	4.29	3.79	0.264	*e*
An (Av.)	5.67	5.17	0.194	*b*
AcA	6.46	5.96	0.168	*b*
AcC (Av.)	5.36	4.86	0.206	*b, d*
$\Sigma^A 1/(R-\rho)$			1.822	

Thorium series	R	$R-\rho$	$(R-\rho)^{-1}$	Reference for R
Th	2.60	2.10	0.477	*f*
RdTh (Av.)	4.00	3.50	0.286	*e*
ThX	4.32	3.82	0.262	*e*
Tn	5.00	4.50	0.222	*b*
ThA	5.64	5.14	0.195	*b*
ThC (Av.)	4.73	4.23	0.080	*b*
ThC′	8.57	8.07	0.082	*b*
$\Sigma^T 1/(R-\rho)$			1.604	

[a] A. F. Kovarik and N. I. Adams, Jr., Phys. Rev. **54**, 413 (1938).
[b] M. G. Holloway and M. S. Livingston, Phys. Rev. **54**, 18 (1938).
[c] W. M. Rayton and T. R. Wilkins, Phys. Rev. **51**, 818 (1937).
[d] F. Rasetti, *Elements of Nuclear Physics* (Prentice-Hall, New York, 1936), pp. 116–7.
[e] G. D. Finney and R. D. Evans, Phys. Rev. **48**, 503 (1935).
[f] G. H. Henderson and G. C. Laurence, Phys. Rev. **52**, 46–47 (1937).

rubber gasket and held down by a 5-kg iron cylinder. Immediately after active stirring, about 10 cc of rock suspension is poured over the aluminum disk, which has been covered previously by a thin layer of alcohol. The alcohol is evaporated in an electrically heated balance case continuously flooded with radioactively dead nitrogen. The deposit adheres strongly to the source disk and, after being weighed and covered with a thin acetate film, described below, is placed in the ionization chamber in an inverted position without any loss of material. The fineness of grain size is checked microscopically. Deposition on glass plates affords a convenient means of observing the uniformity.

The emanating power of these rock deposits is negligibly low for most samples. However, since some sources show an appreciable escape of emanation, manifest by an increase in background following measurement, it is customary to cover each source with a radioactive-free cellulose film. In the measurement of the disintegration constant of thorium, Kovarik and Adams[5] used varnished films of celluloid, 0.2 to 0.3 air-cm thick, for this purpose. Acetate films prepared by the method of Harris and Johnson[6] are mechanically strong and have been found to be completely impervious to Rn and Tn when only 0.05 air-cm thick. A correction for α-ray absorption in the acetate film is included in the equations given below.

D. Efficiency of Counting

Alpha-rays emerge from the rock source into a parallel plate ionization chamber[7] 2 cm deep, filled with nitrogen flowing through at atmospheric pressure. The ion collecting (lower) electrode is 10 cm in diameter, and is surrounded at a distance of 1 mm by a guard ring 2.5 cm wide. Thus the field is essentially normal to the electrodes over the entire area. The source looks down into the ionization chamber through an 8.0-cm diameter opening in the 15-cm diameter upper electrode. Every α-ray emitted from the source must traverse a minimum distance of 1.5 cm before it can emerge from the collecting field. This assures an ionization pulse for every α-ray whose residual range, after its emission from the source, is sufficient to produce a detectable number of ions. The ionization pulses are amplified by a vacuum-tube electrometer, and the output pulses are recorded photographically on a rotating drum camera.[7]

The residual α-ray range corresponding to pulses of various sizes was determined by mounting an electrochemically deposited source of polonium on a calibrated screw so that its α-rays could enter the ionization chamber vertically through a 1-mm hole in the upper electrode. With suitable corrections for the temperature, pressure, and nature of the filling gas, histograms of the number of pulses of various amplitudes were made for two settings, at distances of 1.14 and 1.74 air-cm from the end of the mean range of the polonium α-rays. Using Holloway and Livingston's[8] ionization curve for an individual α-ray, and Kanne and Bearden's[9] data for the relative saturation of α-ray ionization in the collecting fields used, the number of ion pairs per mm of galvanometer deflection was determined from the maxima of the histogram distributions. Separate tests with known voltages applied directly to the grid of the electrometer tube confirmed the linearity of the amplifier response. From an examination of numerous photographic records, a deflection of 0.6 mm was selected as definitely countable and as still exhibiting the characteristic shape of the α-ray pulse. Calculations based on the polonium calibration and the ionization curve for single α-rays then gave $\rho = 0.5$ air-cm.

Where a multi-stage linear amplifier with a message register output is used for recording the α-ray pulses, the rejection of all α-rays whose residual range is less than a fixed value ρ can be accomplished by the grid bias on a thyratron in the output stage.

[5] A. F. Kovarik and N. I. Adams, Jr., Phys. Rev. **54**, 415 (1938).
[6] L. Harris and E. A. Johnson, Rev. Sci. Inst. **4**, 454 (1933).
[7] The ionization chamber used is that described by Finney and Evans (see reference 4). The amplifier has been rebuilt to use a modified Barth circuit [see Penick, Rev. Sci. Inst. **6**, 115–120 (1935)]. The rotating drum cameras are similar to that described by R. D. Evans, Rev. Sci. Inst. **6**, 99–112 (1935).
[8] M. G. Holloway and M. S. Livingston, Phys. Rev. **54**, 18–37 (1938).
[9] W. R. Kanne and J. A. Bearden, Phys. Rev. **50**, 935–938 (1936).

E. Absorption within the Source

An α-ray source whose thickness $\tau \lesssim (R-\rho-a)$, emits[10] a total of

$$n=(N/2)\{1-(\tau+2a)/2(R-\rho)\} \qquad (2)$$

α-rays per gram per hour having a residual range $\gtrsim \rho$, when N α-rays of range R are produced in it per gram per hour, and the source is covered by a protecting film a air-cm thick.

Within each of the three independent radioactive series, the activity of each α-emitter is equal to the activity of its parent, assuming radioactive equilibrium is present. During its disintegration into lead, each initial atom of uranium I eventually produces 8 α-rays, each initial actino-uranium atom 7 α-rays, and each initial thorium atom 6 α-rays. Thus the summations over the three series are:

$$n_U=\sum^U (N_U/2)\{1-(\tau+2a)/2(R-\rho)\}$$
$$=(N_U/2)\{8-(1/2)(\tau+2a)\sum^U 1/(R-\rho)\}, \quad (3)$$
$$n_A=(N_A/2)\{7-(1/2)(\tau+2a)\sum^A 1/(R-\rho)\}, \quad (4)$$
$$n_T=(N_T/2)\{6-(1/2)(\tau+2a)\sum^T 1/(R-\rho)\}. \quad (5)$$

The summations in Eqs. (3)–(5) may be evaluated numerically, as in Table II. Substituting these numerical values, solving for the α-ray production of each series, and expanding in power series, we obtain:

$$8N_U=\frac{2n_U}{1-0.160(\tau+2a)}$$
$$=2n_U\{1+0.160(\tau+2a)$$
$$+0.026(\tau+2a)^2+\cdots\}, \quad (6)$$
$$7N_A=\frac{2n_A}{1-0.130(\tau+2a)}$$
$$=2n_A\{1+0.130(\tau+2a)$$
$$+0.017(\tau+2a)^2+\cdots\}, \quad (7)$$
$$6N_T=\frac{2n_T}{1-0.134(\tau+2a)}$$
$$=2n_T\{1+0.134(\tau+2a)$$
$$+0.018(\tau+2a)^2+\cdots\}. \quad (8)$$

[10] Equation (2) follows immediately from Eq. (4) of Finney and Evans (see reference 4).

Adding Eqs. (6)–(8), we obtain the total rate of production $(8N_U+7N_A+6N_T)$ of α-rays, or helium, within the sample. Factoring the right-hand side, we can express the resulting equation in terms of the observed α-ray counting rate $(n_U+n_A+n_T)$ and correction terms, as follows:

$$(8N_U+7N_A+6N_T)=2(n_U+n_A+n_T)$$
$$\times\left\{1+\frac{(\tau+2a)(0.160n_U+0.130n_A+0.134n_T)}{(n_U+n_A+n_T)}\right.$$
$$+\frac{(\tau+2a)^2(0.026n_U+0.017n_A+0.018n_T)}{(n_U+n_A+n_T)}$$
$$\left.+\cdots\right\}. \quad (9)$$

The correction terms contain ratios of the type $n_U/(n_U+n_A+n_T)$. These represent the fraction of the *observed* α-rays which are due to each of the three radioactive series. Expressions for each of these ratios can be written by substitution from Eqs. (6)–(8). If these are carried through the algebraic steps below, and compared in the final Eq. (16), with $\tau=2$ air-cm, it can be shown numerically that an error of less than 0.1 percent is made in Eq. (16) below by equating these ratios of observed α-rays to the corresponding ratios of α-rays *produced* within the source. Physically, this is because the average internal absorption for α-rays from the uranium series is only slightly greater than for α-rays from the thorium and actino-uranium series. In Eq. (9), we shall write, therefore:

$$\frac{n_U}{n_U+n_A+n_T}=\frac{8N_U}{8N_U+7N_A+6N_T} \qquad (10)$$

with similar expressions for the ratios involving n_A and n_T in the numerator.

The condensation of Eq. (9) into a simpler, practical expression is facilitated by expressing the ratios of Eq. (10) in terms of a single parameter. Let F be the fraction of the total α-rays produced in the source which are due to the uranium and actino-uranium series. Then $(1-F)$ is the fraction due to the thorium series. In all known terrestrial materials, the ratio of the uranium isotopes is such that about 4 α-rays

from actino-uranium are associated with 100 α-rays from uranium I. According to Nier[11]

$$N_A=(0.046\pm0.002)N_U. \quad (11)$$

Combining Eqs. (10) and (11) with the definition of F we have:

$$F=\frac{8N_U+7N_A}{8N_U+7N_A+6N_T}=\frac{8.32N_U}{8N_U+7N_A+6N_T}, \quad (12)$$

$$\frac{n_U}{n_U+n_A+n_T}=\frac{8N_U}{8N_U+7N_A+6N_T}=0.96F, \quad (13)$$

$$\frac{n_A}{n_U+n_A+n_T}=\frac{7N_A}{8N_U+7N_A+6N_T}=0.04F, \quad (14)$$

$$\frac{n_T}{n_U+n_A+n_T}=\frac{6N_T}{8N_U+7N_A+6N_T}=1-F. \quad (15)$$

Combining Eqs. (9), (13)–(15), we obtain

$$(8N_U+7N_A+6N_T)=2(n_U+n_A+n_T)\times\{1+(\tau+2a)(0.134+0.025F)+(\tau+2a)^2(0.018+0.007F)+\cdots\}, \quad (16)$$

which is the final equation relating the true rate of production of helium $(8N_U+7N_A+6N_T)$ to the observed rate of emission of α-rays $(n_U+n_A+n_T)$ from a source τ air-cm thick, covered by an absorber a air-cm thick. Figure 1 is a plot of Eq. (16) for all source thicknesses up to 2 air-cm, and for the limiting and intermediate values of F, employing terms in Eq. (16) through $(\tau+2a)^3$.

For most rocks, accurate knowledge of the relative uranium and thorium activity is unnecessary because F appears in a small correction term only. Thus from Fig. 1, a maximum uncertainty of 1.5 percent is introduced by assuming $F=0.5$, for a source 1 air-cm thick. Most sources are thinner than this, and the great majority of igneous rocks have fractional uranium activities between $F=0.2$ and 0.8, with an average value of about $F=0.5$. When experimental knowledge of F is desirable, it can be determined by analysis of the rock for radium, by the usual emanation technique.[12] Thus from the results of previous work,[13]

$$F=\frac{1.04\ \text{Ra}}{1.04\ \text{Ra}+0.0886\ \text{Th}}=\frac{1040\ \text{Ra}}{8N_U+7N_A+6N_T}, \quad (17)$$

in which Ra is the measured radium content of the rock in 10^{-12} gram per gram of rock, Th is the measured thorium content in 10^{-6} gram per gram of rock, the "activity index" (1.04 Ra +0.0886 Th) is the calculated rate of production of α-rays per milligram of rock per hour, and $(8N_U+7N_A+6N_T)$ is the total rate of production of helium in α-rays per gram per hour as determined from direct α-ray counts with the aid of Eq. (16) or Fig. 1.

Substitution of the appropriate atomic weights and decay constants (see Section III) in Eq. (13) serves to connect F and Th/U, the relative mass concentrations of thorium and uranium in the specimen. This relationship is plotted in Fig. 2, from which the Th/U ratio may be read directly following the determination of F by means of radon and α-ray observations, using Eq. (17). A Th/U ratio of 4.13 corresponds to $F=0.5$, that is, to an equal α-ray contribution from the uranium plus actino-uranium and from the thorium series.[14]

F. Background

With no source in the ionization chamber, the α-ray counting rate is between 10 and 15 α-rays per hour. These α-rays are due to the unavoidable radioactive content of the brass walls of the chamber. Lining the chamber with inserts of sheet electrolytic copper does not reduce this background appreciably, as the effect is due to a volume contamination equivalent to about 4×10^{-14} g Ra per g, rather than surface contamination, in both cases. The metal surfaces are cleaned occasionally with redistilled concentrated nitric acid, and with fine sandpaper. Considering the large area exposed in the chamber, the background is less than 2 α-rays per cm^2 per day.

[11] A. O. Nier, Phys. Rev. **55**, 150–163 (1939); **60**, 112–116 (1941).
[12] R. D. Evans, Rev. Sci. Inst. **6**, 99 (1935).
[13] R. D. Evans, C. Goodman, N. B. Keevil, A. C. Lane, and W. D. Urry, Phys. Rev. **55**, 931 (1939); see Table VI, p. 939.
[14] The value Th/U = 3.7 for this condition, given on p. 932 of reference 13, is superseded by the present value.

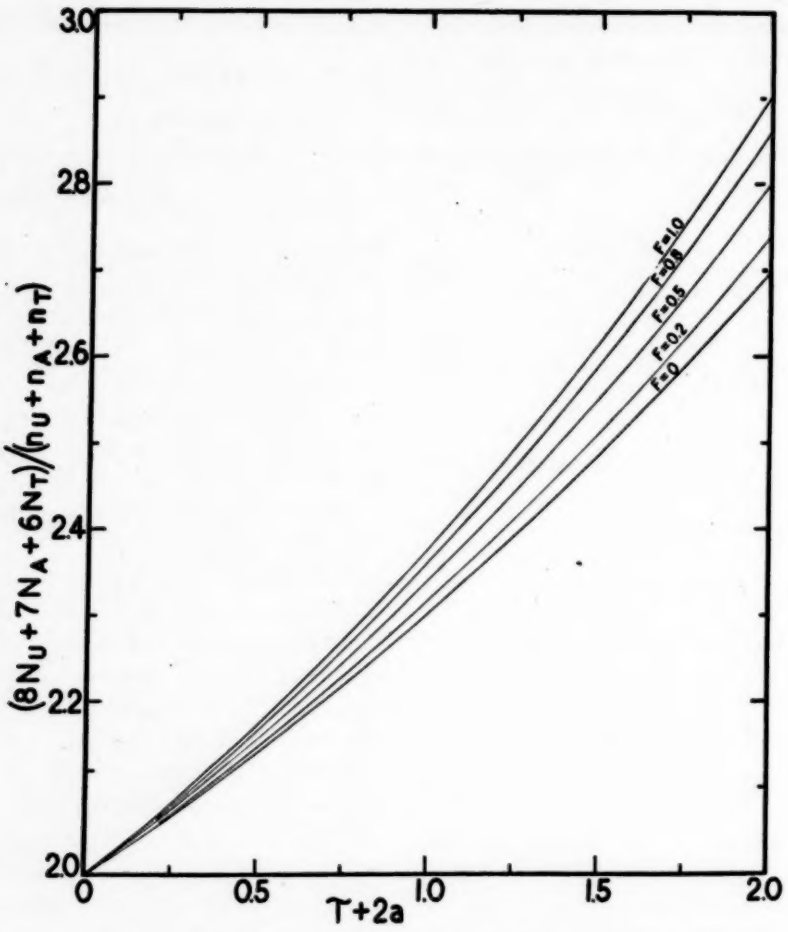

FIG. 1. Graphical relationship between the thickness of the source plus absorber and the ratio of true to observed rate of alpha-emission. For an infinitely thin source and no absorber ($\tau+2a=0$), the true rate of alpha-emission is exactly twice the observed count, because half the α-rays are absorbed in the aluminum source mount. As the source thickness τ and the absorber thickness a (both in air-cm) increases, the ratio, $(8N_U+7N_A+6N_T)/(n_U+n_A+n_T)$, increases in accord with Eq. (16). This equation also involves the fraction F of the total α-rays produced in the source due to the uranium and actino-uranium series. The family of curves shown covers the range of all possible values of F, from 0 to 1.0. In practice $\tau+2a$ is determined from the weight of the source and absorber; F is determined from the observed alpha-count and a separate radium determination.

Between 3 and 5 of the background α-rays per hour come from the aluminum source disk. Disks of brass, copper, iron, and silver have also been tried, but all showed greater contamination than aluminum. The contribution to the background for each disk is determined by observing the decrease in the total background when the disk is covered with a thick deposit ($\gtrsim 4$ milligrams per cm^2) of radioactively inert material. Chemically pure sodium carbonate is generally suitable for this purpose. However, two unusual rock specimens, one a hornblende-hypersthene-diorite and the other a dunite, have been found to have no detectable activity and thus are useful in background studies. They also afford a convenient control measurement of contamination effects in the preparation of the sources. The dunite has been prepared as one of twelve standard rock samples[15] by the Committee on Standards of Radioactivity of the National Research Council and can be obtained from the National Bureau of Standards.

Because of the absorption of the α-rays from

[15] L. F. Curtiss, C. Goodman, A. F. Kovarik, S. C. Lind, C. S. Piggot, and R. D. Evans, Am. J. Sci. **238**, 602–603 (1940).

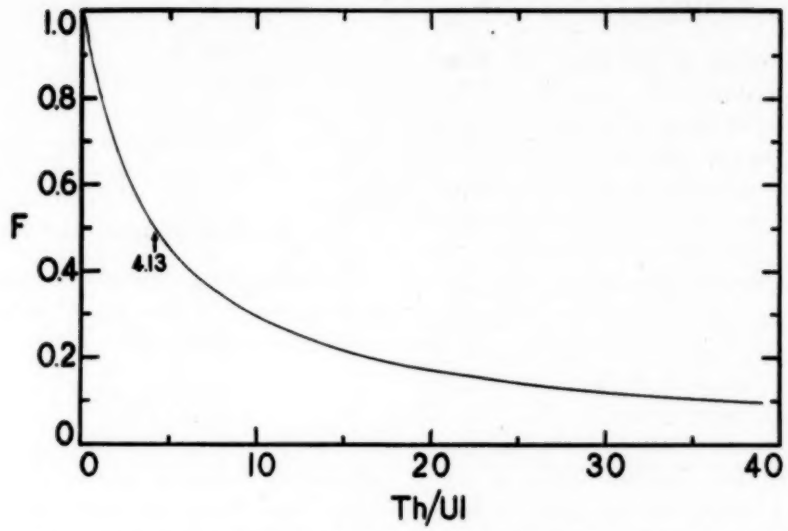

FIG. 2. Relationship between the thorium-uranium ratio, Th/U, and F, the fraction of the total α-rays produced in the source which are due to the uranium and actino-uranium series. At a Th/U ratio of 4.13, the rate of production of helium by the thorium series equals that for the uranium plus actino-uranium series.

the source disk by the rock deposit, there is a small decrease in the effective background when the source is in place. The fractional transmission of the α-rays from the thorium series and from the uranium plus actino-uranium series, as a function of the thickness of the source τ and its acetate film a, is obtained directly by reference to Fig. 3 of Finney and Evans.[4] For example, if $\tau=1$ air-cm and $a=0.07$ air-cm, only 50 percent of the disk background will be transmitted. This correction becomes significant only when the radioactivity of the rock source is unusually small.

G. Samarium

Comparative measurements reported in a previous paper[13] indicate that the α-ray activity of igneous rocks is usually completely accounted for by the radioactive substances known to be members of the uranium, actino-uranium, and thorium series. The only other natural α-ray emitter now known is samarium. Present observations indicate that 1 gram of samarium emits about 150 α-rays per second,[16] all of which appear to be due to the isotope of mass 148,[17] and to have a range[16,18] of 1.28 ± 0.05 air-cm. Thus on a gram-for-gram basis, samarium is 1.2 percent as active as U I.

A limited number of analyses indicate an average content of 10^{-5} g Sm/g rock.[19] At this abundance the Sm α-ray production is only about 0.4 percent of that from the uranium series in an average granite[20] (containing 1.4×10^{-12} g Ra/g). Hence, in most rocks the helium contributed by Sm is negligible compared with that from the other radioactive elements. It is possible, however, that Sm may be an important factor in unusual cases. Fortunately, the Sm α-activity can always be obtained by comparing the activity of two sources of different thicknesses, say 0.8 and 1.6 air-cm. The Sm α-rays from these sources will be equal, since for $\rho=0.5$ both are "thick" for the 1.28 air-cm α-rays, while the uranium, actino-uranium, and thorium series activity will nearly double in the thicker source, since both sources are thin for α-rays of greater than 2.1-air-cm range.

[16] W. F. Libby, Phys. Rev. **46**, 196–204 (1934).
[17] T. R. Wilkins and A. J. Dempster, Phys. Rev. **54**, 315A (1938).
[18] D. Lyford and J. A. Bearden, Phys. Rev. **45**, 743A (1934).
[19] G. Von Hevesy, *Chemical Analysis by X-Rays and Its Applications* (McGraw-Hill Book Company, Inc., New York, 1932), p. 265, and Table LVII.
[20] R. D. Evans and C. Goodman, Bull. Geol. Soc. Am. **52**, 476 (1941), Table XI. R. D. Evans, C. Goodman, and N. B. Keevil, "Radioactivity: The earth's heat and geological age measurements," *Handbook of Physical Constants* (Geological Society of America, Special Paper No. 36, 1942), edited by Francis Birch, Section 18, pp. 267–277.

H. Statistical Fluctuations

Background observations are taken for about 10 hours before and after each rock run, and the rock runs are usually of 10 to 20 hours' duration. The probable error in the observed counting rate depends upon the total number of counts taken, hence, on both the duration of the observations and on the activity of the rock. However, the fluctuations are slightly greater than those predicted by the Poisson distribution law,[21] because all α-counts are not randomly distributed in time.[22] For example, an α-ray from thorium A is dependent upon the prior emission of an α-ray from the thoron atom which is its immediate parent. Accordingly, the probable error of each observation should be computed directly from the squares of the residuals.[23] The probable errors calculated from α-ray counts grouped into 1-hour observations are 1.07 times the Poisson value. This is based on a study of 466 hours of records.

Average granites give observable counting rates of about one α-ray. per milligram per hour, or 50 α-rays per hour in addition to the background of about 15 α-rays per hour. The statistical uncertainty in the observations is usually from 3 to 6 percent.

III. THE ALPHA-HELIUM AGE EQUATIONS

A. Nomenclature and Constants

This section employs the same nomenclature as the preceding sections, and in addition:

U, A, T, H = atoms of uranium I, actino-uranium, thorium, and helium per gram of specimen.

H_U, H_A, H_T = atoms of helium per gram of specimen, originating from the uranium, actino-uranium, and thorium series.

He = total helium per gram of specimen, measured in 10^{-5} cc at 0°C and 76 cm Hg; $=H/2.69\times10^{14}$.

t = helium age of the specimen, in 10^9 years.

t_0 = approximate helium age of the specimen, in 10^9 years.

$\lambda_U = 0.1525$ per 10^9 years, the decay constant[11,24] of uranium I.

$\lambda_A = 0.98$ per 10^9 years, the decay constant[11] of actino-uranium.

$\lambda_T = 0.0498$ per 10^9 years, the decay constant[5] of thorium.

N_U', N_A', N_T' = same as N_U, N_A, N_T, except in α-rays per 10^9 years per gram of source.

B. Derivation of Age Equations

If there were U_0 atoms of uranium I per gram of specimen at a time $t=0$, then the number remaining at a later time t is

$$U = U_0 \exp(-\lambda_U t). \tag{18}$$

Hence, $(U_0 - U)$ atoms have decayed. Since each produces 8 atoms of helium during its complete decay into lead, the number of helium atoms formed is

$$H_U = 8(U_0 - U) = 8U[\exp(\lambda_U t) - 1]. \tag{19}$$

Similar equations for the actino-uranium and thorium series involve 7 and 6 atoms of helium, respectively. We now expand Eq. (19) and its analogs for the actino-uranium and thorium series, obtaining:

$$H_U = 8U[\exp(\lambda_U t) - 1] = 8U\lambda_U t + 8U\lambda_U{}^2 t^2/2 + 8U\lambda_U{}^3 t^3/6 + \cdots, \tag{20}$$

$$H_A = 7A[\exp(\lambda_A t) - 1] = 7A\lambda_A t + 7A\lambda_A{}^2 t^2/2 + 7A\lambda_A{}^3 t^3/6 + \cdots, \tag{21}$$

$$H_T = 6T[\exp(\lambda_T t) - 1] = 6T\lambda_T t + 6T\lambda_T{}^2 t^2/2 + 6T\lambda_T{}^3 t^3/6 + \cdots. \tag{22}$$

From elementary radioactive principles $N_U' = U\lambda_U$; $N_A' = A\lambda_A$; and $N_T' = T\lambda_T$. Making these substitutions, and adding Eqs. (20)–(22), we obtain the total helium produced in the specimen:

$$\begin{aligned} H &= H_U + H_A + H_T \\ &= t(8N_U' + 7N_A' + 6N_T') \\ &\quad + t^2(8N_U'\lambda_U/2 + 7N_A'\lambda_A/2 + 6N_T'\lambda_T/2) \\ &\quad + t^3(8N_U'\lambda_U{}^2/6 + 7N_A'\lambda_A{}^2/6 \\ &\quad + 6N_T'\lambda_T{}^2/6) + t^4(8N_U'\lambda_U{}^3/24 \\ &\quad + 7N_A'\lambda_A{}^3/24 + 6N_T'\lambda_T{}^3/24) \\ &\quad + t^5(8N_U'\lambda_U{}^4/120 + 7N_A'\lambda_A{}^4/120 \\ &\quad + 6N_T'\lambda_T{}^4/120) + \cdots. \end{aligned} \tag{23}$$

[21] R. D. Evans and H. V. Neher, Phys. Rev. **45**, 144–151 (1934).
[22] N. I. Adams, Jr., Phys. Rev. **44**, 651–653 (1933).
[23] See, e.g., Eq. (5), reference 21.
[24] A. F. Kovarik and N. I. Adams, Jr., Phys. Rev. **40**, 718 (1932); J. App. Phys. **12**, 296 (1941).

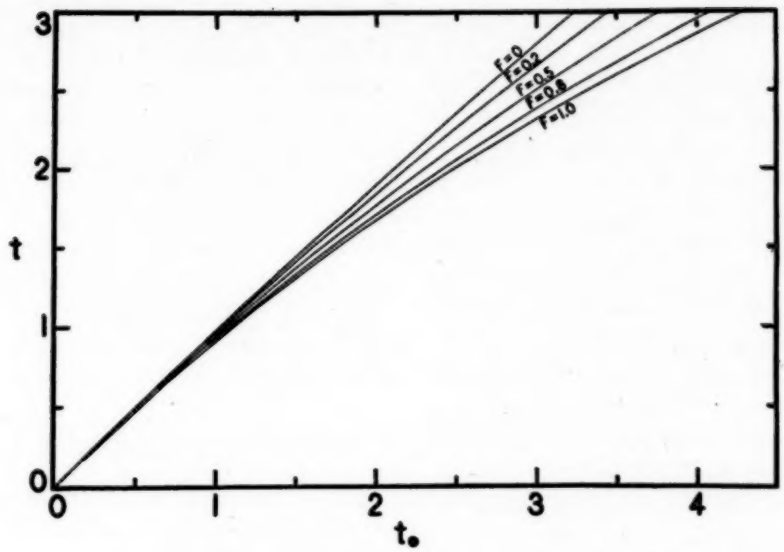

FIG. 3. Relationship between the true age t and the approximate age t_0 both in billions (10^9) of years. The family of curves represents a plot of Eq. (26) for the limiting and intermediate values of F. It is of interest to note that for ages $\leqslant 1$ billion years ($t=1$), a maximum error in t of 5 percent results from the assumption that $F=0.5$ instead of using a more accurate value obtained from a radium determination.

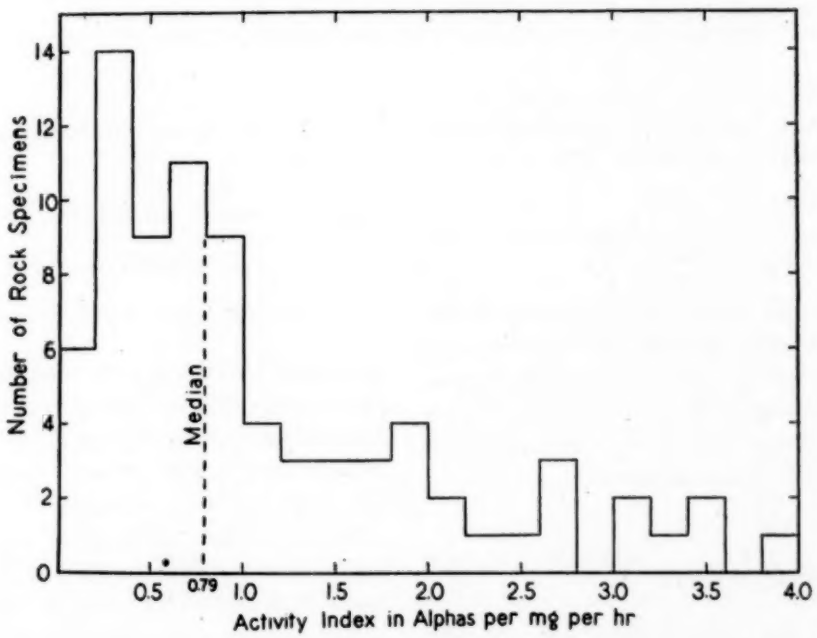

FIG. 4. Distribution histogram of the total alpha-ray activity, in alpha-rays per hour per mg of rock, in 81 rock samples of many lithologic types. The interval width is 0.2 α/hr. mg. Of the 81 samples, two (a granite and a lava) have activities between 5.6 and 5.8 α/hr. mg, and are not shown. The numerical parameters of this distribution are: *average* of all 81 samples, 1.23 α/hr. mg; *modal* (i.e., most probable) activity 0.3 ± 0.1 α/hr. mg; *median* (40 samples have greater activities, 40 samples have smaller activities) activity 0.79 α/hr. mg.

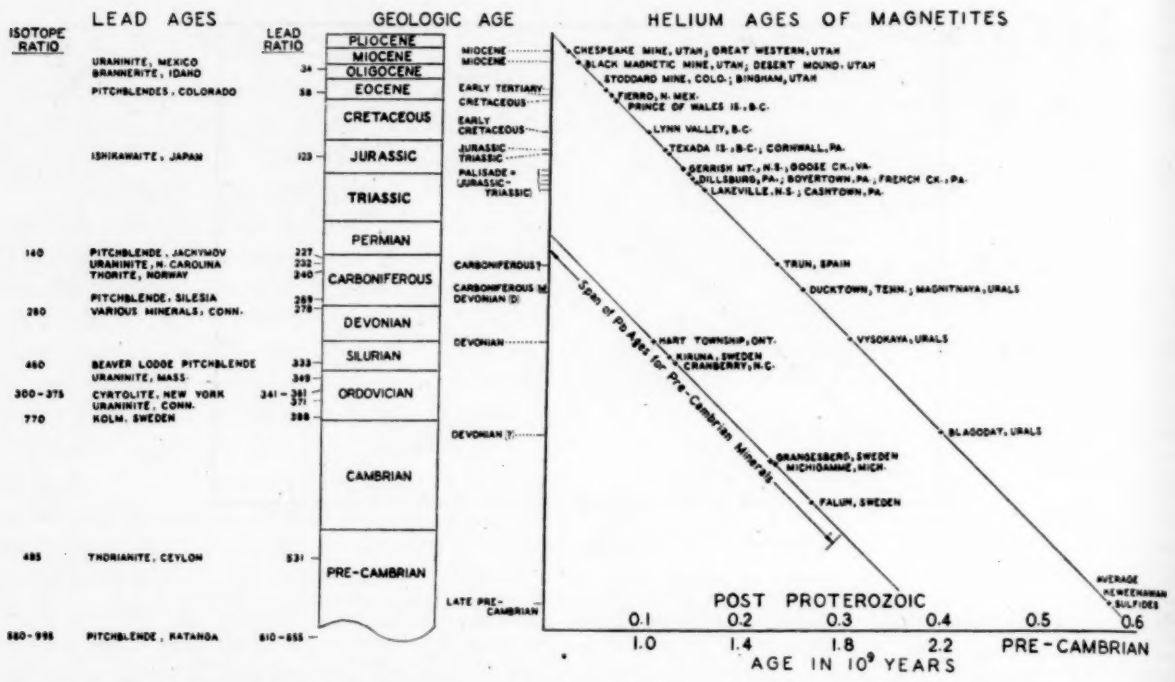

FIG. 5. Geologic time scale based on radioactive methods. The sequence of geologic periods is derived from paleontologic evidence while the quantitative estimates are based largely on the lead ratios of radioactive minerals. With the exception of the Blagodat specimen, which is a questionable Devonian, the helium ages of post Proterozoic magnetites and sulfides (reference 26), shown on the upper scale of abscissas, are in agreement with the limited number of lead ratio ages. The isotope ratio, based on the systematic variation of AcD/RaG with time, in some instances is quite different from the lead ratio on the same mineral (see Nier, reference 11). However, more consistent agreement between the two lead methods is observed for older minerals. Because of the uncertainty in the geologic ages, comparisons between the helium and lead methods have not been made for the earlier pre-Cambrian minerals although both methods show ages ranging up to about 1.7×10^9 years.

The approximate helium age t_0 is obtained by taking the first term only in Eq. (23), that is:

$$t_0=\frac{H}{(8N_U'+7N_A'+6N_T')}\text{ billion years.} \quad (24)$$

This is the quantity which is obtained from the quotient of the observed helium content and α-ray activity of a specimen. Substituting 6.023×10^{23} for Avogadro's number, 22,410 cc for the molecular volume, and 8.766×10^{12} hours per 10^9 years, Eq. (24) takes the form:

$$t_0=30.7\frac{\text{He}}{(8N_U+7N_A+6N_T)}\text{ billion years.} \quad (25)$$

Returning to the general Eq. (23), we now convert it into a usable form by substituting the numerical values of the decay constants given at the beginning of this section, the activity ratio $N_A'=0.046N_U'$ as given in Eq. (11), the fractional uranium activity F as defined by Eqs. (12) to (15), and the approximate age t_0 from Eq. (24), obtaining:

$$t_0/t=1+t(0.0249+0.0675F)+t^2(0.000414+0.00952F)+t^3(0.00166F)+t^4(0.000302F)+\cdots. \quad (26)$$

Equation (26) is the final complete age equation, expressing the relationship between the true age t and the approximate age t_0, obtained from the helium and α-ray observations by means of Eq. (25), for all values of F. Note that for a specimen whose age is small compared with 10^9 years ($t=1$), the true age is given by t_0, and knowledge of the fractional α-ray activity due to uranium [Eq. (17)] is unnecessary. While t can always be obtained from Eq. (26) by successive approximations beginning with t_0, it is much more convenient to use Fig. 3 which is a plot of Eq. (26) for the limiting and intermediate values of F.

The physical interpretation of the terms in Eq. (26) is of interest. The numerical terms represent corrections due to the finite diminution of the parent substances during geological time. When $F=1$, the numerical values reflect the decay of uranium I and actino-uranium. For the term in t^2, about $\frac{2}{3}$ of the correction is due to actino-uranium, while for the higher terms the correction is almost exclusively for actino-uranium. When $F=0$, the numerical values reflect the decay of thorium, their small values being due to the very great half-period of thorium.

IV. RESULTS

Earlier papers[13, 20, 25] have reported in detail seventy-six helium measurements and one hundred and thirty-one alpha-activity determinations, largely using the foregoing techniques. As stated in these papers, the analytical reliability is clearly established. Because of a number of geologic uncertainties, however, the significance of the age values obtained on unseparated igneous rocks is not yet clear.[25, 26] The distribution of helium in rocks has been summarized in a separate paper.[27] A histogram of the observed alpha-activities of 81 rock specimens is presented in Fig. 4.

With few exceptions it has been established[26] that helium ages obtained on rocks can represent only minimal values. Certain common rock minerals, notably the feldspars, appear to lose a large fraction of their radiogenic helium. Thus, all helium ages on rocks as a whole represent mean values dependent upon the proportion and helium retentivity of the mineral components. Some minerals certain metallic sulfides and magnetite[26] in particular, have a much greater retentivity, and show helium ages which approach and may even exceed the lead ages obtained on radioactive minerals from corresponding geologic horizons. Individual helium ages cover the same range of values as lead ages, i.e., from 15 million years for tertiary rocks to 1650 million years ($t=1.65$) for early pre-Cambrian. A graphical tabulation of these results is presented in Fig. 5.

V. ACKNOWLEDGMENTS

The authors appreciate the support of this research given by the Geological Society of America through grants-in-aid to Professors A. C. Lane and W. J. Mead.

[25] C. Goodman and R. D. Evans, Bull. Geol. Soc. Am. **52**, 491–544 (1941).

[26] P. M. Hurley and C. Goodman, Bull. Geol. Soc. Am. **52**, 545–560 (1941); **54**, 305–324 (1943).

[27] C. Goodman and R. D. Evans, Rev. Sci. Inst. (in press).

PHYSICAL REVIEW VOLUME 65, NUMBERS 7 AND 8 APRIL 1 AND 15, 1944

A Generalized Electrodynamics

Part II—Quantum

BORIS PODOLSKY AND CHIHIRO KIKUCHI*
Department of Physics, University of Cincinnati, Cincinnati, Ohio

(Received January 20, 1944)

When the Lagrangian from which the field equations are derived contains second and higher derivatives of the generalized field coordinates, the method of quantizing the field equations developed by Heisenberg and Pauli cannot be immediately applied. By generalizing a method due to Ostrogradsky for converting Lagrange's equations of motion of a particle, when higher derivatives are present, into canonical Hamiltonian form, it becomes possible to perform a similar transformation of the field equations. Applying this method to Podolsky's generalized electrodynamics, we obtain the Hamiltonian of the field and double the usual number of generalized coordinates and momenta. The quantization of the field follows without any special assumptions. The last two sections are devoted to the discussion of the auxiliary conditions and some of their consequences.

1. PRELIMINARIES. EXTENSION OF HEISENBERG AND PAULI'S[1] METHOD

THE basis of generalizing the Heisenberg and Pauli method of quantizing fields to the case when the Lagrangian of the field contains second derivatives of the potentials is contained in a suggestion due to Ostrogradsky.[2] He showed how the Lagrange equations of motion of a particle, when higher derivatives are present, can be transformed into the Hamiltonian form.

Suppose the Lagrangian L is a function of the potentials $\varphi_\alpha=(\mathbf{A}, i\varphi)$ as well as their first and second derivatives:[3]

$$L=L(\varphi_\alpha,\ \varphi_{\alpha,\beta},\ \varphi_{\alpha,\beta\gamma}),$$

where φ_α are functions of the space-time coordinates $x_\alpha=(x_1, x_2, x_3, x_4=ix_0=ict)$, and

$$\varphi_{\alpha,\beta}=\partial\varphi_\alpha/\partial x_\beta,\quad \varphi_{\alpha,\beta\gamma}=\partial^2\varphi_\alpha/\partial x_\beta\partial x_\gamma.$$

The variational equation

$$\delta W=\delta\int\int L\,dV\,dt=0,\quad dV=dx_1dx_2dx_3,$$

or

$$ic\delta W=\delta\int L\,d\Omega=0,\quad d\Omega=dV\,dx_4, \tag{1.1}$$

leads to the field equation

$$\frac{\partial L}{\partial\varphi_\alpha}-\frac{\partial}{\partial x_\mu}\frac{\partial L}{\partial\varphi_{\alpha,\mu}}+\frac{\partial^2}{\partial x_\mu\partial x_\nu}\frac{\partial L}{\partial\varphi_{\alpha,\mu\nu}}=0, \tag{1.2}$$

provided φ_α and $\varphi_{\alpha,\mu}$ are specified and are unvaried over the boundaries of the four-dimensional manifold Ω over which the integration is performed.

We introduce as the new generalized coordinates

$$q_\alpha=\varphi_\alpha,\quad \text{and}\quad Q_\alpha=\partial\varphi_\alpha/\partial t\equiv\dot{q}_\alpha, \tag{1.3}$$

and define the momenta conjugate to q_α and Q_α by

$$p_\alpha=(\partial L/\partial\dot{q}_\alpha)-\partial/\partial t(\partial L/\partial\ddot{q}_\alpha)-\partial/\partial x_i(\partial L/\partial\dot{q}_{\alpha,i}) \tag{1.4}$$

and

$$P_\alpha=\partial L/\partial\ddot{q}_\alpha, \tag{1.5}$$

respectively. The Hamiltonian is then conveniently defined by

$$H=-L+p_\alpha\dot{q}_\alpha+P_\alpha\dot{Q}_\alpha. \tag{1.6}$$

The time derivatives of the coordinates, $\dot{q}_\alpha$ and $\dot{Q}_\alpha$, can in general be eliminated from the Hamiltonian by using Eqs. (1.3) and (1.5). The result is

$$H=H(q_\alpha, p_\alpha, q_{\alpha,i}, q_{\alpha,ij}, Q_\alpha, P_\alpha, Q_{\alpha,i}). \tag{1.7}$$

Taking the differentials of Eqs. (1.6) and (1.7)

* Now at Haverford College, Haverford, Pennsylvania.
[1] W. Heisenberg and W. Pauli, Zeits. f. Physik **56**, 1 (1929).
[2] See E. T. Whittaker, *Analytical Dynamics* (1927), Chapter X.
[3] Greek indices will range from 1 to 4, while Latin subscripts from 1 to 3. Repeated indices are summed.

and equating coefficients we obtain:

$$\begin{aligned} \partial H/\partial Q_\alpha &= -\partial L/\partial \dot{q}_\alpha + p_\alpha, \\ \partial H/\partial q_{\alpha,i} &= -\partial L/\partial q_{\alpha,i}, \\ \partial H/\partial q_{\alpha,ij} &= -\partial L/\partial q_{\alpha,ij}, \\ \partial H/\partial Q_{\alpha,i} &= -\partial L/\partial \dot{q}_{\alpha,i}, \end{aligned} \tag{1.8}$$

and

$$\partial H/\partial p_\alpha = Q_\alpha = \dot{q}_\alpha. \quad \partial H/\partial P_\alpha = \dot{Q}_\alpha = \ddot{q}_\alpha. \tag{1.9}$$

From Eqs. (1.4), (1.5), (1.8), (1.9), and (1.2) it now follows that

$$\partial H/\partial Q_\alpha = -\partial P_\alpha/\partial t - \partial/\partial x_i(\partial L/\partial \dot{q}_{\alpha,i}), \tag{1.10}$$

$$\partial p_\alpha/\partial t = -\partial H/\partial q_\alpha + \partial/\partial x_i(\partial H/\partial q_{\alpha,i}) - \partial^2/\partial x_i \partial x_j(\partial H/\partial q_{\alpha,ij}), \tag{1.11}$$

$$\partial P_\alpha/\partial t = -\partial H/\partial Q_\alpha + \partial/\partial x_i(\partial H/\partial Q_{\alpha,i}). \tag{1.12}$$

But, if we put

$$\begin{aligned} \delta \int H dV \equiv \delta \bar{H} = \int \{ &(\delta \bar{H}/\delta q_\alpha)\delta q_\alpha \\ &+ (\delta \bar{H}/\delta Q_\alpha)\delta Q_\alpha + (\delta \bar{H}/\delta p_\alpha)\delta p_\alpha \\ &+ (\delta \bar{H}/\delta P_\alpha)\delta P_\alpha \} dV, \end{aligned} \tag{1.13}$$

the quantities

$$\delta \bar{H}/\delta q_\alpha = \partial H/\partial q_\alpha - \partial/\partial x_i(\partial H/\partial q_{\alpha,i}) + \partial^2/\partial x_i \partial x_j(\partial H/\partial q_{\alpha,ij}), \tag{1.14}$$

$$\delta \bar{H}/\delta Q_\alpha = \partial H/\partial Q_\alpha - \partial/\partial x_i(\partial H/\partial Q_{\alpha,i}), \tag{1.15}$$

$$\delta \bar{H}/\delta p_\alpha = \partial H/\partial p_\alpha, \text{ and } \delta \bar{H}/\delta P_\alpha = \partial H/\partial P_\alpha \tag{1.16}$$

are the functional derivatives of $\bar{H}$. Hence from Eqs. (1.9), (1.11), (1.12), (1.14), and (1.15), the canonical equations

$$\dot{p}_\alpha = -\delta \bar{H}/\delta q_\alpha, \quad \dot{P}_\alpha = -\delta \bar{H}/\delta Q_\alpha, \tag{1.17}$$

$$\dot{q}_\alpha = \delta \bar{H}/\delta p_\alpha, \quad \dot{Q}_\alpha = \delta \bar{H}/\delta P_\alpha, \tag{1.18}$$

follow. We note that

$$\begin{aligned} d\bar{H}/dt = \int \{ &(\delta \bar{H}/\delta q_\alpha)\dot{q}_\alpha + (\delta \bar{H}/\delta p_\alpha)\dot{p}_\alpha \\ &+ (\delta \bar{H}/\delta Q_\alpha)\dot{Q}_\alpha + (\delta \bar{H}/\delta P_\alpha)\dot{P}_\alpha \} dV = 0. \end{aligned} \tag{1.19}$$

The energy-momentum tensor can be obtained from the variational equation, where now not only the potentials φ_α but also the boundaries are varied. Let the four-dimensional manifold Ω be bounded by two open 3 spaces, having coordinates ξ_α and x_α, respectively. The boundary ξ_α remains fixed; the other x_α is to be displaced by the amount δx_α, while (a) the potentials themselves and their derivatives $\varphi_{\alpha,\mu}$ remain unchanged over the boundary, and (b) Eqs. (1.2) are satisfied for every interior point. Then

$$ic\delta W = \int_{\xi_\beta}^{x_\beta + \delta x_\beta} (L + \delta L) d\Omega - \int_{\xi_\beta}^{x_\beta} L d\Omega, \tag{1.20}$$

where ξ_β and x_β symbolize the original boundaries and ξ_β and $x_\beta + \delta x_\beta$ the new boundaries. Therefore,

$$ic\delta W = \int_{\xi_\beta}^{x_\beta} \delta L d\Omega + \int_{\xi_\beta} L dS_\mu \delta x_\mu, \tag{1.21}$$

where the last integral is a surface integral over the old x_β boundary. From condition (a),

$$\delta \varphi_\alpha = -(\partial \varphi_\alpha/\partial x_\mu)\delta x_\mu$$

and

$$\partial/\partial x_\mu(\delta \varphi_\alpha) = -(\partial^2 \varphi_\alpha/\partial x_\lambda \partial x_\mu)\delta x_\lambda. \tag{1.22}$$

By use of these results and

$$\begin{aligned} \int_{\xi_\beta}^{x_\beta} \delta L d\Omega = \int_{\xi_\beta}^{x_\beta} \{ &(\partial L/\partial \varphi_\alpha)\delta \varphi_\alpha \\ &+ (\partial L/\partial \varphi_{\alpha,\mu})\delta \varphi_{\alpha,\mu} + (\partial L/\partial \varphi_{\alpha,\mu\nu})\delta \varphi_{\alpha,\mu\nu} \} d\Omega \end{aligned} \tag{1.23}$$

Eq. (1.21) can be transformed to

$$\begin{aligned} ic\delta W = \int \{ &L\delta_{\mu\nu} - \varphi_{\alpha,\mu} p_{\alpha\nu} \\ &- \varphi_{\alpha,\mu\lambda} P_{\alpha\lambda\nu} \} dS_\nu \delta x_\mu, \end{aligned} \tag{1.24}$$

where

$$p_{\alpha\beta} = \partial L/\partial \varphi_{\alpha,\beta} - \partial/\partial x_\mu(\partial L/\partial \varphi_{\alpha,\beta\mu}), \tag{1.25}$$

$$P_{\alpha\beta\gamma} = \partial L/\partial \varphi_{\alpha,\beta\gamma}. \tag{1.26}$$

From the definition of the total momentum $\mathbf{P}_\mu$

$$\delta W = \mathbf{P}_\mu \delta x_\mu.$$

We obtain upon comparison with Eq. (1.24)

$$\mathbf{P}_\mu = \int t_{\mu\nu} dS_\nu, \tag{1.27}$$

where the energy-momentum tensor $t_{\mu\nu}$ is given by

$$ict_{\mu\nu} = L\delta_{\mu\nu} - \varphi_{\alpha,\mu} p_{\alpha\nu} - \varphi_{\alpha,\mu\lambda} P_{\alpha\lambda\nu}. \tag{1.28}$$

It can then be shown that this tensor satisfies the equation of conservation of energy and

momentum, namely:

$$t_{\mu\nu,\nu}=0. \tag{1.29}$$

2. PRELIMINARIES. SPECIAL LAGRANGIANS

As an application of the foregoing discussion, consider the Lagrangian proposed by Podolsky.[4]

$$L=-\tfrac{1}{2}\{\tfrac{1}{2}F_{\alpha\beta}F_{\alpha\beta}+a^2F_{\alpha\beta,\beta}F_{\alpha\gamma,\gamma}\}, \tag{2.1}$$

where the field quantities

$$F_{\alpha\beta}=\varphi_{\beta,\alpha}-\varphi_{\alpha,\beta}$$

are now in Heaviside-Lorentz units. The field equations

$$(1-a^2\Box)F_{\alpha\mu,\mu}=0 \tag{2.2}$$

now follow from Eq. (1.2). To compute the energy-momentum tensor we need the quantities

$$\partial L/\partial\varphi_{\alpha,\nu}=F_{\alpha\nu} \tag{2.3}$$

and

$$\partial L/\partial\varphi_{\alpha,\nu\lambda}=-a^2(F_{\nu\beta,\beta}\delta_{\alpha\lambda}-F_{\alpha\beta,\beta}\delta_{\nu\lambda}). \tag{2.4}$$

Hence from Eqs. (1.25) and (1.26) we obtain

$$p_{\alpha\nu}=(1-a^2\Box)F_{\alpha\nu}, \tag{2.5}$$

$$P_{\alpha\lambda\nu}=-a^2(F_{\lambda\beta,\beta}\delta_{\alpha\nu}-F_{\alpha\beta,\beta}\delta_{\lambda\nu}). \tag{2.6}$$

Equation (1.28) thus becomes

$$ict_{\mu\nu}=L\delta_{\mu\nu}-\varphi_{\alpha,\mu}(1-a^2\Box)F_{\alpha\nu}+a^2F_{\alpha\nu,\mu}F_{\alpha\beta,\beta}, \tag{2.7}$$

from which the Hamiltonian is

$$H=-ict_{44}=L$$

$$-\varphi_{\alpha,4}(1-a^2\Box)F_{\alpha4}+a^2F_{\alpha4,4}F_{\alpha\beta,\beta}. \tag{2.8}$$

Care must be exercised in computing the momenta canonically conjugate to φ_α and $\dot{\varphi}_\alpha$ because of the ambiguity in the partial differentiation with respect to $\dot{\varphi}_{\alpha,i}$. We have from Eq. (1.4)

$$p_\alpha=\frac{1}{ic}\Big[\frac{\partial L}{\partial\varphi_{\alpha,4}}-\frac{\partial}{\partial x_4}\frac{\partial L}{\partial\varphi_{\alpha,44}}-\frac{\partial}{\partial x_j}\Big(\frac{\partial L}{\partial\varphi_{\alpha,4j}}+\frac{\partial L}{\partial\varphi_{\alpha,j4}}\Big)\Big]$$

$$=\frac{1}{ic}[F_{\alpha4}+a^2(F_{4\beta,\beta}\delta_{\alpha j}-F_{\alpha\beta,\beta4})]. \tag{2.9}$$

Thus we obtain

$$p_4=\frac{a^2}{ic}F_{j4,j4} \tag{2.10}$$

and

$$p_j=\frac{1}{ic}(1-a^2\Box)F_{j4}; \tag{2.11}$$

having made use of the symmetry properties of $F_{\alpha\beta}$, namely:

$$F_{\alpha\beta}=-F_{\beta\alpha} \quad\text{and}\quad F_{\alpha\beta,\gamma}+F_{\beta\gamma,\alpha}+F_{\gamma\alpha,\beta}=0.$$

Similarly

$$P_\alpha=(a^2/c^2)(F_{4\beta,\beta}\delta_{\alpha4}-F_{\alpha\beta,\beta}) \tag{2.12}$$

or

$$P_4=0, \quad P_j=-(a^2/c^2)F_{j\beta,\beta}. \tag{2.13}$$

In vector notation these quantities become:

$$\begin{aligned} &p_4=i(a^2/c^2)\ \text{div}\ \mathbf{E},\\ &\mathbf{p}=-(1/c)(1-a^2\Box)\mathbf{E},\\ &P_4=0, \quad \mathbf{P}=-(a^2/c^2)(\text{curl}\ \mathbf{H}-(1/c)\dot{\mathbf{E}}). \end{aligned} \tag{2.14}$$

We note that p_4 no longer vanishes, as it does in the usual electrodynamics, but because of the vanishing P_4, we shall encounter the usual difficulty in quantization.

This difficulty can be avoided by using an artifice similar to that used by Fermi[5] and Rosenfeld.[6] Using a modified Lagrangian,

$$L=-\tfrac{1}{2}(\varphi_{\alpha,\beta}\varphi_{\alpha,\beta}+a^2\varphi_{\alpha,\beta\beta}\varphi_{\alpha,\gamma\gamma}), \tag{2.15}$$

we find for the field equations

$$(1-a^2\Box)\Box\varphi_\alpha=0. \tag{2.16}$$

If we further require that these potentials φ_α give the same field equations, Eq. (2.2), we must have

$$(1-a^2\Box)F_{\alpha\mu,\mu}=(1-a^2\Box)\varphi_{\mu,\alpha\mu}$$

$$-(1-a^2\Box)\varphi_{\alpha,\mu\mu}=0 \tag{2.17}$$

or, using Eq. (2.16), we have

$$(1-a^2\Box)\varphi_{\mu,\alpha\mu}=0 \tag{2.18}$$

for the additional conditions to be imposed on the potentials. Since

$$\begin{aligned} &\partial L/\partial\varphi_{\alpha,\nu}=-\varphi_{\alpha,\nu},\\ &\partial L/\partial\varphi_{\alpha,\lambda\nu}=-a^2\varphi_{\alpha,\beta\beta}\delta_{\lambda\nu}, \end{aligned} \tag{2.19}$$

[4] B. Podolsky, Phys. Rev. **62**, 68 (1942), Eq. (3.8). Note the typographical error. This equation should read

$$L_f=-\frac{1}{8\pi}\{\tfrac{1}{2}F_{\alpha\beta}{}^2+a^2(\partial F_{\alpha\beta}/\partial x_\beta)^2\}.$$

Henceforth this paper will be designated by GE.

[5] E. Fermi, Rev. Mod. Phys. **4**, 131 (1932).

[6] L. Rosenfeld, Zeits. f. Physik **76**, 729 (1932).

we have, by Eqs. (1.25) and (1.26),

$$p_{\alpha\nu}=-(1-a^2\Box)\varphi_{\alpha,\nu},\quad P_{\alpha\lambda\nu}=-a^2\delta_{\lambda\nu}\Box\varphi_\alpha. \tag{2.20}$$

Therefore, by Eq. (1.28),

$$ic\mathfrak{l}_{\mu\nu}=L\delta_{\mu\nu}+\varphi_{\alpha,\mu}(1-a^2\Box)\varphi_{\alpha,\nu}+a^2\varphi_{\alpha,\mu\nu}\Box\varphi_\alpha, \tag{2.21}$$

from which follows the Hamiltonian

$$H=-L-\varphi_{\alpha,4}(1-a^2\Box)\varphi_{\alpha,4}-a^2\varphi_{\alpha,44}\Box\varphi_\alpha. \tag{2.22}$$

The momenta canonically conjugate to φ_α and $\dot{\varphi}_\alpha$ are

$$p_\alpha=-(1-a^2\Box)\dot{\varphi}_\alpha \text{ and } P_\alpha=(a^2/c^2)\Box\varphi_\alpha, \tag{2.23}$$

and satisfy the equations

$$\Box p_\alpha=0 \text{ and } (1-a^2\Box)P_\alpha=0. \tag{2.24}$$

3. REDUCTION OF FIELD QUANTITIES AND THE HAMILTONIAN TO FOURIER AMPLITUDES

Following Fock and Podolsky,[7] we shall find it convenient to express the field quantities and the Hamiltonian in terms of the Fourier amplitudes of the potentials. Since,[8] in order to satisfy Eq. (2.16),

$$\varphi_\alpha(\mathbf{r},x_0)=\int(M_\alpha+\tilde{M}_\alpha)dk, \tag{3.1}$$

where

$$\begin{aligned}M_\alpha=\left(\frac{1}{2\pi}\right)^4\{&\varphi_\alpha(\mathbf{k})\exp[i(\mathbf{k}\cdot\mathbf{r}-kx_0)]\\&+\varphi_\alpha^*(\mathbf{k})\exp[-i(\mathbf{k}\cdot\mathbf{r}-kx_0)]\},\\ \tilde{M}_\alpha=\left(\frac{1}{2\pi}\right)^4\{&\tilde{\varphi}_\alpha(\mathbf{k})\exp[i(\mathbf{k}\cdot\mathbf{r}-\tilde{k}x_0)]\\&+\tilde{\varphi}_\alpha^*(\mathbf{k})\exp[-i(\mathbf{k}\cdot\mathbf{r}-\tilde{k}x_0)]\},\end{aligned} \tag{3.2}$$

the notation being the same as in GE, Eq. (6.2). Further, for each field variable F we introduce the Fourier amplitudes defined by the equation

$$\begin{aligned}F=\left(\frac{1}{2\pi}\right)^4\int\{&F(\mathbf{k})\exp[i(\mathbf{k}\cdot\mathbf{r}-kx_0)]\\&+F^*(\mathbf{k})\exp[-i(\mathbf{k}\cdot\mathbf{r}-kx_0)]\\&+\tilde{F}(\mathbf{k})\exp[i(\mathbf{k}\cdot\mathbf{r}-\tilde{k}x_0)]\\&+\tilde{F}^*(\mathbf{k})\exp[-i(\mathbf{k}\cdot\mathbf{r}-\tilde{k}x_0)]\}dk.\end{aligned} \tag{3.3}$$

[7] V. Fock and B. Podolsky, Physik. Zeits. Sowjetunion 1, 801 (1932). This paper will be designated as FP.
[8] GE, Eq. (6.2).

In terms of these quantities then the relations between the field strengths and the potentials become:

$$\begin{aligned}\mathbf{H}(\mathbf{k})&=i\mathbf{k}\times\mathbf{A}(\mathbf{k}),\\ \tilde{\mathbf{H}}(\mathbf{k})&=i\mathbf{k}\times\tilde{\mathbf{A}}(\mathbf{k}),\\ \mathbf{H}^*(\mathbf{k})&=-i\mathbf{k}\times\mathbf{A}^*(\mathbf{k}),\\ \tilde{\mathbf{H}}^*(\mathbf{k})&=-i\mathbf{k}\times\tilde{\mathbf{A}}^*(\mathbf{k}),\\ \mathbf{E}(\mathbf{k})&=i(\mathbf{k}\varphi(\mathbf{k})-k\mathbf{A}(\mathbf{k})),\\ \tilde{\mathbf{E}}(\mathbf{k})&=i(\mathbf{k}\tilde{\varphi}(\mathbf{k})-\tilde{k}\tilde{\mathbf{A}}(\mathbf{k})),\\ \mathbf{E}^*(\mathbf{k})&=-i(\mathbf{k}\varphi^*(\mathbf{k})-k\mathbf{A}^*(\mathbf{k})),\\ \tilde{\mathbf{E}}^*(\mathbf{k})&=-i(\mathbf{k}\tilde{\varphi}^*(\mathbf{k})-\tilde{k}\tilde{\mathbf{A}}^*(\mathbf{k})).\end{aligned} \tag{3.4}$$

The reduction of the Hamiltonian to the Fourier amplitudes is a little more difficult. Putting

$$\begin{aligned}N_\alpha=\left(\frac{1}{2\pi}\right)^4\{&\varphi_\alpha(\mathbf{k})\exp[i(\mathbf{k}\cdot\mathbf{r}-kx_0)]\\&-\varphi_\alpha^*(\mathbf{k})\exp[-i(\mathbf{k}\cdot\mathbf{r}-kx_0)]\}\\ \text{and}\qquad\qquad\qquad\qquad&\qquad\qquad\qquad\qquad\qquad\qquad(3.5)\\ \tilde{N}_\alpha=\left(\frac{1}{2\pi}\right)^4\{&\tilde{\varphi}_\alpha(\mathbf{k})\exp[i(\mathbf{k}\cdot\mathbf{r}-\tilde{k}x_0)]\\&-\tilde{\varphi}_\alpha^*(\mathbf{k})\exp[-i(\mathbf{k}\cdot\mathbf{r}-\tilde{k}x_0)]\},\end{aligned}$$

we obtain for the derivatives of the potentials

$$\begin{aligned}\varphi_{\alpha,4}&=-\int\{kN_\alpha+\tilde{k}\tilde{N}_\alpha\}dk,\\ \varphi_{\alpha,j}&=i\int\{k_jN_\alpha+k_j\tilde{N}_\alpha\}dk,\\ \Box\varphi_\alpha&=(1/a^2)\int\tilde{M}_\alpha dk,\\ (1-a^2\Box)\varphi_\alpha&=\int M_\alpha dk.\end{aligned} \tag{3.6}$$

Adapting FP, Eq. (15) to our need, and after some manipulations, we find

$$\begin{aligned}\bar{H}=&\int\{\varphi_\alpha^*(\mathbf{k})\varphi_\alpha(\mathbf{k})+\varphi_\alpha(\mathbf{k})\varphi_\alpha^*(\mathbf{k})\}k^2dk\\&-\int\{\tilde{\varphi}_\alpha^*(\mathbf{k})\tilde{\varphi}_\alpha(\mathbf{k})+\tilde{\varphi}_\alpha(\mathbf{k})\tilde{\varphi}_\alpha^*(\mathbf{k})\}\tilde{k}^2dk.\end{aligned} \tag{3.7}$$

4. QUANTIZATION

In order to pass from the classical to the quantum equations, without having to make some new postulate for the commutation rules of the potentials, two methods are available. In one, due to Heisenberg and Pauli, the canonically conjugate coordinates and momenta of the field satisfy commutation rules similar to those of the quantum mechanics of a particle, i.e.,

$$[p_\alpha(\mathbf{r}, x_0), q_\beta(\mathbf{r}', x_0)] = -hi\delta_{\alpha\beta}\delta(\mathbf{r}-\mathbf{r}'),$$
$$[P_\alpha(\mathbf{r}, x_0), Q_\beta(\mathbf{r}', x_0)] = -hi\delta_{\alpha\beta}\delta(\mathbf{r}-\mathbf{r}'); \tag{4.1}$$

and

$$\begin{aligned}[q_\alpha(\mathbf{r}, x_0), q_\beta(\mathbf{r}', x_0)] &= [p_\alpha(\mathbf{r}, x_0), p_\beta(\mathbf{r}', x_0)] \\ &= [Q_\alpha(\mathbf{r}, x_0), Q_\beta(\mathbf{r}', x_0)] \\ &= [P_\alpha(\mathbf{r}, x_0), P_\beta(\mathbf{r}', x_0)] \\ &= [p_\alpha(\mathbf{r}, x_0), Q_\beta(\mathbf{r}', x_0)] \\ &= [P_\alpha(\mathbf{r}, x_0), q_\beta(\mathbf{r}', x_0)] \\ &= [q_\alpha(\mathbf{r}, x_0), Q_\beta(\mathbf{r}', x_0)] \\ &= [p_\alpha(\mathbf{r}, x_0), P_\beta(\mathbf{r}', x_0)] = 0. \end{aligned} \tag{4.2}$$

It is interesting to note that now the potentials q_α and their time derivatives Q_β commute, a result which is quite different from that of usual electrodynamics.

Alternatively, we may require that

$$\dot{F} = (i/\hbar)[\bar{H}, F] \tag{4.3}$$

is satisfied for every operator F in the Heisenberg representation. Either method will lead to the same results.

From Eq. (4.3) we have, as special cases,

$$\dot{p}_\alpha = (i/\hbar)[\bar{H}, p_\alpha] \quad \text{and} \quad \dot{P}_\alpha = (i/\hbar)[\bar{H}, P_\alpha]. \tag{4.4}$$

Using Eqs. (2.23) and (3.6) we obtain

$$p_\alpha = (-i/c)\int kN_\alpha dk,$$
$$P_\alpha = (1/c^2)\int \tilde{k}\tilde{N}_\alpha dk. \tag{4.5}$$

The commutation rules for the Fourier amplitudes are now found by expressing both sides of Eq. (4.4) in terms of their Fourier amplitudes and equating coefficients of corresponding exponentials. Thus:

$$[\varphi_\alpha^*(\mathbf{k}), \varphi_\beta(\mathbf{k}')] = -\frac{ch}{2k}\delta_{\alpha\beta}\delta(\mathbf{k}-\mathbf{k}'),$$
$$[\tilde{\varphi}_\alpha^*(\mathbf{k}), \tilde{\varphi}_\beta(\mathbf{k}')] = \frac{ch}{2\tilde{k}}\delta_{\alpha\beta}\delta(\mathbf{k}-\mathbf{k}'). \tag{4.6}$$

All other pairs of the Fourier component of the potentials commute.

The commutation rules for the potentials at different space-time points can be obtained by transforming back to coordinate space. The result is

$$\begin{aligned}&[\varphi_\alpha(\mathbf{r}, x_0), \varphi_\beta(\mathbf{r}', x_0')] \\ &\quad = -\frac{ich\delta_{\alpha\beta}}{(2\pi)^3}\int \exp[i\mathbf{k}\cdot(\mathbf{r}-\mathbf{r}')] \\ &\quad \times\left[\frac{\sin k(x_0-x_0')}{k} - \frac{\sin \tilde{k}(x_0-x_0')}{\tilde{k}}\right]dk. \end{aligned} \tag{4.7}$$

The first term gives the well-known Jordan-Pauli invariant delta function:

$$\begin{aligned}\left(\frac{1}{2\pi}\right)^3\int e^{i\mathbf{k}\cdot\mathbf{R}}\frac{\sin kX_0}{k}dk &= \Delta(X) \\ &= \frac{1}{4\pi|\mathbf{R}|}[\delta(|\mathbf{R}|-X_0) - \delta(|\mathbf{R}|+X_0)]. \end{aligned} \tag{4.8}$$

The second term is proportional to[9]

$$\begin{aligned}\left(\frac{1}{2\pi}\right)^3\int e^{i\mathbf{k}\cdot\mathbf{R}}\frac{\sin \tilde{k}X_0}{\tilde{k}}dk &= -\frac{1}{4\pi|\mathbf{R}|}\cdot\frac{\partial}{\partial|\mathbf{R}|}F(|\mathbf{R}|, X_0), \end{aligned} \tag{4.9}$$

where

$$F(|\mathbf{R}|, X_0) = \begin{cases} J_0\left\{\frac{1}{a}(X_0^2-|\mathbf{R}|^2)^{\frac{1}{2}}\right\} \\ \qquad \text{for } X_0 > |\mathbf{R}|, \\ 0 \quad \text{for } |\mathbf{R}| > X_0 > -|\mathbf{R}|, \\ -J_0\left\{\frac{1}{a}(X_0^2-|\mathbf{R}|^2)^{\frac{1}{2}}\right\} \\ \qquad \text{for } X_0 < -|\mathbf{R}|. \end{cases} \tag{4.10}$$

Equations (4.1) and (4.2) can be obtained immediately from Eq. (4.7). For example, partial differentiation with respect to x_0, and subsequent

[9] P. A. M. Dirac, Proc. Camb. Phil. Soc. **30**, 100 (1934)

substitution of $x_0'=x_0$, gives Eq. (4.2). Later we shall need the relation

$$[\varphi_\alpha(\mathbf{r}, x_0),\ \varphi_{\alpha,i}(\mathbf{r}', x_0)]=0, \tag{4.11}$$

which is easily obtained from Eqs. (4.1).

It is interesting to note that in our formulation the four-divergence of the potentials at different space-time points does not commute. In fact, it can be shown that

$$[\varphi_{\alpha,\alpha}(\mathbf{r}, x_0),\ \varphi_{\beta,\beta}(\mathbf{r}', x_0')] =\frac{-ich}{a^2(2\pi)^3}\int e^{i\mathbf{k}\cdot(\mathbf{r}-\mathbf{r}')}\frac{\sin \tilde{k}(x_0-x_0')}{\tilde{k}}dk. \tag{4.12}$$

The commutation rules for the Fourier components of the field strengths can be obtained from Eqs. (3.4) and (4.6). Thus, since

$$\begin{aligned}
&[A_i^*(\mathbf{k}), A_j(\mathbf{k}')]=-\frac{ch}{2k}\delta_{ij}\delta(\mathbf{k}-\mathbf{k}'),\\
&[\varphi^*(\mathbf{k}), \varphi(\mathbf{k}')]=\frac{ch}{2k}\delta(\mathbf{k}-\mathbf{k}'),\\
&[\tilde{A}_i^*(\mathbf{k}), \tilde{A}_j(\mathbf{k}')]=\frac{ch}{2\tilde{k}}\delta_{ij}\delta(\mathbf{k}-\mathbf{k}'),\\
&[\tilde{\varphi}^*(\mathbf{k}), \tilde{\varphi}(\mathbf{k}')]=-\frac{ch}{2\tilde{k}}\delta(\mathbf{k}-\mathbf{k}'),
\end{aligned} \tag{4.13}$$

it follows that

$$\begin{aligned}
&[E_i(\mathbf{k}), E_j^*(\mathbf{k}')]=\frac{ch}{2k}(k^2\delta_{ij}-k_ik_j)\delta(\mathbf{k}-\mathbf{k}'),\\
&[\tilde{E}_i(\mathbf{k}), \tilde{E}_j^*(k')]=-\frac{ch}{2\tilde{k}}\\
&\qquad\times(\tilde{k}^2\delta_{ij}-k_ik_j)\delta(\mathbf{k}-\mathbf{k}'),\\
&[H_i(\mathbf{k}), H_j^*(\mathbf{k}')]=\frac{ch}{2k}(k^2\delta_{ij}-k_ik_j)\delta(\mathbf{k}-\mathbf{k}'),\\
&[\tilde{H}_i(\mathbf{k}), \tilde{H}_j^*(\mathbf{k}')]=-\frac{ch}{2\tilde{k}}\\
&\qquad\times(k^2\delta_{ij}-k_ik_j)\delta(\mathbf{k}-\mathbf{k}'),\\
&[E_i(\mathbf{k}), H_j^*(\mathbf{k}')]=[E_i^*(\mathbf{k}), H_j(\mathbf{k}')]\\
&\qquad=\frac{ch}{2}k_m\epsilon_{ijm}\delta(\mathbf{k}-\mathbf{k}'),\\
&[\tilde{E}_i(\mathbf{k}), \tilde{H}_j^*(\mathbf{k}')]=[\tilde{E}_i^*(\mathbf{k}), \tilde{H}_j(\mathbf{k}')]\\
&\qquad=-\frac{ch}{2}k_m\epsilon_{ijm}\delta(\mathbf{k}-\mathbf{k}').
\end{aligned} \tag{4.14}$$

All other combinations commute. In the last expression, ϵ_{ijk} is $+1$ or -1, according to whether ijk is an even or odd permutation of 123, and zero otherwise.

The commutation rules of the field quantities can be obtained by the method used in deriving Eq. (4.7). Thus:

$$\begin{aligned}
&[E_i(\mathbf{r}, x_0), E_j(\mathbf{r}', x_0')]\\
&=\frac{ich}{(2\pi)^3}\int\Big\{(k^2\delta_{ij}-k_ik_j)\frac{\sin k(x_0-x_0')}{k}\\
&\times\exp[i\mathbf{k}\cdot(\mathbf{r}-\mathbf{r}')]-(\tilde{k}^2\delta_{ij}-k_ik_j)\\
&\times\frac{\sin \tilde{k}(x_0-x_0')}{\tilde{k}}\exp[i\mathbf{k}\cdot(\mathbf{r}-\mathbf{r}')]\Big\}dk\\
&=\frac{ich}{(2\pi)^3}\left(\delta_{ij}\frac{\partial^2}{\partial x_0\partial x_0'}-\frac{\partial^2}{\partial x_i\partial x_j'}\right)\\
&\times\int\left\{\frac{\sin k(x_0-x_0')}{k}-\frac{\sin \tilde{k}(x_0-x_0')}{\tilde{k}}\right\}\\
&\qquad\times\exp[i\mathbf{k}\cdot(\mathbf{r}-\mathbf{r}')]dk.
\end{aligned} \tag{4.15}$$

Also

$$\begin{aligned}
&[H_i(\mathbf{r}, x_0), H_j(\mathbf{r}', x_0')]\\
&=\frac{ich}{(2\pi)^3}\left(\delta_{ij}\frac{\partial^2}{\partial x_0\partial x_0'}-\frac{\partial^2}{\partial x_i\partial x_j'}\right)\\
&\times\int\left\{\frac{\sin k(x_0-x_0')}{k}-\frac{\sin \tilde{k}(x_0-x_0')}{\tilde{k}}\right\}\\
&\qquad\times\exp[i\mathbf{k}\cdot(\mathbf{r}-\mathbf{r}')]dk
\end{aligned} \tag{4.16}$$

and

$$\begin{aligned}
&[E_i(\mathbf{r}, x_0), H_j(\mathbf{r}', x_0')]=\frac{ch\epsilon_{ijm}}{(2\pi)^3}\\
&\times\frac{\partial}{\partial x_m}\int\left\{\frac{\sin k(x_0-x_0')}{k}-\frac{\sin \tilde{k}(x_0-x_0')}{\tilde{k}}\right\}\\
&\qquad\times\exp[i\mathbf{k}\cdot(\mathbf{r}-\mathbf{r}')]dk.
\end{aligned} \tag{4.17}$$

5. AUXILIARY CONDITIONS

It is customary in the usual quantum electrodynamics to assume, in addition to the wave equation, that the Schrödinger functional Ψ satisfies the condition

$$(\partial\varphi_\alpha/\partial x_\alpha)\Psi=0.$$

However, it is required of an auxiliary condition

of the form $A\Psi=0$ that $A(\mathbf{r}, t)$ commute with $A(\mathbf{r}', t')$ taken at another space-time point. This condition, according to Eq. (4.12), is not satisfied by $(\partial\varphi_\alpha/\partial x_\alpha)$.

A suitable generalization of the above equation can be obtained as follows: Eq. (2.18) is satisfied if we put

$$a(\partial\varphi_\alpha/\partial x_\alpha)+B=0, \tag{5.1}$$

where B is any function satisfying the equation

$$(1-a^2\Box)B=0. \tag{5.2}$$

In terms of the Fourier amplitudes, Eq. (5.2) is equivalent to

$$B=\left(\frac{1}{2\pi}\right)^4\int\{\tilde{B}(\mathbf{k})\exp[i(\mathbf{k}\cdot\mathbf{r}-\tilde{k}x_0)] +\tilde{B}^*(\mathbf{k})\exp[-i(\mathbf{k}\cdot\mathbf{r}-\tilde{k}x_0)]\}dk. \tag{5.3}$$

Following the suggestion due to Stückelberg,[10] we shall take as the auxiliary condition

$$[a(\partial\varphi_\alpha/\partial x_\alpha)+B]\Psi=0, \tag{5.4}$$

and assume that $\tilde{B}(\mathbf{k})$ and $\tilde{B}^*(\mathbf{k})$ satisfy the same commutation rules as the other tilde functions, i.e.,

$$[\tilde{B}(\mathbf{k}), \tilde{B}^*(\mathbf{k}')]=-(ch/2\tilde{k})\delta(\mathbf{k}-\mathbf{k}'), \tag{5.5}$$

and commute with the amplitudes of the potentials. Hence from Eqs. (5.3) and (5.5)

$$[B(\mathbf{r}, x_0), B(\mathbf{r}', x_0')]=\frac{-ich}{(2\pi)^3}\times\int\frac{\sin\tilde{k}(x_0-x_0')}{\tilde{k}}\exp[i\mathbf{k}\cdot(\mathbf{r}-\mathbf{r}')]dk. \tag{5.6}$$

Using this result and Eq. (4.12), we have

$$[a\varphi_{\alpha,\alpha}(\mathbf{r}, x_0)+B(\mathbf{r}, x_0), a\varphi_{\beta,\beta}(\mathbf{r}', x_0')+B(\mathbf{r}', x_0')]=0. \tag{5.7}$$

Equating coefficients of corresponding exponentials, the auxiliary condition can be written in terms of the Fourier amplitudes, i.e.,

$$\begin{gathered}[\mathbf{k}\cdot\mathbf{A}(\mathbf{k})-k\varphi(\mathbf{k})]\Psi=0,\\ [a(\mathbf{k}\cdot\tilde{\mathbf{A}}(\mathbf{k})-\tilde{k}\tilde{\varphi}(\mathbf{k}))-i\tilde{B}(\mathbf{k})]\Psi=0,\\ [\mathbf{k}\cdot\mathbf{A}^*(\mathbf{k})-k\varphi^*(\mathbf{k})]\Psi=0,\\ [a(\mathbf{k}\cdot\tilde{\mathbf{A}}^*(\mathbf{k})-\tilde{k}\tilde{\varphi}^*(\mathbf{k}))+i\tilde{B}^*(\mathbf{k})]\Psi=0.\end{gathered} \tag{5.8}$$

[10] E. C. G. Stückelberg, Helv. Phys. Acta 11, 225–299 (1938).

The operators occurring in these equations commute among themselves and also with the Hamiltonian.

6. FIELD WITH CHARGED PARTICLES

The present formulation can be extended to fields containing charged particles exactly as was done by Dirac, Fock, and Podolsky.[11] As in DFP, we shall find again that the operators in Eqs. (5.8) do not commute with the operator[12]

$$R_s-ih(\partial/\partial t_s). \tag{6.1}$$

This difficulty can be overcome by introducing operators

$$\begin{aligned}C(\mathbf{k})&=i[\mathbf{k}\cdot\mathbf{A}(\mathbf{k})-k\varphi(\mathbf{k})]+f(\mathbf{r}_s, t_s),\\ \tilde{C}(\mathbf{k})&=i[\mathbf{k}\cdot\tilde{\mathbf{A}}(\mathbf{k})-\tilde{k}\tilde{\varphi}(\mathbf{k})]+\frac{1}{a}\tilde{B}(\mathbf{k})+\tilde{f}(\mathbf{r}_s, t_s),\end{aligned} \tag{6.2}$$

and their complex conjugates, where $f(\mathbf{r}_s, t_s)$ and $\tilde{f}(\mathbf{r}_s, t_s)$ are chosen so as to make the C's commute with the operators (6.1). A short calculation shows that

$$\begin{aligned}f(\mathbf{r}_s, t)&=\frac{i}{2(2\pi)^3}\sum_s\frac{\epsilon_s}{k}\times\exp[-i(\mathbf{k}\cdot\mathbf{r}_s-kx_{0s})],\\ \tilde{f}(\mathbf{r}_s, t)&=-\frac{i}{2(2\pi)^3}\sum_s\frac{\epsilon_s}{\tilde{k}}\times\exp[-i(\mathbf{k}\cdot\mathbf{r}_s-\tilde{k}x_{0s})].\end{aligned} \tag{6.3}$$

Then, the modified auxiliary conditions are given by:

$$\begin{aligned}C(\mathbf{k})\Psi=0, &\qquad \tilde{C}(\mathbf{k})\Psi=0,\\ C^*(\mathbf{k})\Psi=0, \text{ and} &\qquad \tilde{C}^*(\mathbf{k})\Psi=0.\end{aligned} \tag{6.4}$$

Transforming (6.4) to coordinate space, we obtain

$$C(\mathbf{r}, x_0)=\operatorname{div}\mathbf{A}+\frac{\partial\varphi}{\partial x_0}+\frac{1}{a}B(\mathbf{r}, x_0) -\frac{1}{(2\pi)^3}\sum_s\epsilon_s\int\left\{\frac{\sin k(x_0-x_{0s})}{k} -\frac{\sin\tilde{k}(x_0-x_{0s})}{\tilde{k}}\right\}\exp[i\mathbf{k}\cdot(\mathbf{r}-\mathbf{r}_s)]dk. \tag{6.5}$$

[11] Dirac, Fock, and Podolsky, Physik. Zeits. Sowjetunion 2, 473 (1932). Hereafter referred to as DFP.

[12] For the definitions of these quantities see reference 11, Eqs. (1) to (11), inclusive.

The field equations can be obtained by procedure similar to that used in DFP. From the defining equations, GE Eq. (3.3), or

$$\mathbf{E}=-\operatorname{grad}\varphi-(1/c)(\partial\mathbf{A}/\partial t)$$
$$\text{and} \tag{6.6}$$
$$\mathbf{H}=\operatorname{curl}\mathbf{A},$$

it follows immediately that

$$\operatorname{curl}\mathbf{E}+(1/c)(\partial\mathbf{H}/\partial t)=\mathbf{0} \quad \text{and} \quad \operatorname{div}\mathbf{H}=0, \tag{6.7}$$

so that these remain as quantum mechanical equations. The other two equations can only be derived with the aid of Eq. (6.5).

Recalling Eq. (2.16), and observing that the first and the second terms under the integral sign of Eq. (6.5) satisfy Maxwell's and Yukawa's wave equations, respectively, we obtain from Eq. (6.6)

$$(1-a^2\Box)\left(\operatorname{curl}\mathbf{H}-\frac{1}{c}\frac{\partial\mathbf{E}}{\partial t}\right)\Psi$$
$$=\left[\operatorname{grad}\sum_s\frac{\epsilon_s}{4\pi}\Delta(X-X_s)\right]\Psi, \tag{6.8}$$

where X is the four-vector (x_1, x_2, x_3, x_0) and $\Delta(X)$ the invariant delta function defined in Eq. (4.8). Similarly

$$(1-a^2\Box)\operatorname{div}\mathbf{E}\Psi$$
$$=-\frac{1}{c}\left[\frac{\partial}{\partial t}\sum_s\frac{\epsilon_s}{4\pi}\Delta(X-X_s)\right]\Psi. \tag{6.9}$$

Now putting the various times equal to each other, we get for the equations corresponding to DFP Eqs. (45), (46), and (47) the generalized results:

$$(1-a^2\Box)\left(\operatorname{div}\mathbf{A}+\frac{1}{c}\frac{\partial\varphi}{\partial t}\right)\Psi=0, \tag{6.10}$$

$$(1-a^2\Box)\left(\operatorname{curl}\mathbf{H}-\frac{1}{c}\frac{\partial\mathbf{E}}{\partial t}\right)\Psi=0, \tag{6.11}$$

and

$$(1-a^2\Box)\operatorname{div}\mathbf{E}\Psi$$
$$=-\sum_s\frac{\epsilon_s}{4\pi}\left[\frac{1}{c}\frac{\partial}{\partial t}\Delta(X-X_s)\right]_{t_s=t}\Psi. \tag{6.12}$$

The argument leading from DFP Eqs. (48) to (49) has to be modified slightly in view of the fact that the momenta conjugate to A_i are not $-(1-a^2\Box)E_i$, but $(1/c^2)(1-a^2\Box)A_i$. Thus

$$[R_s, (1-a^2\Box)\mathbf{E}]$$
$$=-\epsilon_s\Big[\varphi(\mathbf{r}_s, t_s)-\boldsymbol{\alpha}_s\cdot\mathbf{A}(\mathbf{r}_s, t_s),$$
$$(1-a^2\Box)\nabla\varphi(\mathbf{r}, t)+\frac{1}{c}(1-a^2\Box)\dot{\mathbf{A}}(\mathbf{r}, t)\Big]$$
$$=ic\hbar\epsilon_s\boldsymbol{\alpha}_s\delta(\mathbf{r}-\mathbf{r}_s). \tag{6.13}$$

Since

$$\left[\frac{1}{c}\frac{\partial}{\partial X_0}\Delta(X)\right]_{X_0=0}=-4\pi\delta(|\mathbf{R}|),$$

Eqs. (6.11) and (6.12) become

$$(1-a^2\Box)\left(\operatorname{curl}\mathbf{H}-\frac{1}{c}\frac{\partial\mathbf{E}}{\partial T}\right)\Psi$$
$$=\Big(\sum_s\epsilon_s\boldsymbol{\alpha}_s\delta(\mathbf{r}-\mathbf{r}_s)\Big)\Psi \tag{6.14}$$

and

$$(1-a^2\Box)\operatorname{div}\mathbf{E}\Psi=\Big(\sum_s\epsilon_s\delta(\mathbf{r}-\mathbf{r}_s)\Big)\Psi. \tag{6.15}$$

These are natural generalizations of the equations of ordinary quantum electrodynamics.

PHYSICAL REVIEW VOLUME 65, NUMBERS 7 AND 8 APRIL 1 AND 15, 1944

Experimental Verification of the Theory of the Continuous Spectra of H_2 and D_2

ALBERT SPRAGUE COOLIDGE
Harvard University, Cambridge, Massachusetts

(Received February 21, 1944)

The continuous spectra of molecular hydrogen and deuterium have been produced and studied under conditions permitting control of the excitation processes involved, the electron beam being subjected to definite accelerating potentials. An immediate comparison of the results with those predicted on purely theoretical grounds in previous papers by the author and others was not possible because of the unavoidable thermal spread in the kinetic energies of the electrons, an effect which had not been considered in those papers. The necessary modification in the theoretical predictions has been carried out, the essential result being that no sharp separation of even the lowest vibrational level of the radiating electronic state can be expected at any accelerating potential; consequently, even at the lowest potential at which any radiation is perceptible, that coming from the lowest vibrational level will be appreciably contaminated by the contribution from the next higher. The form of functional relationship between the rate of excitation of a given level and the accelerating potential is investigated and found to be linear if the latter is higher than the critical excitation potential of the given level (but not too much higher), and exponential if it is lower. Advantage is taken of this relationship to determine the corrections due to contact potentials and possible other causes which prevent the true accelerating potential in a thermionic device from being read directly from a voltmeter connected between the source of electrons and the collector. It has been shown that at certain wave-lengths the observed radiation can come only from a single vibrational level; when the corresponding intensity is plotted as a function of the voltmeter reading, a curve of the form described is obtained, and the point at which the linear and exponential parts merge is taken as that at which the true accelerating potential is equal to the (known) critical potential. When the true potential scale has been thus established, it is found that there is good agreement between calculated and observed spectral energy distribution. Thus the original calculations, which were in painful disagreement with the only quantitative experimental data then extant, are now satisfactorily confirmed.

INTRODUCTION

THE quantitative theory of the relative energy distribution in the continuous spectrum of hydrogen and deuterium has been given in two previous papers.[1,2] This spectrum is produced by transitions from the stable $1s\sigma 2s\sigma\ ^3\Sigma_g$ electronic state of the molecule to the unstable $1s\sigma 2p\sigma\ ^3\Sigma_u$ state, and consists of contributions from each of the vibrational levels of the upper state. We presented a complete theoretical calculation of the composition of the contributions from the first four or five such levels, making use of no assumptions or numerical constants other than those of basic theory, and no approximations which could not be shown by internal evidence to be legitimate. In addition, we made rough estimates of the relative populations of the several levels which should be maintained when molecules in the ground state are excited by electrons with definite homogeneous kinetic energies, and of the character of the resulting composite radiation. Comparison with the existing experimental evidence was very unsatisfactory. The only work with which our accurate calculations could be compared was that of Smith,[3] who attempted to isolate the radiation from the lowest vibrational level by using a great excess of helium in his discharge tube; his results bore no resemblance to ours. The older work of Finkelnberg and Weizel[4] on the composite spectrum could be given an interpretation in harmony with our calculations, but it was not sufficiently quantitative to be regarded as definite confirmation.

In order to clear up the matter, it was decided to undertake the analysis of the spectrum radiated under simple, known conditions, with excitation produced at low pressure (0.015 mm) by thermionic electrons under controlled acceleration. It was at first hoped to be able to reproduce the conditions assumed in the calculations of II, and in particular to isolate the radiation

[1] A. S. Coolidge, H. M. James, and R. D. Present, J. Chem. Phys. **4**, 193 (1936).
[2] H. M. James and A. S. Coolidge, Phys. Rev. **55**, 184 (1939). These two papers will hereafter be referred to as I and II, respectively.
[3] N. D. Smith, Phys. Rev. **49**, 345 (1936).
[4] W. Finkelnberg and W. Weizel, Zeits. f. Physik **68**, 577 (1931).

from the level $v=0$ by keeping the electron velocities below the critical velocity for $v=1$, which lies 0.3 volt higher (for H_2). This would have been desirable because it would have provided a direct test of that part of our calculations which was wholly independent of all assumptions about the nature of the excitation process. But consideration showed that this hope could not be realized because the inevitable thermal spread in the energies of the electrons must, no matter what the accelerating voltage, produce an appreciable contamination by radiation from the next higher level. Fortunately, it is possible to modify the theoretical predictions in order to allow for this effect and thus to obtain an experimental test in which the excitation process is involved only in the determination of a correction term.

THEORY

It will be assumed, as before, that when an electron with a given kinetic energy encounters a normal hydrogen molecule, the probability of excitation to a particular vibrational level of the upper (electronic) state is zero if the electron possesses less than a certain critical energy (the excitation energy), and otherwise is directly proportional to the amount by which the electronic energy exceeds the critical value. (A discussion of this assumption will be found in I.) Actually, the relation stated is expected to break down for excess energies more than a fraction of a volt, the true excitation being less than predicted, but this will be disregarded in making the calculations.

Suppose electrons are emitted from a hot cathode and travel through an accelerating field, some of them arriving at a point of observation where the potential difference is known with respect to a point just outside the cathode surface. We wish to calculate their distribution with regard to kinetic energy and the corresponding excitation produced to various levels. Since the original velocities are small in comparison with those acquired from the field, we may ignore any differences between the paths followed by electrons of different original speeds, and assume that the same fraction of those emitted with all initial speeds arrive at the observation point. Then the final energy distribution can be found from the initial distribution simply by taking account of the fact that the increase in energy is the same for all electrons. They are emitted with a Maxwellian distribution about a mean value $2kT$. (The extra $\frac{1}{2}kT$ as compared with the mean value for the molecules in a fixed sample of gas is due to the fact that, of all the electrons of given energy present, the proportion emitted increases with the energy.) Consequently, upon arrival at the observation space, they will have a similar distribution about a mean value equal to the accelerating potential plus $2kT$, and none will have energy less than the accelerating potential. If the latter is not less than the critical potential for a given upper level, all arriving electrons can produce excitation to that level. In view of the linearity of the excitation function (the relation between the rate of excitation and the kinetic energy), the mean rate of excitation will be just that corresponding to the mean kinetic energy; the thermal energy will simply lower the apparent critical potential by $2kT$. But if the accelerating potential is lower than the critical value this reasoning fails, for the value $2kT$ represents the energy averaged over all the electrons, while the excitation rate has to be averaged only over those electrons which started with at least sufficient thermal energy to make up the deficiency between accelerating and critical potentials. The excitation rate is therefore greater than that corresponding to the mean kinetic energy, and indeed remains positive even if the latter falls below the critical value (accelerating potential more than $2kT$ below excitation potential), for there are always some exceptionally fast electrons capable of overcoming the deficiency. But this number decreases exponentially as the deficiency becomes greater. The complete prediction for the apparent excitation function (relation between rate of excitation and accelerating potential) is therefore a linear part for accelerating potentials greater than the true critical potential, joined smoothly to a curved portion which vanishes exponentially with decreasing accelerating potential.

It might appear possible to reduce the thermal spread by introducing a very slight retarding field near the cathode, so as to reflect electrons having low initial velocities and permit only the faster ones to pass. Consideration shows, how-

ever, that no diminution in spread would really occur because there would also be a reflection of fast electrons which happened to be moving obliquely. The energy distribution of the electrons passing the barrier would still be Maxwellian, and the only modification necessary in the reasoning of the previous paragraph is that the accelerating potential should be measured from the barrier instead of from the cathode surface.

To get a quantitative theory, let V be the accelerating potential and let V_0, V_1, $\cdots$, be the critical potentials for the vibrational levels $v=0$, $v=1$, $\cdots$. For convenience put $V-V_0=\Delta_0$, $V-V_1=\Delta_1$, $\cdots$. Let E' be the kinetic energy (in volts) of an electron issuing from the cathode (or crossing the potential minimum), and $E=E'+V$ its energy upon arrival at the point of observation. The distribution-in-energy of the electrons is originally that given by the equation

$$dn/dE=CE'e^{-E'\epsilon/kT},$$

where dn is the number of electrons having energies within the range dE, C is a constant which need not concern us, and ϵ is the elementary charge. [This apparently unfamiliar expression can be easily derived from any of the usual statements of the Maxwellian law. For example, Kennard[5] states that the rate at which particles cross a plane with speed in dv at v and at an angle to the normal in $d\theta$ at θ is

$$2\pi nAv^3 \exp(-mv^2/2kT)dv \sin\theta\cos\theta d\theta,$$

where n is the number present per unit volume and A is a constant. Upon putting $2v^3dv=v^2d(v^2)=4E'dE'/m^2$ (with m the mass of a particle) and integrating over the appropriate angle, an expression in the given form is obtained.]

The electrons arrive at the point of observation with energy distribution

$$dn/dE=C(E-V)e^{-(E-V)\epsilon/kT}, \quad E>V.$$

For small positive $E-V_v$ an electron has a probability $K_v(E-V_v)$ of producing excitation to the level v, K_v being the excitation constant. (K_v is the quantity $KM^2_{v,v'v'}$ of Eq. (11) of I, for which revised values are given in Table II of II.) The total rate of excitation to each level v is therefore

$$R_v=CK_v\int(E-V_v)(E-V)e^{-(E-V)\epsilon/kT}dE.$$

The upper limit of integration may be taken as infinity since the smallness of the Boltzmann factor for high electron energies prevents the failure of the assumption of a linear excitation function from producing an appreciable error. The lower limit is to be taken as V or V_v, whichever is the higher, that is, accordingly as Δ_v is positive or negative. The integration is readily performed, leading to the formulas

$$R_v=C'K_v[1+\Delta_v\epsilon/2kT], \qquad \Delta_v>0,$$

$$R_v=C'K_v[1-\Delta_v\epsilon/2kT]e^{\Delta_v\epsilon/kT}, \quad \Delta_v<0.$$

Here C' stands for the new constant $2C(kT/\epsilon)^3$. The two formulas join smoothly at $\Delta_v=0$, as can be seen by expanding the exponential. For positive Δ_v, R_v is a linear function of Δ_v, while for large negative Δ_v, $\log R_v$ becomes linear in Δ_v. The functional form of R_v, plotted logarithmically against Δ_v, is shown (except for an additive

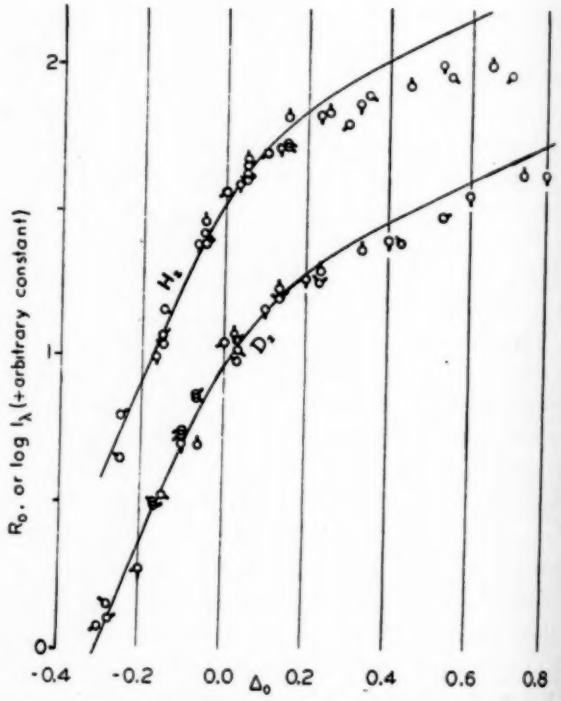

FIG. 1. Determination of absolute potential scale. Curves show calculated log R_0 plotted against Δ_0. Symbols show observed log intensity plotted against voltmeter readings and displaced so as to coincide with curves. Data for H_2 are for line 12. Data for D_2 are for line 10.

[5] E. H. Kennard, *Kinetic Theory of Gases* (McGraw-Hill Book Company, New York, 1938), Eq. (71*b*).

constant) by either solid curve in Fig. 1. For large positive Δ_v its true value must be expected to fall below that given by the above formula, in view of the known breakdown of the linear relation for the true excitation function.

The remaining calculation of the radiation predicted at any potential V is made exactly as before in II, substituting R_v for $F_{ev,e'v'}$ of Eq. (11) of I. Briefly summarized, the method calculates the population of each level as the product of the appropriate R_v multiplied by the mean lifetime τ_v as taken from Table I of II. The calculated radiation from each level, as shown in Figs. 2 and 3 of II, is then multiplied by the population of that level, and the contributions are added to give the final composite result.

The degree to which the radiation from $v=0$ can be isolated depends principally on the amount of contamination from $v=1$, which is determined by the relative intensities at each wave-length of the radiations from the two pure levels and by the ratio of their populations. For $V<V_0$, this ratio is

$$\frac{\tau_1 R_1}{\tau_0 R_0}=\frac{\tau_1 K_1}{\tau_0 K_0}\,\frac{1+(V_1-V)\epsilon/2kT}{1+(V_0-V)\epsilon/2kT}\times\exp\left[-(V_1-V_0)\epsilon/kT\right].$$

As V becomes negatively infinite, the second factor approaches unity. With a cathode temperature of 1100°K, ($\epsilon/kT=10.52$ v), we may substitute the values for hydrogen:

$\tau_1=1.10\times10^{-8}$ sec., $K_1=1.13$ arbitrary units,
$\tau_0=1.19\times10^{-8}$ sec., $K_0=1.00$ arbitrary units,
$V_1=12.03$ v.
$V_0=11.72$ v.

Then the limiting value of the population ratio is 0.04, while in the range of V within which a perceptible radiation intensity may be expected, it has the following values:

V	11.42	11.52	11.62	11.72	11.82	11.92	12.02	12.12
ratio	0.066	0.073	0.083	0.106	0.159	0.252	0.382	0.495.

The resulting contamination will vary with the wave-length, being zero at 2800A where the radiation from $v=1$ vanishes, and increasing most rapidly toward shorter wave-lengths, at which the radiation from $v=1$ is much greater than that from $v=0$. It appears that for wave-lengths greater than about 2500A, and accelerating potentials in the neighborhood of the critical potential for $v=0$, the contamination should not be serious, and could be adequately accounted for by this somewhat crude method of estimating the effective excitation functions. Evidently there is nothing to be gained by attempting to push the potential far below 11.72 v, as the slightly more favorable population ratio will be more than outweighed by the loss in accuracy caused by the exponential decrease in total intensity.

For deuterium the relations are much less favorable. This is due to the facts that the vibrational levels lie closer together, that the excitation constants for the higher levels are nearly twice as great as for hydrogen in comparison to the ground level, and that the radiation from pure $v=1$ exceeds that from $v=0$ at longer wave-lengths than for hydrogen.

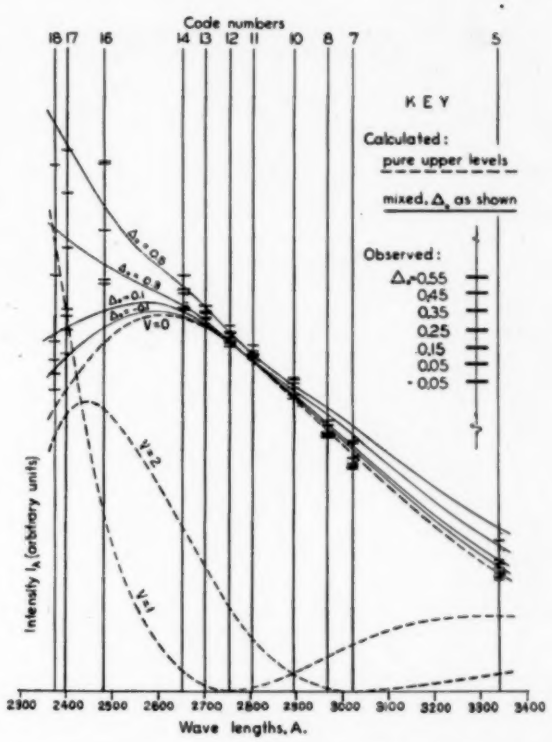

FIG. 2. Spectral energy distribution for hydrogen at various accelerating potentials. Dashed curves show theoretical distribution for pure vibrational levels. Solid curves show distributions calculated for the mixtures of levels produced at potentials $11.72+\Delta_0$ ev, with Δ_0 as indicated. Short horizontal lines show observed intensities at the wave-lengths of the standard mercury lines (indicated by code numbers) at potentials as indicated in the Key. For details see Table I. For normalization of curves, see text.

TABLE I. Relative intensities I_λ (in arbitrary units) calculated and observed for H_2 at various wave-lengths and values of Δ_0 (accelerating potential relative to the critical excitation potential for $v=0$, 11.72 v).

Code number	5		7		8		10		11		12		13		14		16		17		18	
Wave-length	3341		3023		2967		2894		2804		2758		2699		2654		2481		2400		2378	
Δ_0	calc.	obs.	calc.	obs.	calc.	obs.	calc.	obs.	calc.	obs.	calc.	obs.	calc.	obs.	calc.	obs.	calc.	obs.	calc.	obs.	calc.	obs.
−0.1	268	242	518	490	571	552	639	640	706	728	745	745	782	818	806	837	779	880	714	730	691	650
0.0	272	248	521	482	573	550	639	633	707	735	746	752	784	820	807	837	789	890	733	780	714	685
0.1	281	258	526	485	577	557	642	640	707	722	747	756	786	820	811	840	811	892	778	823	766	714
0.2	296	267	535	502	584	560	646	655	709	720	748	775	790	807	819	837	851	890	857	810	859	755
0.3	317	285	548	540	594	585	652	665	712	730	751	765	796	817	830	860	910	1000	970	960	991	900
0.4	336	326	560	534	603	560	657	677	717	730	756	777	807	833	848	870	971	1150	1078	1230	1115	1140
0.5	351	326	568	534	610	577	663	672	725	748	767	790	824	833	871	900	1033	1145	1172	1255	1218	1140
0.6	—		—		—		—		—		—		—		—		—		—		—	
0.7		335		540		582		662		740		825		905		913		1330		1405		1325
1.2		340		530		593		705		805		915		985		1080		1570		1615		1505
1.9		335		524		600		720		833		920		1055		1120		1590		1700		1580

TABLE II. Relative intensities I_λ (in arbitrary units) calculated and observed for D_2 at various wave-lengths and values of Δ_0 (accelerating potential relative to the critical excitation potential for $v=0$, 11.76 v.).

Code number	5		7		8		10		11		12		13		14		16		17		18	
Wave-length	3341		3023		2967		2894		2804		2756		2699		2654		2481		2400		2378	
Δ_0	calc.	obs.	calc.	obs.	calc.	obs.	calc.	obs.	calc.	obs.	calc.	obs.	calc.	obs.	calc.	obs.	calc.	obs.	calc.	obs.	calc.	obs.
−0.1	350	299	614	576	663	640	721	733	792	808	824	840	853	885	877	889	910	900	879	775	860	725
0.0	362	305	619	580	666	641	725	743	798	815	834	842	869	920	901	918	982	985	981	845	968	735
0.1	388	352	633	620	677	685	734	782	815	840	858	902	906	945	956	966	1141	1150	1204	1140	1204	1050
0.2	428	387	654	651	694	720	755	820	845	885	901	935	970	999	1049	1064	1388	1375	1544	1450	1564	1350
0.3	464	426	677	651	717	715	778	822	893	915	968	1028	1058	1130	1164	1218	1620	1830	1846	1900	1883	1740
0.4	491		702		748		821		969		1066		1178		1304		1810		2066		2115	
0.5	—	440	—	670	—	755	—	895	—	1070	—	1190	—	1335	—	1450	—	2120	—	2170	—	2030
0.7		443		693		792		983		1160		1320		1490		1585		2180		2400		2240
1.2		440		770		897		1065		1230		1355		1495		1575		2380		2520		2420
1.9		465		795		922		1105		1280		1420		1580		1670		2500		2310		2250

The detailed structure of the radiation predicted for various accelerating potentials is shown in Tables I, II, and Figs. 2, 3. (In these tables and figures the code numbers at the top refer to the wave-lengths of certain lines in the mercury comparison spectrum which was used in the experimental part.) In computing these values, the calculated values for the pure states were first carefully interpolated at the desired wave-lengths from large drawings of the theoretical curves and were then combined as explained. At the higher potentials there is considerable structure, due to contributions from the increasingly narrow maxima in the separate terms, which would be missed if the attempt were made to interpolate from the composite curves. In the figures, the first three pure state curves are shown for comparison, being merely copied from Figs. 2 and 3 of II. In calculating the composite curves, the increase in absolute intensity with increasing potential has been neglected in order to facilitate comparison; each curve has been scaled down by a factor such that the contribution from $v=0$ is exactly the same as shown for that pure state. The height of the curve above that for $v=0$ at any wave-length is therefore a direct measure of the contamination from other states, mostly from $v=1$. The vanishing of the latter at 2800A causes the first three curves for H_2 to coincide at this wave-length.

PRODUCTION OF RADIATION

The radiation to be studied was produced in a tube shown in Fig. 4, which also indicates the essential parts of the electrical connections. Electrons were drawn from an internally heated oxide cathode *c* in the form of a flattened tube 3 cm in length, mounted in an aperture in a supporting plate *s*, to which was attached the negative lead *2* common to both heating and electronic circuits. Heating current from the battery B_h, rheostat R, and ammeter A_h was led in at *1*, the cathode

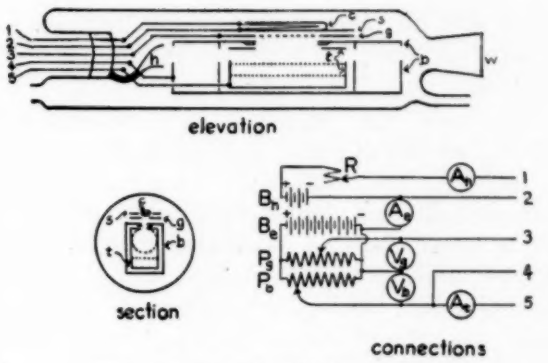

FIG. 4. Source of radiation studied.

being maintained at about 1100°K as determined by an optical pyrometer focused on one of the surface cracks in order to get the best approximation to blackbody radiation. The rate of electron emission, measured by the milliammeter A_e, was controlled by the accelerating grid *g*, maintained at a potential of about 7 v by means of the lead *3* from the battery B_e, potentiometer P_g, and voltmeter V_g. A portion of the electron stream entered the constant-potential box *b* by means of the double-walled slit, and passed down into the collecting trap *t*, the slit of which was wide enough to admit the total beam passed by the first slit. Box and trap were maintained at the same potential by means of leads *4* and *5*, respectively, from the potentiometer P_b and voltmeter V_b, this potential being varied from 14.6 v to 18 v (by the meter) during the course of the work. The microammeter A_t (in which the potential drop was negligible) served to measure the current to the trap, which was maintained at 25 microamperes by suitable slight adjustments of the grid potential. Within the trap were two gauze screens in order to assist in the capture of electrons.

Box and cage were provided with holes at the ends, permitting observation through the quartz window *w*, attached by a graded seal to the Pyrex tube which housed the assembly. Reflection at the rear was prevented by the internal black glass horn *h*. Except for the lead wires in the press, all metal parts were of nickel, and were thoroughly outgassed by induction heating in vacuum before measurements were made. In spite of this treatment, it was found impossible to get clean spectra except by constructing parts *2* and *3*, which ran hot during operation, of metal

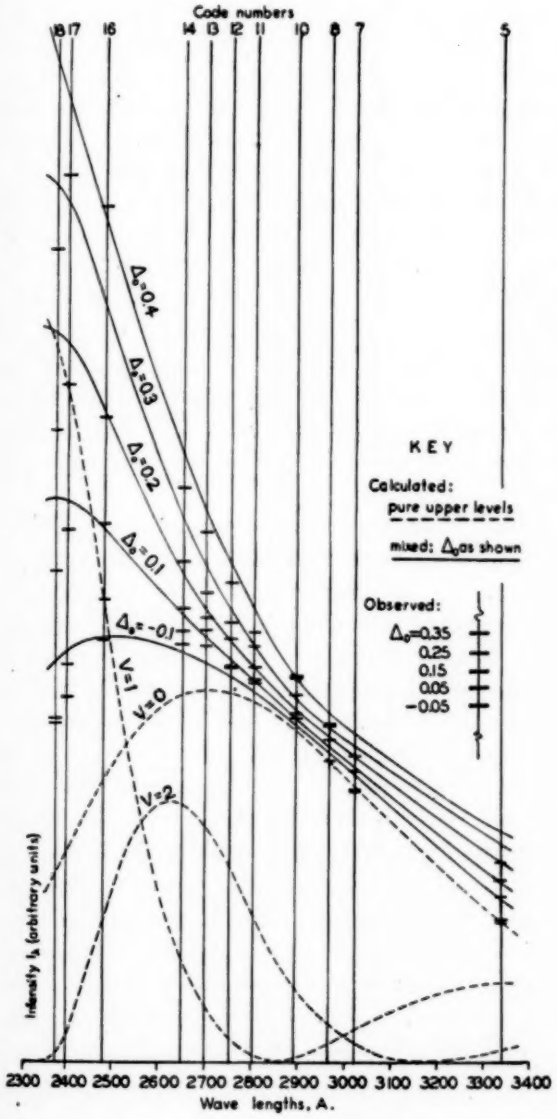

FIG. 3. Spectral energy distribution for deuterium at various accelerating potentials. Explanation as for Fig. 2, except that the potentials are $11.76+\Delta_0$ v. For details see Table II.

which had first been heated nearly to fusion for several minutes in hydrogen at atmospheric pressure.

The tube was operated in a continuously flowing stream of gas at a pressure of 0.015 mm of mercury. To provide this, commercial hydrogen or deuterium was drawn from a cylinder to fill a mercury-sealed gasometer holding about 300 cc, enough for two days' operation. From here it passed through a parallel pair of electrically heated palladium thimbles into a small space where the pressure was kept constant at about half an atmosphere by means of a barostat controlling the heating circuit of the thimbles. Although the current was carefully limited to the least value which would supply enough gas, the thimbles repeatedly failed through the development of small holes, and had to be repaired with gold solder or replaced. From the intermediate space gas leaked into the observation tube through a long fine capillary, and was continuously removed by a diffusion pump connected through a pinhole in a diaphragm, the capillary and pinhole being so matched as to maintain the desired pressure in the tube. Both entrance and exit connections passed through dry ice traps in order to exclude mercury vapor.

When deuterium was being used, a certain amount of water invariably collected in the jackets housing the palladium thimbles. The source could not be determined. According to the label on the cylinder, the deuterium had been dried over liquid air. At first it was thought that the moisture might come from the asbestos upon which the heating coils were wound, but the effect persisted in spite of vigorous preliminary heating and pumping. In the first experiments, hydrogen had been stored over water; but in the final work only the mercury gas holder was used, and no moisture appeared except when the gas was deuterium. Of course, no moisture could penetrate the palladium, and the only cause for concern was that if ordinary water was present from any source, the exchange reaction with deuterium might contaminate the latter with hydrogen.

MEASUREMENT OF INTENSITIES

The radiation was analyzed by photographic comparison with the standard mercury arc of Krefft, Rössler, and Rüttenauer,[6] and the use of a small Hilger quartz spectrograph. When the results were computed on the basis of the calibration of this standard given by Rössler,[7] irregularities appeared which strongly suggested errors in this calibration. A new calibration was therefore carried out, and did indeed lead to revisions in the expected directions. This work is reported in a separate paper,[8] and as many details of the method there described applied also to the work on the H_2 and D_2 spectra, only the special features of the latter need discussion here. These features arose, first, from the extreme feebleness of the spectra to be measured (due to the desirability of working at the lowest possible accelerating potentials), and second, from the fact that instead of sampling light from all parts of the source, as is necessary with the mercury standard, it was essential to isolate that emitted from a small region, namely, a thin horizontal slice across the electron beam, in order to minimize the effects of possible stray fields. Because of the proximity of metal surfaces or gauzes parallel to the line of sight through the observation space, any such fields would tend to be perpendicular to that line, and such a slice should constitute a very nearly equipotential region.

These two facts made it imperative to focus the source as well as possible upon the spectrograph slit and to perform the photometric analysis upon the dispersed image produced by light passing through a single short section of the slit, and hence originating in a single zone of the luminous beam. By use of an aluminum-sputtered concave mirror in order to avoid chromatic aberration, the edgewise view of the electron beam as seen through the window of the tube was focused so as to produce the maximum illumination in the spectrograph. To facilitate making this adjustment the radiation was temporarily made visible by raising the voltage until bright lines could be seen on looking through the instrument with an eyepiece. In order to make possible accurate location of the points at which the spectrographic image was to be measured, the

[6] H. Krefft, F. Rössler, and A. Rüttenauer, Zeits. f. tech. Physik **18**, 20 (1937).
[7] F. Rössler, Ann. d. Physik [5] **34**, 1 (1939).
[8] To appear in J. Opt. Soc. Am., hereafter cited as III.

slit was provided with an aperture plate sharply defining the portion exposed, and hence the breadth of the dispersed image. For the lowest voltages, the short wave portion was too feeble for accurate registration by this means. It was therefore arranged that by sliding the aperture plate in its ways, the portion of the slit used for the main exposure could be covered, and additional short sections just above and below could be exposed for a minute or two to strong radiation obtained by momentarily raising the voltage, thus producing two gauge marks on the plate whose relation to the main image was known once for all. To provide a wave-length scale, another short section of the slit was exposed to feeble mercury radiation, conveniently produced by holding in front of the slit an evacuated quartz tube containing mercury (actually one of the standard lamps) and operating an induction leak tester in the neighborhood. It was not necessary for an actual spark to jump.

Because of the absence of detail in the spectrum, it was permissible to operate with a slit width of 1 mm without perceptible error through loss of resolution. Satisfactory densities were obtained with exposures on Eastman 1–0 or 103–0 spectroscopic plates, ranging between one-half and two hours, according to the excitation voltage.

The comparison spectra were obtained with the standard mercury arc, essentially as described in III, except for modifications made necessary by the different character of the continuous source being measured. A very great attenuation was needed, and was obtained in part by using a narrow slit on the lamp house, and in part by providing the sector wheel with a second disk, geared to that in which the steps were cut and carrying an opening which exposed only one out of every sixteen of their transits across the slit. (In view of the prolonged exposure, the frequency of the flashes produced was still ample to prevent errors due to reciprocity failure.) No bromine filter was required, and the diffusing quartz disk could not be used because it would have prevented focusing of the hydrogen source. In order to secure a similar distribution of light entering the spectrograph, the radiation from the mercury source was reflected into the slit by the same mirror as used for hydrogen, but both source and mirror were placed so far from the slit as to form an image, acting effectively as a point source, about a meter in front of the slit. By mounting the mirror slightly askew on the end of a motor shaft, this point was spun out into a ring about 2 cm in diameter, thus providing the "narrow beam" type of illumination discussed in III.

The photometry was conducted essentially as in III, except that each hydrogen exposure yielded a single set of readings instead of a set of six. These readings were taken at wave-lengths corresponding to the mercury calibration points, and at points accurately located at a fixed fraction of the width of the image or of the distance between the gauge marks (which varied somewhat with the wave-length), in order to correspond to the same point in the slit and hence to the same portion of the luminous source. It was noticed that the intensity varied considerably along the length of the slit, particularly at the lower voltages. This could be due partly to spreading and extinction of the electron beam, but the dependence on voltage suggests the presence of some real inhomogeneity in the supposedly uniform potential space, which would naturally produce a greater relative variation in the intensity radiated near the critical potential than at higher potentials. In order to minimize errors due to faulty registration, the points chosen for analysis were selected close to the maximum of intensity with respect to the length of the slit.

Each plate carried two comparison exposures and a series of hydrogen or deuterium spectra obtained by stepping up the accelerating voltage. The comparison exposures were combined to plot a set of characteristic curves, as described in III, except that in order to accommodate the feeble intensities obtained for short wave-lengths and low voltages, it was necessary to extend the characteristic curves so as to include as much as possible of their initial non-linear portions. For this portion of the curves it was found convenient to use semi-log paper, thus in effect plotting the optical densities against the exposures themselves, as recommended by Tien Kiu,[9] rather than against their logarithms. An example of

[9] Tien Kiu, Comptes rendus **207**, 1394 (1938). The exposure was varied by varying time, not intensity.

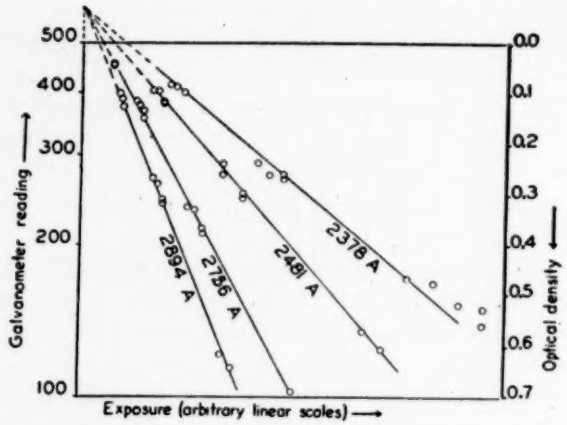

FIG. 5. Characteristic curves for small exposures at different wave-lengths. The abscissae are exposures on arbitrary scales, different for each wave-length. The scale on the left (logarithmic) shows the galvanometer reading of the densitometer, which is proportional to the light transmitted by parts of the plate receiving the exposure indicated. The reading 500 corresponds to unexposed emulsion. The optical densities (above fog) are shown by the linear scale on the right. When extrapolated back to zero exposure, the characteristic curves appear to radiate from a false zero of density.

such curves is shown in Fig. 5, and it will be seen that they are remarkably straight for densities between 0.1 and 0.5. Extrapolation to zero exposure appears to give a negative density (transmission greater than 100 percent), but this is, of course, only a convenient aid in drawing the usable portion of the curves; at very low exposures the actual curves bend over and tend to zero density. Since the ordinary logarithmic characteristic curves are practically straight at densities above 0.7, there is but a narrow range where neither form of plotting gives linear results, and since slight curvature does not interfere with accurate interpolation, there is considerable overlapping of the ranges in which the two methods are useful.

For the ordinary density range, the plates used developed to a contrast of about $\gamma=1.7$; this showed a tendency to increase with successive batches of plates supposedly of the same type of emulsion. This high contrast was undesirable in the present work, as it limited the useful range of exposures to about a ratio of 12 to 1. Attempts to reduce it by modifying the method of development lead to irregular results and were abandoned. It did not seem feasible to use plates with softer emulsions since none were available with the requisite high sensitivity in the ultraviolet.

To judge from internal evidence, the precision of the photometry was about 4 percent at either end of the range covered, and somewhat better for intermediate values.

RESULTS AND DISCUSSION

Before comparing the results of these measurements with the theory as developed above, it is necessary to consider whether there could be any appreciable modification of the distribution-in-energy of the electrons as a result of collisions with molecules. According to Brode,[10] in hydrogen at 1-mm pressure the number of collisions of all kinds made by an electron with a velocity of a few volts is of the order of 20 per cm of path. This corresponds to about one collision every 3 cm at the prevailing pressure of 0.015 mm; hence very few electrons can have made more than one collision. Because of the disparity in mass, the energy lost in an elastic collision is negligible; the same applies to any collision producing only rotational excitation, while any vibrational or electronic excitation would remove so much energy that the electron could not take part in any further production of radiation. It seems safe to neglect the effects of previous collisions.

In order to apply the theory, some method of determining the actual accelerating potential must be found—it is notorious that the reading of a meter connected between cathode and collector may be in "error" by several volts because of the effects of contact potentials, space charges, and ohmic drops, some of which are highly inconstant and difficult to determine. It seemed best to make this determination from internal evidence in each series of exposures, and to assume that the corrections would not change appreciably during the few hours required for a single series. This was done on the basis of the theoretical apparent excitation function, giving the relation between the true accelerating potential and the intensity of radiation from a particular vibrational level at a given wave-length. It happens that in the spectrum from $v=1$ there is a region of zero intensity, falling at the

[10] R. B. Brode, Phys. Rev. **25**, 636 (1925).

wave-length of line 12 for H_2 and near that of line 10 for D_2. (See Figs. 2, 3.) Hence, at these wave-lengths the entire radiation comes from $v=0$ until the voltage is raised sufficiently to excite $v=2$. This permits a direct test of the form of the apparent excitation function for $v=0$. On plotting the logarithm of the observed I_λ against the voltmeter reading, a curve should be obtained which can be brought into coincidence with the theoretical curve of log R_0 against Δ_0 by suitable vertical and horizontal displacements. It is thus possible to determine what voltmeter reading corresponds with $\Delta_0=0$, that is, with true potential equal to critical potential for $v=0$. Since the latter is known from spectroscopic evidence to be 11.72 v for H_2 and 11.76 v for D_2, the voltmeter correction can be determined at once.

The application of this device is shown in Fig. 1. Points indicated by the same symbol represent a single series of exposures, plotted so as to secure the best possible correspondence with the theoretical curve. The horizontal displacements used represent corrections of from -3.28 v to -3.45 v. It will be seen that below $\Delta_0=0.1$ there is satisfactory agreement with theory and that a horizontal displacement differing by 0.1 v would lead to a definitely poorer fit. The fact that the observed points lie too low for larger positive Δ_0 is entirely to be expected since it is known that the true excitation function for a triplet state rapidly drops below the linear form which was assumed in constructing the present theoretical curve, the linear form holding only for a few tenths of a volt. It seems safe to conclude that the value of the true potential was known relative to the critical potential for $v=0$ to within 0.1 v. The absolute value of this critical potential was not determined directly. But in some preliminary experiments the voltage was run up until certain identifiable lines of the molecular spectrum appeared, and it was verified that the voltmeter readings at which these lines and the continuum, respectively, first appeared were consistent, within 0.1 v, with the spectroscopically known excitation energies of the states concerned.

When interpreted in this way, each exposure furnished a set of relative values of the radiation intensity I_λ (in the notation of III) at eleven selected wave-lengths produced at a known accelerating potential. It was found that considerable variation occurred in the actual intensities obtained in different exposures even at the same accelerating potential, but this did no harm, as only the ratios are given by the theory. For comparison with theory, the results of each exposure were multiplied by an arbitrary constant so selected as to bring the average of the intensities between 2700A and 3000A into good agreement with the calculated values. Some sixty exposures were analyzed, but a complete presentation of the results would be needlessly

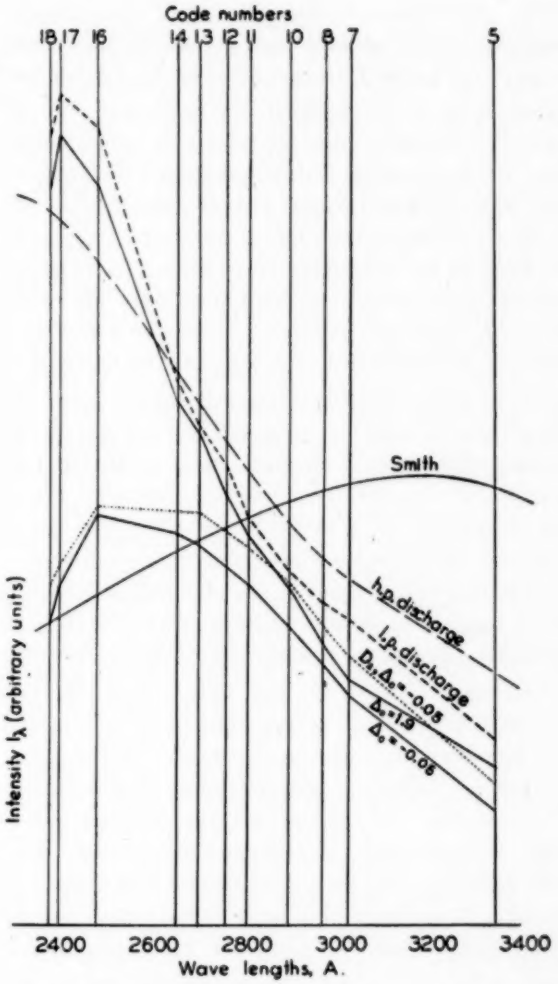

FIG. 6. Hydrogen and deuterium spectra produced under various conditions. All data are for H_2 except the curve marked D_2. The curves marked $\Delta_0=-0.05$ and $\Delta_0=1.9$ are from the data of Tables I and II. The l.p. discharge curve is from measurements on a low pressure discharge lamp. The h.p. discharge curve is given by Chalonge for a lamp with pressure 35 mm. Smith's curve is for a discharge in the presence of helium.

bulky, and some condensation by averaging is necessary. In Tables I and II the entries under "calc." are each the average of several exposures which have been individually analyzed and adjusted as described and for which the accelerating potentials have been determined to lie between the two tabulated round values indicated by the position of the entry. Thus, the first entry is the average of six exposures for which Δ_0 was determined to lie between -0.1 and 0.0. The same data are represented in Figs. 2 and 3 by short horizontal lines drawn across the vertical lines showing the selected wave-lengths. Unfortunately it did not seem possible to indicate the values of Δ_0 on the figures; in general, they increase by tenths from -0.05 for the lowest short lines to 0.55 (Fig. 2) or 0.35 (Fig. 3) for the highest, but there are some transpositions as the tables show. Above these voltages there is little reason to expect the theoretical values to be valid, because of breakdown of the assumption of a linear excitation function. No calculated values are therefore given, and the normalization of the observed values is entirely arbitrary.

For purposes of comparison, the data for H_2 and for D_2 at the lowest potential used ($\Delta_0=-0.05$) are shown together in Fig. 6, in the form of broken lines drawn between successive experimental points. There are also included the data for H_2 at the highest potential ($\Delta_0=1.9$), and a set of points obtained with a conventional hydrogen discharge lamp having a narrow capillary tube with gas at a fraction of a millimeter pressure and operating at about 50-ma current. In addition, there are included a curve given by Chalonge[11] for a discharge at 35-mm pressure, and the curve determined by Smith in the presence of helium.

On the whole, the present experimental results are in gratifying agreement with theory, both with respect to the form of the spectral distribution curves for low Δ_0, where it is almost pure radiation from $v=0$, and with respect to the magnitude and character of the contamination from higher levels when Δ_0 is increased. The differences between H_2 and D_2 are also in good accord with theory, the maximum for D_2 being at longer wave-lengths, as shown in Fig. 6 of II (the fact that the curves cross in that figure, but not in Fig. 6 of the present paper, has no significance, as the normalizations are different). The disturbing discrepancy between our calculations and Smith's results can be definitely set aside as due to some unknown source of error in the latter. It seems possible to assert that the essential correctness of the basic theory of molecular spectra has been experimentally established by a direct test.

It must, however, be admitted that the results leave something to be desired, with respect both to self-consistency and to agreement with theory. On the first score, the irregular spacing and occasional inversion of the data for a single wave-length and varying accelerating potential indicate that the conditions of production or analysis of the radiation have not been sufficiently well controlled. Particularly at the short wave end, where the effects of contamination by higher vibrational levels are most serious and most sensitive to variations in the potential, the results must be regarded with some suspicion. Above 2500A the data are more nearly self-consistent, but there appears to be a small systematic discrepancy as compared with theory, the observed curves being a little steeper than the calculated. Until more accurate data are forthcoming, it does not seem worth while to speculate as to possible explanations of the discrepancy.

It is interesting to note that the spectral distribution for $\Delta_0=1.9$ is already practically the same as for the several thousand volts in the low pressure discharge, except at the longest wave-length measured.

[11] D. Chalonge, Comptes rendus **192**, 1551 (1931).

Letters to the Editor

PROMPT publication of brief reports of important discoveries in physics may be secured by addressing them to this department. The closing date for this department is the third of the month. Because of the late closing date for the section no proof can be shown to authors. The Board of Editors does not hold itself responsible for the opinions expressed by the correspondents. Communications should not in general exceed 600 words in length.

Thixotropy in Silver Amalgams

DOUGLAS RENNIE HUDSON
Heriot-Watt College, Edinburgh, Scotland
March 25, 1944

SILVER and mercury form two well-defined intermetallic compounds, approximately AgHg and Ag_3Hg_4, by peritectic reactions at 276° and 127°C. For each lattice the range of stability is small, about ½ percent Ag_3Hg_4—the alchemists' *Arbor Dianae*—is also obtained by action of either ion in solution on the other element. Further, it exists as a mineral amalgam (*argental* or *landsbergite*) in beautifully formed crystals in the cubic system. In dentistry it is formed in the setting of tooth stoppings by the reaction [Black (1896), Troiano (1938)]

$$Ag_3Sn + Hg \rightleftarrows Ag_3Hg_4 + Sn(Hg)$$
filings liquid dendrites solid solution.

Since the only trustworthy data regarding the densities of silver amalgams are those of Maey (1905), these were redetermined. This investigator concluded that up to 35 percent silver, the density varied little from that of pure mercury. The present results are more consistent among themselves and are believed to be more accurate. There are small but definite peaks at 15 percent and 28 percent silver on the density/composition curve. The plot specific volume/composition consists of straight lines intersecting at minima at 13 percent and 25 percent; consequently the partial specific volumes are constant for both components over corresponding ranges of composition (see Table I). The densities of all heterogeneous alloys are consistently above the values calculated for a conglomerate by summation of volumes.

PHYSICAL CHARACTERISTICS OF THE AMALGAMS

The solubility of silver in mercury is only 0.03 percent at room temperature, and above this the amalgams are heterogeneous, but up to about 8 percent silver they are quite fluid. Between 8 percent and 20 percent they are plastic on formation but "set" on standing overnight; above 20 percent they are remarkably rigid in the set state. By very gentle handling it was found possible to use Archimedes' method for determining specific gravity down to 13 percent silver; below this a specially blown s.g. bottle was used successfully.

THE SOLID PHASE

The maximum silver content attainable by expulsion of the liquid phase under pressure was found in two separate determinations to be 27.43 percent and 27.72 percent, in good agreement with previously published values. This is about halfway between $(Ag_3Hg_4)_4$ 28.74 percent suggested by Weryha, and $(Ag_2Hg_3)_{10}$ 26.4 percent by Berman and Harcourt, both from x-ray data. Preston guardedly indicated $(Ag_{10}Hg_{13})_2$ to correspond with the phase identified by Murphy by microscopical technique, but Westgren favoured a γ-brass structure. The corresponding Hume-Rothery composition $(Ag_5Hg_8)_4$ 25.14 percent is unequivocally excluded by metallographic, mechanical, and radiological results.

TABLE I.

Range (Percentage silver)	Partial specific volmue Silver	Mercury
0 –13	0.0771	0.0736
13 –15	0.0423	0.0790
15 –16.7	0.1690	0.0566
16.7–20.7	0.1053	0.0798
20.7–25	0.0858	0.0711
25 –28	0.0400	0.0865
Over 28	0.0980	0.0640

SETTING

Above 8 percent the amalgams set like plaster of Paris, but the process is really very distinct, being reversible by pressure alone. During setting, hardness gradually increases, the very robust mass which the 20 percent analgam yields on setting becomes perfectly fluid on kneading. The process is a remarkable exhibition of thixotropy; a well-defined réseau of acicular crystals is formed and becomes degraded readily under local pressure. As a result of its high surface energy, liquid mercury is held very tenaciously in the sponge but in the lower amalgams some liquid will appear as Fig. 1A shows for an amalgam with about 8 percent.

EFFECT OF SETTING ON DENSITY

Setting is accompanied by a drop of 1–1½ percent in density in a few days. In one extreme case a 15 percent amalgam which had stood undisturbed for over two years segregated into hard discrete lumps immersed in fluid argentiferous mercury. Hard grinding was required to

A B

FIG. 1. An amalgam containing approximately 8 percent mercury in the set and fluid states. (A), Set, showing liquation of liquid mercury from the dry spongy réseau. (B), Liquified by shaking the bottle

restore this to the plastic state in which the density was found to be normal and as much as 4 percent greater than in the (pea plus liquid) state. This complete segregation is regarded as the extreme attainable in thixotropic setting.

EQUILIBRIA

Two explanations are suggested. 1. That pressure causes Murphy's peritectic reaction at 127°C to go leftward $\beta+Hg\rightleftarrows\gamma$ or very nearly

$$3AgHg+Hg\rightleftarrows Ag_3Hg_4.$$

2. That the réseau consists of a new intermetallic species, formed on standing and restored under pressure to the Ag_3Hg_4 originally present. This might be either the same phase (27.7 percent silver) in a new space-lattice with different physical properties, or a new intermetallic compound, possibly richer in mercury.

DENTAL AMALGAMS

The unexpectedly low density of the structure (spongy réseau plus liquid mercury) accounts very happily for the paradoxical expansion of dental stoppings too rich in silver—a sharp change in setting characteristics occurs at 25.5–26 percent silver. This phenomenon has long been known but has hitherto been a bugbear in any theory of setting. *Faute de mieux*, Troiano and Gayler have both accepted the void formation theory formulated by Gray. However, in the 15 percent amalgam described, in which thixotropy had proceeded to the extreme, the measured 4 percent difference in density would require an unoccupied volume of as much as one-eighth in the peas. In view of their hardness and jagged characteristics this is absurd.

Sullivan's copper amalgam formerly used in dentistry was plastic when excess mercury had been squeezed out, but in a few hours set hard and could then be rolled or hammered. On kneading or heating the mass recovered its plasticity.

THIXOTROPY AND OTHER ANOMALOUS PROPERTIES OF AMALGAMS

It is formally suggested that other anomalous properties of amalgams of the alkalies and other metals which have been reported (*e.g.*, viscosity, surface tension, electrical conductance) may also be attributable to thixotropy.

It is hoped to publish a detailed account of the experimental work shortly in *Metallurgia*.

Erratum: Influence of Pressure on Intermetallic Diffusion

[Phys. Rev. 65, 62A (1944)]

F. J. RADAVICH AND R. SMOLUCHOWSKI
General Electric Company, Schenectady, New York

IN accord with the contents of the presented paper, the last sentence of the abstract should read: "Also at 7000 kg/cm² no definite change was found although at lower concentrations, the depth of penetration was slightly decreased."

Magnetic-Dipole Transitions in the Configurations $5p^5$, $5p^4$, and $6p^5$ of Xenon and Radon*

BENGT EDLÉN
Physics Institute of the University, Upsala, Sweden
March 20, 1944

IN the course of a recent examination[1] of existing data on rare-gas spectra, it was found (as shown in Table I) that three unidentified lines in the tables[2] for Xe I and Xe II correspond to transitions between the series limits of these spectra. The perfect wave-number agreement with the ground-level separations of Xe II and Xe III as obtained from the extreme ultraviolet spectrum[3] leaves no doubt as to the reality of the coincidences. Because of the low energy of the levels involved, it is natural that these Xe II and Xe III transitions have been experimentally referred to Xe I and Xe II, respectively. The lines are due to magnetic-dipole transitions, the theoretical probability[4] of which is shown in the last column of Table I.

TABLE I.

Configuration	Transition	Int. and wave number	Trans. prob.
Xe II $5p^5$	$^3P_{1\frac{1}{2}}-{}^3P_{\frac{1}{2}}$	(4) 10537.01	21 sec.$^{-1}$
Xe III $5p^4$	$^3P_2-{}^3P_1$	(1) 9794.6	19 sec.$^{-1}$
	$^3P_2-{}^1D_2$	(6) 17098.97	21 sec.$^{-1}$
Rn II $6p^5$	$^3P_{1\frac{1}{2}}-{}^3P_2$	(5) 30895.1	531 sec.$^{-1}$

The transitions $^3P_1-{}^1S_0$ of $5p^4$ cannot be found in the Xe II table,[2] which is surprising, since its calculated transition probability is considerably higher than that of the two actually observed lines and the analogous transition in $4p^4$ has been observed by Ruedy and Gibbs[5] as a rather strong line in selenium. The line might have been referred to Xe III, however, for which no complete line table has been published. Another possible explanation for its absence might be an incorrect locating of the ^1S level.

Radon is the only rare gas besides xenon where the p^5 transition falls within the observable spectral range. In this case the level separation is not accurately known since Rn II is still unanalyzed. However, an approximate value around 31,000 cm^{-1} was indirectly deduced[1] from a certain perturbation in the observed md_6 series of Rn I. As the transition probability is proportional to ν^3 one would expect a relatively intense line in radon. These arguments immediately suggest an identification (Table I) with the radon arc line observed by Rasmussen[6] at ν30895, the only unidentified line of that spectrum. This identification might become of importance as the clue to the analysis of Rn II.

* Dr. P. Swings has asked that the following remark be published: "A faint unidentified emission line has been observed by A. B. Wyse [Astrophys. J. 95, 356 (1942)] at λ5847 in the Orion nebula. It is very probably the forbidden transition $^3P_2-{}^1D_2$ of Xe III."

[1] Some results of this examination have already been published in Arkiv f. Mat. Astron. Fysik, **A29**, Nos. 21 and 32 (1943).

[2] C. J. Humphreys and W. F. Meggers, Bur. Stand. J. Research **10**, 139 (1933); C. J. Humphreys, Bur. Stand. J. Research **22**, 19 (1939).

[3] J. C. Boyce, Phys. Rev. **49**, 730 (1936).

[4] Cf. G. H. Shortley, L. H. Aller, J. G. Baker, and D. H. Menzel, Astrophys. J. **93**, 178 (1941), and references there; cf. also discussion of coronal lines by B. Edlén, Zeits. f. Astrophys. **22**, 30 (1942).

[5] J. E. Ruedy and R. C. Gibbs, Phys. Rev. **46**, 880 (1934).

[6] E. Rasmussen, Zeits. f. Physik **62**, 494 (1930); **80**, 726 (1933).

Note on the Spectrum of N_2

R. E. WORLEY
Department of Physics, University of California, Los Angeles, California
March 11, 1944

IN a recent article[1] on the ultraviolet spectrum of N_2, smaller letters $i, j \ldots v$ were used by me to designate a number of u-type singlet states, reached by absorption from $X\,{}^1\Sigma_g^+$. I have learned that prior to publication of this article, Gaydon[2] reported to the Royal Society several g-type singlet states (found in transitions to $a\,{}^1\Pi_u$), in the same high energy range, and that he used some of the same letters to designate them. In order to avoid confusion, Dr. Gaydon and I are agreed that it would be desirable in the future to affix primes to those states of g symmetry where duplication has occurred. Elsewhere, we plan to list the singlet states, in the revised notation.

I take this occasion to correct an error in Table V of my article. Opposite $J_P=12$ of the band $\lambda 991.87$, the wave number should read: 100,698.3. Such other errors as have been noticed are minor.[3] However, as reference 62 may be misleading, it is again emphasized that the potential curves of Fig. 4 are only approximate.

As a plausible explanation for Hopfield's Rydberg series in emission, I suggested[1] that the upper levels may be of a hybrid $^3\Sigma$ type, corresponding to $3pns\,{}^3P_u$ terms in Si I, and remarked upon the possibility of transitions between these states and known triplet states of N_2. However, as the proposed terms would be of type $^3\Sigma_u^+$, only transitions to $B\,{}^3\Pi_g$ are anticipated, and the strongest bands would lie in the far ultraviolet. I have examined Kaplan's[4] unassigned bands ($\lambda\lambda 2100$–2700) to see whether any might be attributed to the proposed new levels and to some heretofore unknown levels, but it appears that no definite conclusion can be drawn without a more precise determination of his wave-lengths.

[1] R. E. Worley, Phys. Rev. **64**, 207 (1943).
[2] A. G. Gaydon, Proc. Roy. Soc. **A182**, 286 (1944). Professor Kaplan kindly loaned me a copy of the manuscript sent him by Gaydon.
[3] On p. 210, column 3, the final digits of entries 13 and 22 should be inferior. For footnote 34, read "Cf. ref. 21 (b), §F3." On p. 219, third line from foot of column 1, read "$a \leftarrow X$."
[4] J. Kaplan, Phys. Rev. **46**, 534, 631 (1934).

Note Concerning the Multiple Production of Penetrating Secondary Cosmic Rays in Lead

WAYNE E. HAZEN
Department of Physics, University of California, Berkeley, California
March 13, 1944

IN an earlier letter and again in a recent paper,[1] it was mentioned that there are many cloud-chamber photographs which indicate a multiple production of penetrating particles by cosmic-ray neutrons and protons, but that none of the photographs indicates a "cascade" process. Therein lay an apparent contradiction to the theory of Hamilton, Heitler, and Peng.[2]

However, Jánossy[3] has since shown that the theory of HHP gives such a large cross section for the production of mesotrons in collisions between fast protons or neutrons and a nuclear particle that several mesotrons will almost certainly be emitted in the traversal of a single heavy nucleus such as lead. If the fast neutron or proton has an energy $\leq 2\times 10^{10}$ ev, it is highly probable that essentially all of its energy will be dissipated in traversing a single lead nucleus. Therefore the above-mentioned photographic observations are in essential agreement with the theory of HHP if we assume that no protons or neutrons with energies much greater than 2×10^{10} ev traversed the lead plates during a photographed expansion.

[1] W. E. Hazen, Phys. Rev. **64**, 257 (1943); Phys. Rev. **65**, 67 (1944).
[2] Hamilton, Heitler, and Peng, Phys. Rev. **64**, 78 (1943).
[3] L. Jánossy, Phys. Rev. **64**, 345 (1943).

A New Representation of Types of Nuclear Forces

MARIO BUNGE
Instituto de Física, Facultad de Ciencias Físicomatemáticas, La Plata, Argentina
March 15, 1944

IN the ordinary representation of nuclear forces, due to Heisenberg, Majorana, and others, two new features appear: the fact that nuclear forces depend, already in non-relativistic approximation, essentially on the particle spin; and the introduction of a new independent variable called "isotopic spin," represented by a set of three operators τ_ξ, τ_η, τ_ζ.

We shall show here that the physical meaning and, in particular, the spatial symmetry properties of a system of nuclear particles, can be put in evidence by a representation which considers spin and isotopic spin to be components of a single, tetravalent variable. Indeed, four possible quantum states of the nucleon have to be considered already in non-relativistic approximation. In order to deal with these four possible states, we have to use operators represented by matrices of four rows and columns which are, *formally*, identical with the ones used in Dirac's electron theory. Correspondingly, we shall describe a nucleon by a spinor of four components

$$\psi^1=\psi_p{}^\alpha, \quad \psi^2=\psi_p{}^\beta, \quad \psi^3=\psi_n{}^\alpha, \quad \psi^4=\psi_n{}^\beta$$

where α and β refer to the two spin directions, p = proton, n = neutron. In terms of Dirac's notations, there are 16 linearly independent matrices

$$1,\ \beta,\ \tau,\ i\beta\tau;\ \boldsymbol{\alpha},\ i\boldsymbol{\gamma},\ \boldsymbol{\sigma},\ \beta\boldsymbol{\sigma} \qquad (1)$$

where τ stands for $\frac{1}{3}(\boldsymbol{\alpha}\boldsymbol{\sigma})$. The spatial transformation properties of these quantities may be derived from the fact that the operator describing the kind of the particle is a scalar quantity, while the spin operator $\boldsymbol{\sigma}$ represents an axial vector.

The operators (1) permit one to form the following scalar expressions, symmetrical in two particles, which commute with the total kind $(-{}^1\beta-{}^2\beta)$:

$$\begin{gathered} {}^1\mathbf{1}\cdot{}^2\mathbf{1};\quad {}^1\beta\cdot{}^2\beta \\ {}^1\boldsymbol{\sigma}\cdot{}^2\boldsymbol{\sigma};\quad {}^1\beta{}^1\boldsymbol{\sigma}\cdot{}^2\beta{}^2\boldsymbol{\sigma} \\ \tfrac{1}{2}(1-{}^1\beta{}^2\beta)\cdot{}^1\tau{}^2\tau;\quad \tfrac{1}{2}(1-{}^1\beta{}^2\beta)\cdot{}^1\boldsymbol{\alpha}{}^2\boldsymbol{\alpha}. \end{gathered}$$

In this notation, the isotopic spin no longer appears explicitly in Heisenberg's and Majorana's operators,

$$P^H = \tfrac{1}{2}(1 - {}^1\beta \cdot {}^2\beta) \cdot {}^1\tau \cdot {}^2\tau$$
$$P^M = \tfrac{1}{2} \cdot P^H + \tfrac{1}{2}(1 - {}^1\beta \cdot {}^2\beta) \cdot {}^1\alpha \cdot {}^2\alpha.$$

This representation of nuclear forces, however, does not furnish an indication how to obtain a relativistic generalization of our formulae. In particular, it does not show whether a relativistic theory of the nucleon can be built without introducing four more states (antiproton and antineutron).

The Retraction of Stretched Rubber

R. B. STAMBAUGH
Goodyear Research Laboratories, Akron, Ohio
March 31, 1944

FOR some time we have been making measurements of the velocities acquired by rubber strips when retracting after being stretched. The rubber band is stretched in front of two photo-cells, cutting off two sharply focused light beams. When the strip is released, the beams impinge successively on the photo-cells, the first of which starts the charging of a condenser, and the second of which stops the charging current. The resulting voltage on the condenser is thus a measure of the time required for the free end of the rubber strip to traverse the distance between the two light beams. Retraction velocities of the order of several hundred miles per hour have been observed.

To explain some of our results and to secure a more detailed picture of the mechanism of retraction, we have also taken pictures of retracting rubber strips with a high speed stroboscopic lamp. These seemed to be of sufficient general interest to present here.

Parallel, equidistant lines were ruled across the strips before they were stretched. The spacings of these lines were then measured in the photographs of the retracting strips to study the local elongation at any point during the retraction.

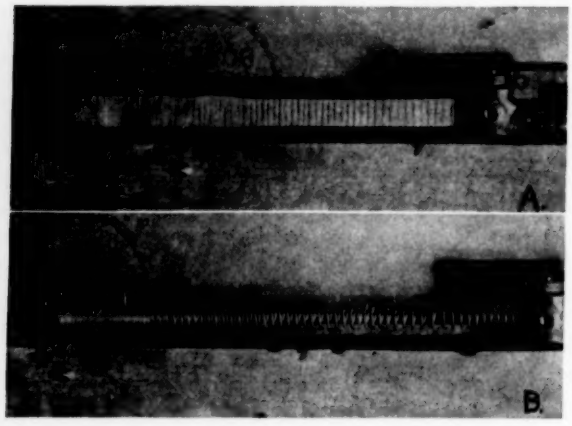

FIG. 1. High speed photographs of a freely retracting rubber strip and a steel spring. *A*, Hevea gum stock; *B*, steel spring.

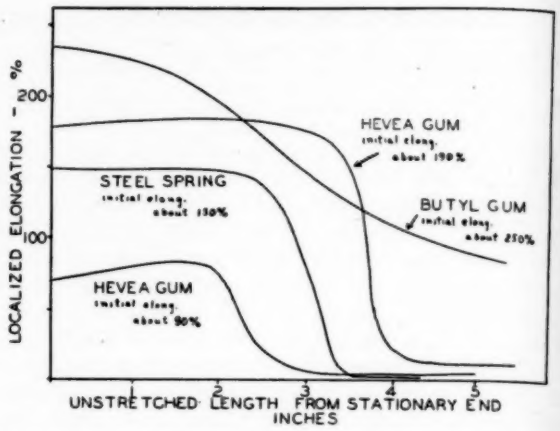

FIG. 2. Curves showing the wave front for free retraction. Local elongation obtained from photographs plotted against the normal length.

The photographs show that a rubber stock having low internal friction, such as a Hevea rubber cured gum stock, retracts very much like a steel spring. The retraction starts at the released end and progresses in a wave until it reaches the stationary end. This effect is shown in the photographs of Fig. 1 and also by the measurements of local elongation taken from the photographs which are plotted in Fig. 2.

It is interesting to note that the sharpness of this retraction wave front is dependent on the internal friction of the elastic material. Butyl rubber gum stock shows practically no wave front but merely a progressively lower elongation along the strip.

It is planned to publish a complete description and the results of the experiments at an early date.

The Method of Shower Anticoincidences for Measuring the Meson Component of Cosmic Radiation

VIKRAM SARABHAI
Department of Physics, The Indian Institute of Science, Bangalore, India
March 4, 1944

THE meson intensity measured in counter experiments where absorbers are used to filter out the soft electronic component refers only to fast mesons. The slow mesons which get cut out by the absorber can so far be estimated only indirectly, as, for instance, by the method adopted by Auger[1] and Greisen.[2] There is evidence, however, that the proportion of slow mesons increases rapidly with altitude, and it would be of great advantage if there were a direct method for measuring the total meson intensity. Bhabha[3] has recently suggested on grounds of reducing the weight of lead carried by balloons measuring the meson intensity in the stratosphere that the production of secondaries by the electronic component can be used to advantage in cutting them out. But this principle could be used for the more important purpose of bringing for the

first time the slow mesons in the field of direct experimental observations. While a great proportion of cosmic-ray electrons in the atmosphere are already associated with other ionizing particles, the number so associated can be increased by a lead plate of thickness corresponding to the maximum of the Rossi curve. By means of an anti-coincidence arrangement working along with a vertical counter telescope, it is possible to exclude events in which associated particles arrive in the telescope. This can be done with side anticounters arranged as shown in Fig. 1a, but here the main cone of measured radiation is not utilized for detecting the showers and those that are generated in the lead above on account of their narrow angular spread might avoid detection. The actual arrangement used is shown in Fig. 1b, where the sets of counters II and III are used to register the showers. A shower coincidence II, III gives rise to an antipulse which is fed to the coincidences of the main telescope formed by counters I, IV. The lead placed in position X is to increase the associated soft particles, and the lead placed in position Y is to study the absorption of the radiation without interfering with the efficiency of shower anticoincidences. The basic circuit used has been shown in Fig. 1c.

Preliminary results obtained with this arrangement of the total intensity given by coincidences I, IV and the meson intensity given by shower anticoincidences I, IV —(II, III) at various altitudes up to 13,900 ft. in Kashmere illustrate the working of the arrangement. Figure 2 shows the absorption curve at two altitudes of these two counting rates with lead placed at positions X and Y. The difference

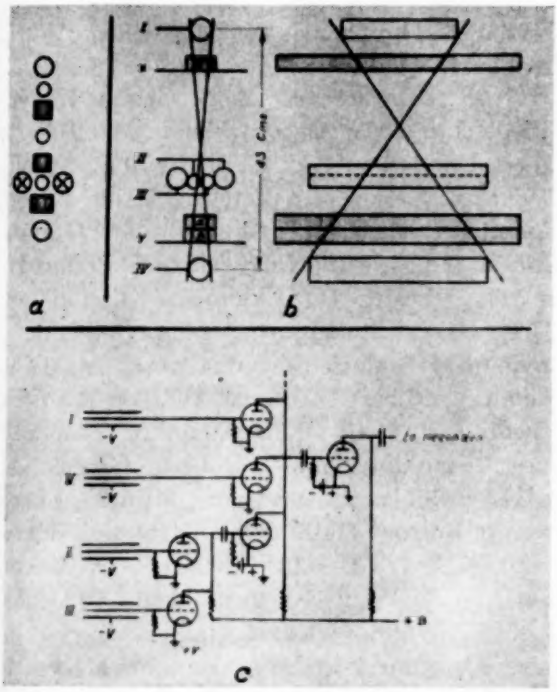

FIG. 1. (a) Arrangement showing anticounters outside the main cone of measured radiation. (b) Arrangement used for measuring shower anticoincidences. (c) Basic circuit for registering shower anticoincidences.

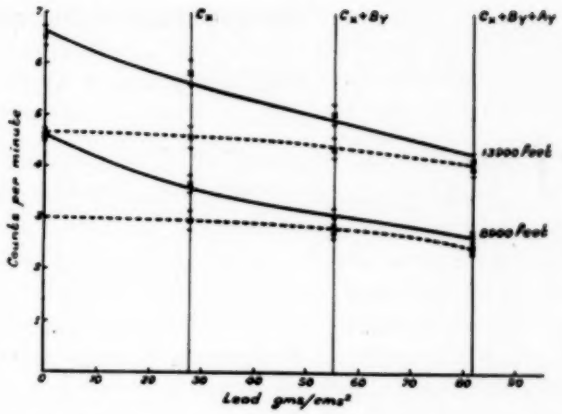

FIG. 2. Curves showing for two altitudes the absorption of the total intensity measured by coincidence rate I, IV (full lines) and the meson intensity measured by shower anticoincidence rate I, IV–(II, III) (broken lines).

between the two curves diminishes rapidly with increasing thickness of lead absorber as the electronic component gets progressively absorbed; and while the slope of the total intensity curve increases with diminishing thickness of lead, the slope of the meson intensity curve varies in an opposite direction. The tendency of the shower anti-coincidence curve to become horizontal for zero thickness of lead is a striking indication of the fact that it measures chiefly the meson intensity. The altitude intensity curves from readings at 4 elevations in Kashmere at geomagnetic latitude 25°N show that above 10,000 ft. the meson intensity increases less rapidly than the total intensity and the atmospheric shower intensity. At 13,900 ft. the proportion of mesons was 64 percent, of which about 18 percent consisted of slow mesons, but the accuracy of these estimates is not high. A full report of the results obtained at Kashmere and repeated with the same arrangement at Bangalore will appear shortly.[4]

The errors in this experiment might be due to three causes. Firstly, due to the contribution of side showers to the double coincidences that were measured. This would give an underestimate of the proportion of electrons. Secondly, due to electrons of low energy which do not produce large enough showers to be detected and cut out by the anticoincidence arrangement, and lastly, due to mesons which are associated by other mesons or knock-on electrons and which get cut out by the anticoincidence arrangement. These two errors will tend to give an over-estimate of the proportion of slow mesons. With the help of an accurate experiment that is now being performed with quadruple coincidences measuring the vertical intensity, it is hoped to correct for these errors.

I am indebted to Professor C. V. Raman for support and assistance, and to Professor Bhabha for helpful discussions. The Kashmere trip would not have been possible but for the willing help given by the state officials and friends.

[1] P. Auger, Phys. Rev. **61**, 684 (1942).
[2] K. Greisen, Phys. Rev. **63**, 323 (1943).
[3] H. J. Bhabha, Proc. Ind. Acad. Sci. (A), in press.
[4] V. Sarabhai, Proc. Ind. Acad. Sci. (A), in press.

Proceedings of the American Physical Society

Meeting in New York City, January 14–15, 1944

THE 259th meeting of the American Physical Society, being the "1943 Annual Meeting," was held at Columbia University in New York City on Friday and Saturday, January 14 and 15, 1944. Meetings of the American Association of Physics Teachers and of the newly-organized Electron Microscope Society of America were held conjointly, and we to some extent subordinated our programme to theirs, arranging for ourselves only the Retiring Presidential Address and two sessions of contributed ten-minute papers. We were co-sponsors of the Symposium on Training Programmes for Army and Navy Personnel in the Field of Physics, but the entire credit for arranging this important and successful affair belongs to the A.A.P.T. Three hundred and forty people registered at the desks shared by the three societies and the dinner was attended by as many as the Columbia University Faculty Club could accommodate, two hundred and sixty-three. Regrets are expressed to those who could find no place at the dinner, and grateful acknowledgments for his work in arranging rooms and services for the meetings to Professor H. W. Farwell, Chairman of the Local Committee.

At the business meeting of the Society the tellers of election (W. H. Crew and S. A. Korff) reported the election of the following candidates for the stated offices and terms:

A. J. Dempster, *President*, 1944.
Harvey Fletcher, *Vice President*, 1944.
K. K. Darrow, *Secretary*, 1944.
G. B. Pegram, *Treasurer*, 1944.
J. T. Tate, *Editor*, 1944–1946.
A. C. G. Mitchell, H. B. Wahlin, *Members of the Council*, 1944–1947.
J. W. Beams, V. Rojansky, F. Seitz, *Members of the Board of Editors*, 1944–1946.

The business meeting was followed by the Retiring Presidential Address, "Physics in Industry," by A. W. Hull and by the (third) Richtmyer Memorial Lecture of the American Association of Physics Teachers, "The Future of Physics, Past and Present," by K. K. Darrow.

The Council met on Thursday evening, January 13, and elected to fellowship the six candidates and to membership the eighty-three candidates whose names are appended. The Council, acting on a report from the Organizing Committee of the Division authorized at its Evanston meeting, adopted for this new division the name "Division of High Polymer Physics" and defined its field in the following words: "the advancement and diffusion of knowledge of the physical properties of high polymeric materials such as rubbers, textiles, and plastics." The announcement and form of enrollment for this Division will soon be distributed to all members of the Society.

The Society has lost through death the following Fellows and Members: Leon W. Hartman (Nevada) and Thomas MacFadden (North Ireland). On January 16 occurred the death of L. T. More (Cincinnati), long a member of the Society.

Elected to Fellowship: A. Gemant, A. W. Lawson, E. Lorenz, J. H. MacMillen, W. E. Stephens, G. Wannier.

Elected to Membership: Abel, George K., Jr.; Allred, Harry M.; Arsove, Melvin W.; Baietti, Albert L.; Bailey, Jack Cecil; Benton, Arnold; Blachman, Nelson M.; Bletcher, Arthur Lester; Block, Edward; Boyd, George; Branch, Garland Marion, Jr.; Brown, J. Oliver; Brown, Robert H.; Buxton, Chester L.; Cahnman, Gisella Levi (Mrs.); Cioffard, Bernard; Collins, Donald L.; Covington, Arthur Edwin; Crowe, M. O'L.; Dunaway, Robert E.; Faust, William R.; Fast, Edwin; Feit, Louis; Finkelstein, A. Theodore; Furst, Franklin; Ginell, Robert; Givens, M. Parker; Goldsmith, Adrian Milton; Hales, Everett Burton; Hall, William Hansen; Harris, Franklin S., Jr.; Herold, Edward W.; Hinshaw, Robert A.; Iskraut, Richard; Hughes, Gordon; Hushley, Walter J.; Ivie, James O.; Jacobsmeyer, Vincent P. (Rev.); Jurman, Harry R.; Karush, Fred; Kass, Sholom; Kaufman, Raymond; Keene, Lester F.; Kehl, William; Kurmer, John; Lasof, Solomon; LeCorbeiller, Philippe E.;

Lindsay, Edwin M.; Livingston, Donald C.; Major, John Keene; Marcinkowski, Chester J.; McFerrin, W. V.; Miller, Ray L. (Miss); Nedelsky, Leo; Novey, Theodore B.; Oravec, Ralph J.; Pondrom, Walter Lewis, Jr.; Reddan, Martin Joseph; Reynolds, Charles Barton; Richman, Chaim; Rogers, Marguerite M.; Rothlein, Bernard; Sabel, Reina G. (Miss); Salkovitz, Edward I.; Scag, Dane; Scharff-Goldhaber, Gertrud; Schuette, Oswald F., Jr.; Schulz, LeRoy Gregor; Seiler, Karl, 3rd; Shaw, Milton C.; Sibbitt, Wilmer Lawrence; Sliverman, Daniel; Snow, Olive Bremner (Mrs.); Steinitz, Robert; Tiffany, O. Lyle; Van Horn, John Robert; Wannlund, Arthur Leonard, Jr.; Weaver, Harry E., Jr.; Weissler, Pearl G. (Mrs.); Whitesell, Robert O.; Wilkinson, Roger G.; Winkler, Marion R.; Zyve, David Leonard.

Abstracts of Contributed Papers

A1. A Determination of the Rate of Production in Paraffin of Neutrons by the Cosmic Radiation at Sea Level. Max Kupferberg and S. A. Korff, *New York University.*—A determination of the rate of production in paraffin of neutrons by the cosmic radiation at sea level has been carried out. A large boron trifluoride counter was employed, 75 cm long and 14.6 cm in diameter. The counter was surrounded by about 50 cm of paraffin on all sides. Arrangement was made for surrounding the counter by a cadmium or a boron carbide shield. Counting rates unshielded and with each shield were obtained and the pulse size distribution was determined at several voltages by a biased diode skimmer. The difference in counting rates between the shielded and unshielded counter permits approximate evaluation of the rate of production of neutrons in the paraffin through the relations developed by Bethe, Korff, and Placzek. The counting rate produced by the neutrons was about nine per minute in this counter, which corresponds to a rate of production of about 2.4×10^{-5} neutron per gram of paraffin per second at sea level, if the capture cross section of paraffin for thermal neutrons is taken as 0.5×10^{-24} square cm, the rate of production being directly proportional to the paraffin capture figure.

A2. A Determination of Mesotron Mass-Lifetime Ratio by Correlation with Meteorological Data. K. Kupferberg and F. Reines, *New York University.*—A method is presented for correlating vertical mesotron intensity at a given elevation with atmospheric fluctuations to determine the rest mass to lifetime ratio. The analysis is based on the well-known equation for the decay of a radioactive particle. Previous methods of correcting daily mesotron intensity for variations of temperature and pressure at the instrument are insufficient, inasmuch as the distribution of air mass above the instrument is not taken into account. Our method of correcting for the daily variations is to correlate the mesotron intensity with the distance between the upper and lower limits of a selected pressure interval as determined by radiosonde measurements. Because of the dependence of lifetime on momentum, the expansion or contraction of the atmosphere affects most markedly those particles having lower momenta. As a result, the incremental mesotron spectrum can be reasonably replaced by a monoenergetic beam. A narrow-angle, wide-aperture telescope is under construction for the purpose of determining the angular distribution of mesotrons. With this information the analysis is applicable to such wide-angle devices as Millikan-type integrating electroscopes.

A3. The Quenching Mechanism in "Self-Quenching" Counters. S. A. Korff and R. D. Present.—The role of the polyatomic molecule in "quenching" the secondary emission by positive ions in a "self-quenching" Geiger-Mueller counter has been investigated. The polyatomic gas serves a twofold purpose: (1) quenching of ultraviolet photons and (2) quenching of secondary emission by positive ions reaching the cathode. The characteristic property of a polyatomic gas, which is of importance for the operation of a fast counter, is the large probability of predissociation from excited electronic states. The quenching of ultraviolet photons occurs through photodecomposition. In a fast counter containing a self-quenching mixture, the polyatomic gas has invariably a lower ionization potential than the monatomic constituent. The positive ions make 10^5 collisions in crossing the counter, and the electron transfer probability ensures that the positive ion sheath, when it reaches the cathode, is composed entirely of polyatomic ions. These are neutralized at about 10^{-7} cm from the wall and the excited neutral molecules predissociate in 10^{-13} sec. before they can liberate a secondary electron by an inelastic collision with the wall. This is why a polyatomic vapor counter needs no quenching resistance. We have performed experiments to test some of these points.

A4. Experiments on Large Cosmic-Ray Bursts in Relation to *A* Showers. R. E. Lapp and J. H. Alexander, *Ryerson Physical Laboratory, University of Chicago.*—Experiments on large cosmic-ray bursts in relation[1] to *A* showers (extensive atmospheric showers) are being continued. In line with the finding that at sea level large bursts in an unshielded ionization chamber (t_0 bursts) are coincident with *A* showers, the experiments have been extended by using two unshielded ionization chambers in coincidence with sets of Geiger-Mueller counters. In addition a further point on the transition curve for large bursts in iron has been investigated for a uniform 5-cm iron shield. The results show that a large fraction of the bursts under 5 cm of iron originate from *A* showers (t_0 bursts);

the remaining fraction of the bursts is due to mesotrons (t_μ bursts).

[1] R. E. Lapp, Phys. Rev. **64**, 129 (1943).

A5. Auger Electrons Resulting from *K* Capture. FRANKLIN MILLER, JR., *Rutgers University.*—The most intense group of Auger electrons due to x-rays associated with *K* capture in Zn^{65} would have energies lying in a narrow band within about 150 ev of 6850 ev ($H\rho$ 276 gauss-cm). These would arise from a K–L^2 transition in the resulting Cu atom. Electrons from the K–LM transition would be about $\frac{1}{3}$ as numerous, lying within 60 ev of 8000 ev ($H\rho$ 298). The soft electrons which are emitted copiously from Zn^{65} were found to have an absorption limit in collodion of 0.15 ± 0.03 mg/cm², approx. 7500 ev. When the samples were placed 0.6 to 1.3 cm from the screen of a screen wall counter in a longitudinal magnetic field, filled with H_2 at 2-cm Hg pressure, the upper limit (by inspection) was found to be at $H\rho$ 300 ± 30. Scattering in the counter gas and absorption in the sample are believed negligible. For an old sample of Fe, presumably Fe^{55}, as well as for a recent sample, soft electrons of $H\rho$ 220 ± 30 were found. Theoretical values are $H\rho$ 237 (K–L^2) and $H\rho$ 252 (K–LM). There is some indication of a weaker group of electrons of about 20,000 ev max. energy from the recent Fe sample. These data are consistent with the hypothesis that the soft electrons from Zn^{65} and Fe^{55} are Auger electrons resulting from *K* capture.

A6. The Evaluation of the Intensities of Line Patterns Recorded on a Moving Film in its Application to the Measurement of X-Ray Intensities. J. C. M. BRENTANO AND H. FROULA, *Northwestern University.*—In evaluating the intensities of x-ray reflections recorded photographically as "lines" each line comprises a density distribution extending from a peak value to the density of the background. The evaluation of such a density range is unfavorable, particularly so when the distribution comprises a central band of high density which is narrow accompanied by a broader band in which the density "tails off" and when the latter represents an appreciable part of the total intensity. By rocking the photographic film during the exposure with uniform velocity in a direction normal to the lines a more even density distribution is obtained. When the range of rocking attains and exceeds the line width the density distribution shows flat plateaux. The intensities can then be assessed from the densities of these plateaux without requiring an evaluation of the range of uneven densities. A limitation arises where the permissible range of rocking is restricted by the closeness of the line pattern, but this limitation can be partially overcome.

A7. Thermionic Effects of Thin Films of Alkaline Earth Oxides on Metals. GEORGE E. MOORE AND H. W. ALLISON, *Bell Telephone Laboratories, Inc.*—Data are presented which indicate that approximately 0.001 monomolecular layer of alkaline earth oxide adsorbed on tungsten or molybdenum filaments produces optimum thermionic emission which is approximately the equivalent of that obtained with conventional oxide coated cathodes, using the same oxide. An effort was made to eliminate the effects of free alkaline earth metal. It was found that the heats of adsorption of the oxides to either tungsten or molybdenum are equivalent to the heats of formation of stable compounds and are in the order BaO, SrO, CaO; and that for SrO (and probably for BaO) the tenacity of adsorption to the support metal is in the order Mo, W, Ta, Pt–Rh. The order of the thermionic emission is the same in the various systems investigated. The chemical activity of the oxides is in the same order. It is suggested that differences in the dipole characteristics of the three alkaline earth oxide molecules are responsible for the differences in thermionic emission, adsorption, and chemical activity. A theory involving oriented adsorption is proposed which appears to account for the observed phenomena. The work suggests possible modifications in existing theories of the oxide-coated cathode.

A8. Electric Birefringence of Colloidal Solutions. B. W. SAKMANN, *Lubrication Laboratory, Massachusetts Institute of Technology.*—Measurements of the electro-optical effect of colloidal solutions may lead to an understanding of the interaction between the micelles in an electric field. The double refraction of colloids in alternating electric fields of low frequency consists of a direct and an alternating part. Both components have been measured in monodisperse bentonite sols of various particle size in dependence of field strength, frequency of the applied field, temperature, and concentration of the solution. The dependence of the vibrating part of the birefringence on the different parameters investigated is in good agreement with existing theories. Likewise the direct component of the double refraction of sols of large particle size and small concentration can be explained by the orientation theory in a satisfactory way. However, the direct part of the birefringence of sols of small particle size and high concentration cannot be explained by the orientation of anisotropic particles in the electric field. Measurements of the concentration dependence of the electric birefringence of those solutions indicate that part of the double refraction is due to an interaction between the micelles.

B1. Free Vibrations of Aeolotropic Bodies. H. EKSTEIN, *Research Laboratory, Commercial Equipment Co., Kansas City, Missouri.*—An approximation method similar to the perturbation theory of quantum mechanics is used to obtain frequencies and modes of crystal vibrations. First, a set of functions is selected whose linear combinations can be expected to be similar to the solutions sought. These functions are then subjected to a perturbation calculus which leads to a secular determinant of the usual form. The characteristic values of the secular equation give the frequencies. The method is applied to the extensional vibrations of thin rectangular plates. The zero-order solutions are rigorous solutions for the case of a square isotropic plate with vanishing Poisson's ratio. The perturbation calculus yields the frequencies and modes for the general case of the aeolotropic rectangular plate. The calculated frequencies and modes are compared with observations found in the bibliography (resonant fre-

quencies and lycopodium powder patterns of piezoelectrically excited quartz and tourmaline plates). The agreement is satisfactory.

B2. The Effect of Rate of Shear on the Viscosity of Oils. F. MORGAN AND M. MUSKAT, *Gulf Research and Development Company, Pittsburgh, Pennsylvania.*—In the design of machine bearings the viscosity of the lubricating oil is normally assumed to be independent of the rate of shear. Recently,[1] however, a report has appeared of experiments which have been interpreted as indicating that all oils are probably thixotropic plastics at values of viscosity times rate of shear above approximately 7000 dynes/cm². This assumption has been tested with various lubricants in a journal bearing having a ratio of radius to clearance of about 970. Temperatures were measured by thermocouples set flush with the bearing surface. For highly refined oils the apparent deviation from linearity of plots of coefficient of friction against product of viscosity and rate of shear up to values of 20,000 can be readily accounted for by the measured elevation in lubricant temperature. However, large deviations, exceeding those due to temperature rise, result for oils containing appreciable quantities of normally thixotropic materials. The results therefore indicate that for conventional, well-refined lubricating oils, the viscosity is usually independent of rate of shear at least over the practical range of speeds. On the other hand, many high viscosity compounded oils do undoubtedly behave as thixotropic plastics.

[1] Ruth N. Weltmann, Ind. Eng. Chem., Anal. Ed. **15**, 424 (1943).

B3. A Method of Determining the Energies and Wave Functions in Solids. H. A. BETHE AND F. C. VON DER LAGE, *Cornell University.*—The method differs from that of Wigner-Seitz-Slater in two respects: (1) Proper linear combinations of the usual spherical harmonics of order l are first constructed so that the sought one-electron ψ_k satisfies the symmetry required of a ψ_k belonging to the k in reduced wave vector space. This permits effectively a larger number of terms in ψ with a reduction of labor. (2) The boundary conditions on the surfaces of the crystal cell are essentially satisfied at points other than the center of the faces *ei* at more representative points as dictated by a Shockley "empty lattice" test. The method was applied in determining the lower lying energy levels at the center and far corners of the sodium k space. The results indicate that width of the first and second Brillouin zones along the (1, 0, 0) direction differs from the free electron approximation by about 4 percent. This is in marked contrast to Slater's result of about 50 percent. On the other hand the empty lattice test made upon two energy levels by Von der Lage and five by Bowers all yielded agreement within less than 1 percent of the known free electron energies.

B4. Kinematical Probability. BENJAMIN LIEBOWITZ, *Trubenizing Process Corporations, New York.*—As an inversion of quantum-mechanical ideas, a calculus is proposed in which the *density of solutions* P_a of a differential equation is sought rather than the solutions themselves. Thus, if a is a constant whose values are all equally probable, and $\delta\sigma$ is the normal distance between neighboring solutions $y(x, a)$ and $y(x, a+\delta a)$ of $y'=F(x, y)$, then by definition $P_a=|\delta a/\delta\sigma|=|(1+y'^2)^{\frac{1}{2}}/(\partial y/\partial a)|$. Alternatively, P_a is defined by means of the ratio of lengths cut by a sheaf of solutions from neighboring orthogonal trajectories. Let $1/R_\sigma$ be the curvature of these trajectories and s the length measured along a solution; then $d\log P_a/ds=-1/R_\sigma$. Similarly we define *orbital density* for a particle by means of the ratio of areas cut by a sheaf of orbits from neighboring action surfaces, $W(x, y, z, t)=C$ and $W(x, y, z, t)=C+\delta C$ at $t=t_0$. Dividing this ratio by the momentum ratio yields the *kinematical probability* P which satisfies $\partial\log P/\partial n=-\nabla^2 W/p$ (dn parallel to momentum $\mathbf{p}=\nabla W$). Putting $W=\pm k\log\psi$ transforms this into $(k^2/p^2\psi)\nabla^2\psi=1-d\log P/d\log\psi$. If we make the assumption $\nabla\cdot\mathbf{p}=\pm 2p^2/k$, then $P=\text{const.}\times\psi^2$ and $\nabla^2\psi+(p^2/k^2)\psi=0$. Some insight into the significance of this assumption is obtained from the fact that it has $\mathbf{p}=\dfrac{\mp k}{2}\cdot\dfrac{li+mj+nk}{lx+my+nz+f(t)}$ as a "plane" solution.

B5. Exchange Forces Between Li^+ and He, and The Mobility of Li^+ in He. ROLAND MEYEROTT AND HENRY MARGENAU, *Yale University.*—A calculation of the exchange force between Li^+ and He has been made with the use of a simple hydrogenic state function to represent the charge distribution of the ion. The force so obtained was added to that arising from the polarizability and the Van der Waals interaction between Li^+ and He. The result was then used to calculate the mobility of Li^+ in He gas. The theoretical value thus found, 19.4 cm²/sec. volt at a temperature of 18°C, is somewhat lower than the experimental one of 25.8 cm²/sec. volt, reported by Hoselitz.[1]

[1] K. Hoselitz, Proc. Roy. Soc. **A177**, 200 (1940).

B6. On the Application of Dirac's Method of Field-Quantization to the Problem of Emission of Low Frequency Photons. W. PAULI, *The Institute for Advanced Study* AND J. M. JAUCH, *Princeton University.*—The bremstrahlung emitted by an electron in an external field of force can in general be treated according to the usual perturbation theory with respect to the small parameter $e^2/\hbar c$. This is no longer the case for the emission of many photons with a small frequency and a given amount of total energy which is lost by the electron, because the total cross section for the deflection of the electron through a given angle turns out to be infinite in first approximation. A more rigorous treatment of this problem was given by Bloch and Nordsieck using a suitable canonical transformation. A closer investigation by Pauli and Fierz showed, however, that it is necessary to introduce an arbitrary cutting off by large frequencies of some integrals in order to obtain a satisfactory result. It was therefore interesting to apply to this problem the new formalism of Dirac[1] which avoids all divergencies by using negative energy photons in a hypo-

thetical world. According to Dirac's physical interpretation of his formalism one has to compute the probability of an emission process, where no negative energy photon is emitted in order to obtain the probability of the emission of low frequency photons in the actual world, which is here considered. The result is, however, not satisfactory. It does not seem that the difficulty can be removed without arbitrary changes of the rules applied for the physical interpretation of Dirac's formalism.

[1] P. A. M. Dirac, Proc. Roy. Soc. **A180** 1 (1942). Compare also the report of W. Pauli, Rev. Mod. Phys. **15**, 175 (1943).

B7. Continuation of Experiments with the Magnetic Current. FELIX EHRENHAFT, *New York.*—Five independent facts: movement of particles in the homogeneous magnetic field, reversing their direction of movement with the reversal of the field; the appearance of oxygen if the two ends of one piece of soft Swedish iron immersed in acidulated water are magnetized north and south; circulation of positively and negatively charged gas bubbles and solid bodies in the same plane around the constant magnetic field, reversing their direction of circulation with the reversal of the electric as well as the magnetic field; spiral tracks of particles upwards and downwards in the constant vertical magnetic field in gases as well as in liquids; the magnetization north or south of particles through illumination by a beam of light, have to be explained by the magnetic current. Stefan, Hertz, and Heaviside had the presentiment of magnetic currents. By adding the terms for the magnetic current to the equation of electrodynamics, (defining magnetism also by two constants—conductivity for magnetism and permeability), these equations become entirely symmetrical concerning H and E. The tracks of the same particle carrying simultaneously electric and magnetic charges moving with three degrees of freedom have to be investigated separately in the homogeneous electric and homogeneous magnetic field, and jointly with these fields parallel as well as perpendicular to each other. New experiments will be described in magnetolysis and electrolysis.

T1. A Simplified Method of Plate Calibration for Analytical Spectroscopy. SAUL LEVY, *Carnegie-Illinois Steel Corporation, Gary Works.*—Theoretical considerations (Silberstein-Webb) as well as experiments lead to the conclusion that the sensitometric curves for pure silver bromide unsensitized photographic emulsions are represented closely by expressions with one parameter, of importance in determination of the relative intensities. This feature can be utilized for simplification of plate calibration by preparing permanent curves for different contrasts and using a pair of spectral lines of a stable intensity ratio (gamma-pair) for determining the proper calibration curve. This procedure involves the experimental determination of a calibration curve of one particular contrast value (basic calibration). The curves for other contrast values, as measured with the gamma-pair ratio using the basic curve, can be obtained by changing the unit of abscissa according to the gamma-pair ratio. The transparencies (or the galvanometer deviations) can be projected on the log intensity axis and scales thus obtained used with the scales for concentration—log intensity relation (Owens). Since the true intensity ratios are of no importance in the analytical spectroscopy, the basic curve can be found, in absence of a step-weakener of known transparencies, by measuring the gamma-pair lines on several spectrograms on the same plate made with weakeners of unknown transparencies.

T2. The Tensile Strength of Water. ALLEN KING, *Dartmouth College.*—From experiment and theory the tensile strength of water has been assigned values within three ranges: 0–50, 150–300, and above 20,000 atmospheres. Independent evidence for the 150–300 atmosphere range is obtained from a study of the spore discharge mechanism of common ferns. Reasonable values for Young's modulus of the annular arc ($\sim 4\times 10^{11}$ dynes/cm^2) and for the range of spores ($\sim$5 cm) are found, if the tensile strength of water is assumed to be about 200 atmospheres. The calculated range is 2–3 times observed maximum values; but, since the computations are based on an idealized model, the result is not unexpected. Ripe sporangia of Polypodiaceae also can be shown to have diameters not exceeding 16 and not less than 5.5 annular cell lengths. Measurements on several species lie well within these limits.

Proceedings of the American Physical Society

Meeting of the Metropolitan Section, February 25–26, 1944

THE second meeting of the Metropolitan Section of the American Physical Society for the season 1943–1944 was held on Friday and Saturday, February 25–26, 1944, at the Polytechnic Institute of Brooklyn, 99 Livingston Street, Brooklyn, New York, as a joint symposium with the Polytechnic Institute on the Industrial Applications of X-Ray Diffraction. The program was as follows:

Friday Evening, February 25, 1944

8:00 P.M.

1. **The Ideas Behind X-Ray Diffraction.** A. L. Patterson, *Bryn Mawr College.*
2. **X-Ray Diffraction as a Tool in Metallurgy.** C. S. Barrett, *Carnegie Institute of Technology.*

Saturday, February 26, 1944

10:30 A.M.

3. **Diffraction Methods in Analytical Chemistry.** L. K. Frevel, *The Dow Chemical Company.*
4. **Diffraction Methods in Organic Chemistry.** J. D. H. Donnay, *Hercules Powder Company.*

2:30 P.M.

5. **X-Ray Diffraction in High Polymers.** W. O. Baker, *Bell Telephone Laboratories.*
6. **X-Ray Diffraction in the Study of Soap.** M. J. Buerger, *Massachusetts Institute of Technology.*

A buffet lunch for those attending the symposium was held at 1 o'clock on Saturday.

At 10 o'clock on Saturday a business meeting of the Metropolitan Section was held, and the following officers were elected for the season 1944–1945:

Chairman, L. H. Germer,
Vice Chairman, Charles M. Slack,
Secretary-Treasurer, W. S. Gorton.

Elected Members of the Executive Committee:

G. Failla,
Bernhard Kurrelmeyer.

W. S. Gorton,
Secretary-Treasurer